AD-A124 093 OSCILLATING FLOW ABOUT YAWED CYLINDERS(U) NAVAL 1/2
POSTGRADUATE SCHOOL MONTEREY CA T SARPKAYA MAR 83
NPS-69-83-001 NSF-CEE82-10248

UNCLASSIFIED F/G 20/4 NL

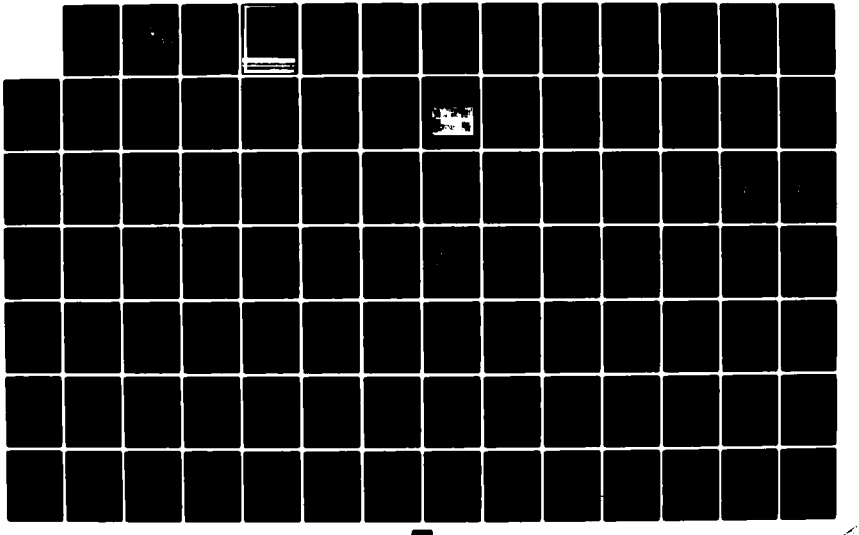

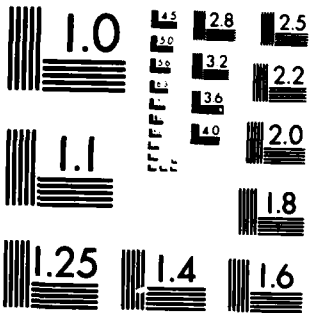

NPS-69-83-001

NAVAL POSTGRADUATE SCHOOL

Monterey, California

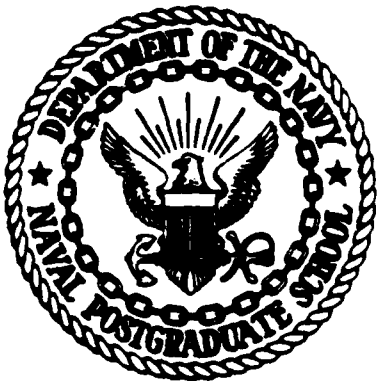

OSCILLATING FLOW ABOUT YAWED CYLINDERS

by

T. SARPKAYA

March 1983

Prepared for: NATIONAL SCIENCE FOUNDATION
WASHINGTON, D. C.

NAVAL POSTGRADUATE SCHOOL

Monterey, California

J. J. Ekelund, RADM, USN
Superintendent

D. A. Schrady
Provost

The work reported herein was supported by the National Science Foundation.

This report was prepared by:

TURGUT SARPKAYA
Distinguished Professor of
Mechanical Engineering

Reviewed by:

Paul J. Marto, Chairman
Department of Mechanical
Engineering

Released by:

William M. Tolles
Dean of Research

TABLE OF CONTENTS

Unclassified

SECURITY CLASSIFICATION OF THIS PAGE (When Data Entered)

REPORT DOCUMENTATION PAGE		READ INSTRUCTIONS BEFORE COMPLETING FORM
1. REPORT NUMBER NPS-69-83-001	2. GOVT ACCESSION NO. AD-A124093	3. RECIPIENT'S CATALOG NUMBER
4. TITLE (and Subtitle) OSCILLATING FLOW ABOUT YAWED CYLINDERS		5. TYPE OF REPORT & PERIOD COVERED Progress Report Sept. 82 - March 83
		6. PERFORMING ORG. REPORT NUMBER
7. AUTHOR(s) Professor Turgut Sarpkaya		8. CONTRACT OR GRANT NUMBER(s) CEE-8210248
9. PERFORMING ORGANIZATION NAME AND ADDRESS Naval Postgraduate School Monterey, California 93940		10. PROGRAM ELEMENT, PROJECT, TASK AREA & WORK UNIT NUMBERS
11. CONTROLLING OFFICE NAME AND ADDRESS National Science Foundation, Water Resources & Environmental Engineering (Attn: Dr. A. A. Ezra) Washington, D. C. 20550		12. REPORT DATE March 1983
		13. NUMBER OF PAGES 125
14. MONITORING AGENCY NAME & ADDRESS(if different from Controlling Office)		15. SECURITY CLASS. (of this report) Unclassified
		15a. DECLASSIFICATION/DOWNGRADING SCHEDULE

16. DISTRIBUTION STATEMENT (of this Report)

Approved for public release; distribution unlimited.

17. DISTRIBUTION STATEMENT (of the abstract entered in Block 20, if different from Report)

18. SUPPLEMENTARY NOTES

19. KEY WORDS (Continue on reverse side if necessary and identify by block number)

Yawed Cylinders; Wave Forces; Drag and Inertia Coefficients;
Wave Forces on Cylinders; Vortex Shedding

20. ABSTRACT (Continue on reverse side if necessary and identify by block number)

The forces acting on yawed smooth and rough circular cylinders in oscillating flow have been investigated for the purpose of determining the appropriate force-transfer coefficients and the applicability of the "independence principle." The results have shown that the flow about each cylinder is unique and the independence principle does not hold true over the range of Reynolds numbers and Keulegan-Carpenter numbers covered by the investigation. It has further been shown that Morison's equation

DD FORM 1 JAN 73 1473 EDITION OF 1 NOV 65 IS OBSOLETE
S/N 0102-014-6601 |

SECURITY CLASSIFICATION OF THIS PAGE (When Data Entered)

predicts the measured force with the same degree of accuracy as that for the normal cylinder provided that the force-transfer coefficients appropriate to each yaw angle, Reynolds number, Keulegan-Carpenter number, and the relative roughness are used.

ABSTRACT

The forces acting on yawed smooth and rough circular cylinders in oscillating flow have been investigated for the purpose of determining the appropriate force-transfer coefficients and the applicability of the "independence principle." The results have shown that the flow about each cylinder is unique and the independence principle does not hold true over the range of Reynolds numbers and Keulegan-Carpenter numbers covered by the investigation. It has further been shown that Morison's equation predicts the measured force with the same degree of accuracy as that for the normal cylinder provided that the force-transfer coefficients appropriate to each yaw angle, Reynolds number, Keulegan-Carpenter number, and the relative roughness are used.

PREFACE

The work reported herein is part of a basic research on "yaw and current effects on the hydrodynamic resistance of smooth and rough cylinders in harmonic flow" and was performed during the period 1 September 1982 to 1 March 1983. The principal investigator is Dr. T. Sarpkaya, Distinguished Professor of Mechanical Engineering. The project was supported by the Water Resources and Environmental Engineering Program of the National Science Foundation under Agreement No. CEE-8210246. The cognizant NSF Program Officer is Dr. Arthur A. Ezra.

The writer wishes to acknowledge the generous support of the National Science Foundation and the constructive comments of Dr. Arthur A. Ezra. A special note of thanks is extended to Mr. Thomas S. Raines and Mr. Dean O. Trytten for their assistance with the experiments during the course of the investigation.

TABLE OF CONTENTS

LIST OF FIGURES

TABLE OF SYMBOLS AND ABBREVIATIONS

C	Normalized force coefficient, $C = 2F/(\rho DLU_m^2)$
C_d	Drag coefficient
C_{lrms}	RMS value of the normalized lift force
C_m	Inertia coefficient
D	Diameter of the test cylinder
F	In-line force
F_m	Measured force
K	Keulegan-Carpenter number, $K = U_m T/D$
k	Roughness height
k/D	Relative roughness
L	Length of the test cylinder
Re	Reynolds number, $Re = U_m D/\nu$
t	Time
T	Period of flow oscillation
U	Instantaneous velocity, $U = -U_m \cos(2\pi t/T)$
U_m	Maximum velocity in a cycle
α	Yaw angle, measured between ambient flow direction and cylinder axis
β	Frequency parameter, $\beta = Re/K = D^2/\nu T$
ν	Kinematic viscosity
ρ	Density of water

I. INTRODUCTION

The study of time dependent flow about yawed cylinders is a topic which presently has great interest, both theoretically and practically. Of the great variety of time-dependent flows about yawed cylinders, the wave motion and sinusoidally oscillating flow are of such importance as to demand immediate investigation. For lack of adequate information concerning time-dependent flows, industry is often forced to adopt steady flow relations to time-dependent flow situations. This research proposes to investigate the forces acting upon yawed circular cylinders immersed in sinusoidally-oscillating planar flow and to examine the validity or limitations of the present methods of analysis.

In 1950, Morison et al. [Refs. 1 and 2] introduced an equation for calculating the in-line force acting on a vertical pile due to unbroken surface waves. For a cylinder of diameter D, the force per unit length is expressed as

$$F = 0.5\rho D\, C_d U|U| + 0.25\,\pi\rho D^2 C_m (DU/Dt) \qquad (1)$$

where U represents the incident flow velocity; C_d, the drag coefficient; and C_m, the inertia coefficient. The coefficients C_m and C_d were considered time-invariant and constant along the length of the cylinder. Morison's paper was intended as a preliminary report with follow-on studies to be done on other structures in various wave actions. Morison et al. did not consider the contributions of transverse forces and vortex shedding in the calculation of the in-line forces.

Attempts have been made to extend this rather simple relationship to far more complex situations such as combined wave and current flow, hydroelastic oscillations, and yawed cylinders. Heideman et al. [Ref. 3] studied

the validity of Morison's equation using ocean data. Although Heideman et al. concluded that Morison's equation was satisfactory for normal cylinders, the utilization of an equation unproven even under ideal flow situations [Ref. 2] to analyze ocean data so as to prove the validity of the equation is not a very meaningful exercise, (for additional details see Ref. 4).

It is obvious that there is a great need for an idealization of the problem, or an experiment which is more manageable (e.g., a sinusoidally oscillating planar flow). Only in this way can all the complex interactions be separately taken into account.

Engineers faced with the problem of dealing with wave forces on yawed members and having no other recourse drew upon previous work with steady flow. Hoerner [Ref. 5] proposed the "independence principle", which stated that the normal pressure forces are independent of the tangential velocity for subcritical values of Re_n, where Re_n is the Reynolds number based upon the flow velocity normal to the cylinder. This principle allowed the decomposition of forces and velocities into normal and tangential components and the neglecting of the tangential components. Bursnall and Loftin [Ref. 6] found that the independence principle does not apply to the critical and transcritical flow regimes. Norton et al. [Ref. 7] found that the independence principle does apply to post-critical as well as subcritical flow, but not to the critical and transcritical regions in between. Thus, recent research has shown that the independence principle applies when the boundary layer is wholly laminar (Hoerner) or wholly turbulent (Norton), but its use in the critical and transcritical regions is uncertain.

The designers of offshore structures were thus led to adopt the independence principle for the wave force calculations, and in doing so, to generalize the Morison equation. This has been accepted practice in industry

for lack of a better relation. It can be asked what would be anticipated for oscillating flow or waves on the basis of what is known for steady flow. The instantaneous Reynolds number in such a flow will vary from $-Re_{max}$ to $+Re_{max}$ during a complete flow cycle. It could be postulated that the boundary layer would, at times, be fully laminar; at other times fully turbulent; and the rest of the time be in transition. In light of this, it is rather doubtful that the independence principle applies at all to oscillating or wave flow.

The study of forces acting on yawed cylinders can be carried out either by oscillating a yawed cylinder in a tank, or using small amplitude waves in a laboratory channel, oscillating the flow about a fixed cylinder, or by using ocean data if available. Oscillating the cylinder has proven to be impractical [Ref. 8] because of difficulties of accounting for the inertial force acting on the body, producing repeatable oscillations, vibrations in the system, and difficulties in measuring the in-line and transverse forces simultaneously. Waves have relatively more complex flow kinematics due to the orbital motion of particles and the decay of wave amplitude with depth. Ocean data are not available for such a study. Oscillation of the flow past the cylinder has proved to be the best method [Refs. 9 and 10].

The primary objective of this investigation was to study the forces exerted by a sinusoidally oscillating planar flow on yawed circular cylinders to determine whether the independence principle is applicable or not. If so, the force transfer coefficients calculated by Fourier analysis using the normal velocity component should reduce identically to the normal cylinder case at corresponding values of K, Re, and k/D. If the independence principal does not apply, it is desired to determine what the coefficients are

as functions of yaw angle, roughness ratio k/D, Re, and K. It would also be necessary to determine how well Morison's equation works with the new force coefficients.

With the foregoing objectives in mind a detailed investigation has been undertaken using smooth and rough cylinders of nominal 6 inch, 4.5 inch, and 3 inch diameters at yaw angles of 45 degrees, 60 degrees, and 90 degrees (as measured between the ambient flow direction and the cylinder axis). The relative sand-roughness for all rough cylinders was k/D = 1/100.

II. EXPERIMENTAL EQUIPMENT AND TEST CYLINDERS

The equipment consists of a large U-shaped oscillating flow tunnel. It was first constructed in 1975. Since then the length of the tunnel has been increased from 30 feet to 35 feet and its height from 16 feet to 22 feet. The cross-section of the 35 ft long horizontal test section has been increased from 3 ft by 3 ft to 3 ft by 4.7 ft. Furthermore, the oscillation mechanism has been completely modified so that mono-harmonic oscillations can be generated and maintained indefinitely at the desired amplitude. For this purpose the output of a 2 Hp fan was connected to the top of one of the legs of the tunnel with a large pipe (D = 3 ft). A small butterfly valve, placed in a special housing, outside the tunnel, between the top of the tunnel and the supply line, oscillated continuously and sinusoidally at a frequency equal to the natural frequency of the oscillations of water in the tunnel. The oscillation of the valve was perfectly synchronized with that of the flow through the use of an electronic feedback control system, coupled to a DC motor oscillating the valve plate. The circuit maintained the period of oscillations of the valve within 0.0005 seconds. The amplitude of the oscillations was varied by constricting or enlarging an orifice at the

exit of the fan. The flow oscillated at a given amplitude as long as desired, (see Fig. 1 for a picture and schematic drawing of the tunnel).

The velocity in the tunnel has been determined through the use of a capacitance wire, hotfilm anemometer, perforated ball, magnetic flow meter, an accelerometer (which measured the instantaneous acceleration of flow in the test section), and by visual measurement of the water level at its heighest and lowest points in the legs of the tunnel. It is safe to state that the velocity could not have been measured more accurately. The only other means by which the velocity could have been measured was the use of a laser device. In view of its cost and in view of the fact that the other means of measurement yielded the ambient velocity within 2 percent of each other it was decided to forsake the laser system.

Mounting pads for the strain gage housings were placed on opposite sides of the tunnel in such a manner so as to accommodate the yawed cylinders. A separate mounting had to be installed for each angle of yaw. The mounting pad on one side of the tunnel was fitted with an adjustable slide so that the pad could be moved horizontally small distances to exactly match the cylinder length. The force transducers and housings were unchanged from descriptions in [Refs. 9 and 10].

The cylinder ends, cut exactly at the desired angle of yaw, were parallel to the tunnel walls with a 1/32 inch gap at each end. This gap was filled with a soft foamy material glued to the ends of the cylinder. Ball bearings were mounted in the ends of the cylinder with the outer bearing faces flush with the face of the cylinder. Careful calibration and extensive testing proved that this mounting system allowed accurate and repeatable recording of the normal and transverse forces upon the test cylinder.

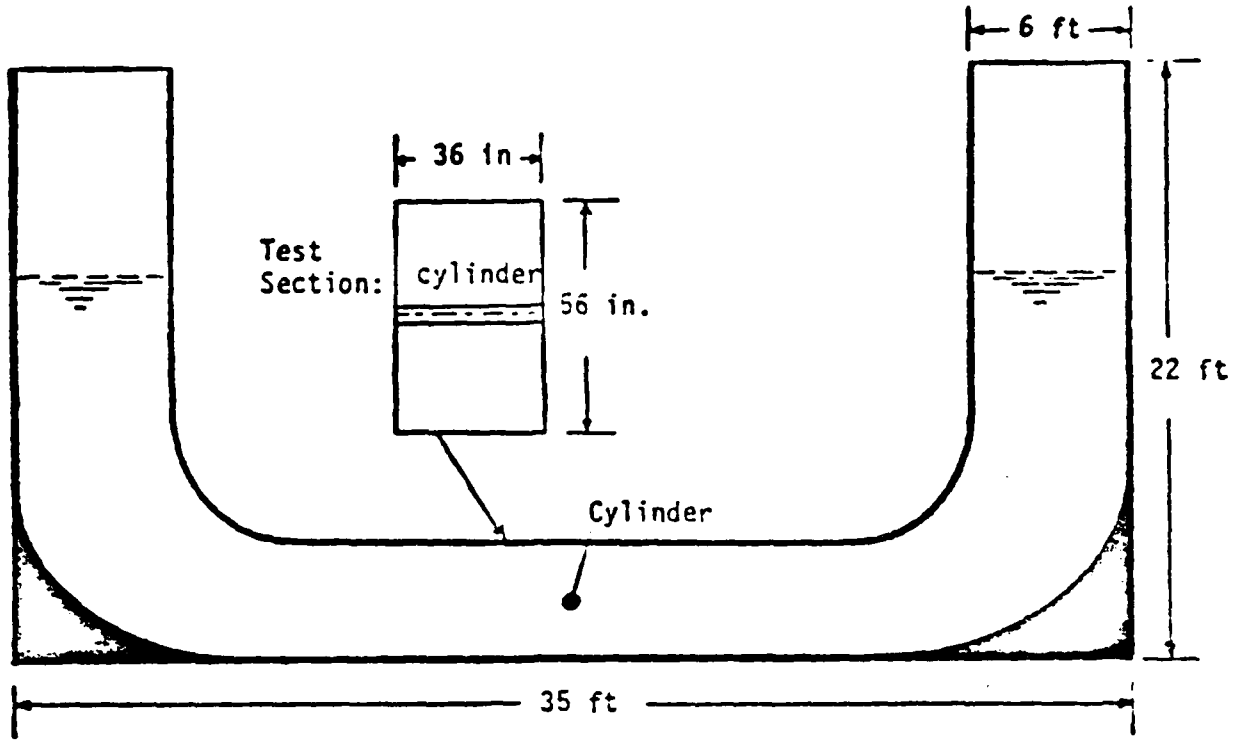

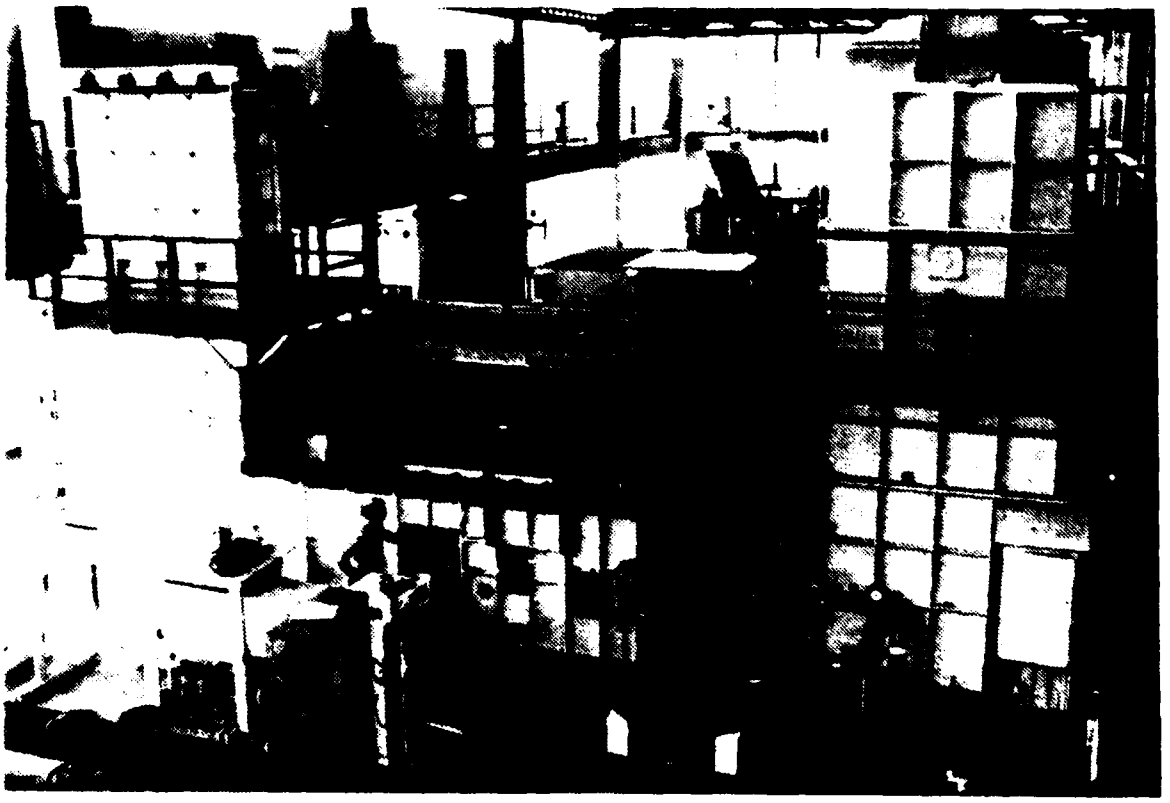

Fig. 1 A schematic drawing and picture of the water tunnel

The calibration of the cylinder was first conducted in a vertical direction, since yaw would not affect the total force in this direction. Weights were hung from the center of the cylinder, and calibration factors were obtained by converting the sum of the signals of two force transducers to either pounds/mm or pounds/volt. The strain gages were found to be exactly linear throughout the range of expected forces. Ideally, the horizontal forces normal to the cylinder should be related to the streamwise force by the sine of the yaw angle α (as measured between the cylinder axis and the ambient flow direction). A system of supports and pulleys allowed applying horizontal force at the center of the cylinder and normal to it. The sum of the outputs of the two transducers was recorded on the strip chart recorder, establishing the necessary relationship between the normal in-line force F and the total electrical output of the gages. The same gages were used to measure the lift force or the in-line force by rotating the gages 90 degrees. It is easy to show that the calibration factor for the lift force (here in the vertical direction, up or down), expressed in terms of pounds or millimeter deflection, is $\sin\alpha$ times the calibration factor for the in-line force. This proved to be true experimentally also and demonstrated independently the validity of the measurement technique.

The following cylinder sizes and angles were tested:

90 degrees, 6.5 in. and 6 in., smooth and rough;

60 degrees, 6.0 in., 4.45 in., and 3 in., smooth and rough;

45 degrees, 6 in., 4.45 in., 3 in., smooth and rough.

Relative sand roughness of k/D = 1/100 was used for all rough cylinders.

III. DATA ACQUISITION AND PROCESSING

The data were acquired using an HP-3052A automatic data acquisition system. The system consisted of an HP-3495A 20 channel scanner and an HP-3437A system voltmeter, both controlled by an HP-9845B desk top computer. The in-line and transverse force signals, originating as a voltage from the strain gages, was then amplified and sent to the strip chart recorder. This amplified signal was also sent to the scanner as one channel of data. The flow amplitude signal, originating from a differential pressure transducer, was similarly amplified and sent to both the strip chart recorder and the scanner as another channel of data. The strip chart data was maintained as a visual record of the flow amplitude and force. The scanner switched between the two channels at designated intervals when triggered by the voltmeter. The voltmeter read each one of these voltage values and transferred them to the computer for immediate calculation of the governing parameters or for further transfer to floppy disc storage to allow for analysis at a later time.

At least six cycles of in-line force data, digitized at 0.5 degree intervals, were acquired with the HP-3052A - HP-9845B system. The data were then averaged to give one cycle from which the governing parameters were calculated. Ten cycles of transverse force data, digitized at one degree intervals, were acquired with the same system. These data were not averaged before calculating the governing parameters.

The use of the data acquisition system proved to be highly beneficial for a number of reasons. The calculated parameters were available on a real time basis, allowing for detailed study of anomalies in the force patterns. Taking data over a larger number of cycles removed more of the

small randomness of the flow forces. This was particularly valuable for analyzing the transverse force data.

IV. GOVERNING PARAMETERS

Data reduction for the in-line forces is based on Morison's equation using the normal component of velocity. The derivation of the governing parameters is described in detail in [Refs. 2, 9-11]. Here only a brief description of the parameters will be given.

The force per unit length of a cylinder of diameter D is represented by Morison's equation as

$$C = \frac{2F}{\rho D U_m^2} = \frac{\pi^2}{K} C_m \sin\theta - C_d |\cos\theta| \cos\theta \qquad (2)$$

For an oscillating flow represented by $U = -U_m \cos\theta$ with $\theta = 2\pi t/T$, where U_m represents the maximum flow velocity, the Fourier averages of C_m and C_d are given by

$$C_m = \frac{2K}{\pi^3} \int_0^{2\pi} \frac{F_m \sin\theta}{\rho D U_m^2} d\theta \qquad (3)$$

and

$$C_d = -\frac{3}{4} \int_0^{2\pi} \frac{F_m \cos\theta}{\rho D U_m^2} d\theta \qquad (4)$$

where F_m represents the measured force.

The transverse force data are represented by the normalized rms value of the measured lift force ($C_{l_{rms}}$). The lift data were also analyzed using a Fourier transform to obtain frequency information. The first 15 Fourier coefficients, with corresponding magnitude and phase angles, were

calculated. Finally, C_d, C_m, and C_{lrms} were plotted in terms of the Keulegan-Carpenter number K, the 'frequency parameter' $\beta = Re/K = D^2/\nu T$, the relative roughness k/D, and the yaw angle α.

V. EXPERIMENTAL RESULTS

A. CYLINDERS AT 90 DEGREE YAW ANGLE

Attempts to achieve as high Reynolds numbers as possible in conducting wind-tunnel and water-tunnel experiments invariably give rise to wall-interference effects which, of course, influence whatever measurements are made. There are several blockage correction formulas for steady flows which might be used so that the wall-interference effects on the calculated force coefficients might be minimized. Unfortunately, none of these formulas could be used in the present study for no one has demonstrated that the blockage effects in oscillatory flows are identical to those experienced in steady flows [Ref. 9].

In view of the foregoing it was decided to repeat the experiments reported in 1976 [Refs. 9 and 10] with a 6.5 inch smooth and sand-roughened cylinder (k/D = 1/100). Originally the experiments were conducted in the first version of the U-shapped water tunnel which had a length of 30 ft, a height of 16 ft, and a cross-section of 3 ft by 3 ft. Subsequently, the length of the tunnel has been increased from 30 ft to 35 ft and its height from 16 ft to 22 ft. The cross-section of the 35 ft long horizontal test section has been increased from 3 ft by 3 ft to 3 ft by 4.7 ft, as noted earlier. Finally, the data acquisition system and other refinements have been incorporated into the system. Experiments with the 6.5-inch cylinder have been repeated following each change in the tunnel.

The drag and inertia coefficients obtained in 1976 with a D = 6.5 in. smooth cylinder are shown in Figs. 2 and 3. The data obtained with the same cylinder in the larger tunnel in 1981 and in 1982 are shown in Figs. 4 through 7. Finally, the entire data for C_d and C_m are shown in Figs. 8 and 9. Evidently, the data obtained with the enlarged tunnel agree extremely well with those obtained in 1976 [Ref. 9]. No clearer proof can be presented than these figures in eliminating the possibility of any blockage effect on the data reported previously by Sarpkaya [Refs. 9 and 10], particularly at large values of K and Re.

Figures 8 and 9 show that the only difference between the 1976 data and those obtained in 1981 and 1982 is the occurrence of two distinct modes of vortex shedding for a given K in the region of K values from 9 to 16. The observations of the in-line and transverse-force traces over several hundred cycles of flow oscillation in the said region of K values (the drag-inertia dominated regime) have revealed that the dominant mode of flow is as shown in Fig. 10a. For this mode, the in-line force trace does not exhibit large second order oscillations and the transverse force is both small and irregular. In other words, at such large Reynolds numbers (Re varied from about 47,000 to 85,000 as K varied from 9 to 16) the spanwise coherence of vortices is not perfect. The in-line force corresponding to this dominant mode yields drag and inertia coefficients identical to those shown in Figs. 2 and 3 (the 1976 data). From time to time, however, the spanwise coherence of the vortices improves dramatically and the the in-line and transverse forces change to those shown in Fig. 10b. In this second mode of flow, the in-line force exhibits large oscillations and the magnitude of the transverse force increases dramatically. This second mode gives rise to the larger drag and smaller inertia coefficients shown in Figs. 8 and 9 in the region $9 < K < 16$.

Thus, it is clear that one can obtain two different drag coefficients and hence two different inertia coefficients for the same K (in the drag-inertia dominated regime), depending on the flow mode. The occurrence of the second mode in the drag-inertia dominated regime for Reynolds numbers smaller than about 30,000 is quite common [Ref. 9]. As the Reynolds number increases, however, the first mode becomes the dominant mode. Then the variation of the transverse force with time becomes a non-stationary random process.

It is clear from the foregoing that unique values of C_d, C_m, and $C_{l_{rms}}$ do not exist for certain values of K and Re. It is also clear that the orbital motion of the fluid particles and the omnidirectionality of the waves and currents in the ocean environment give rise to the first flow mode and result in smaller drag and lift coefficients. In laboratory experiments the coherence length emerges as an important parameter, particularly in the drag-inertia dominated regime. It is thus possible to choose and L/D radio for which the flow will be in the first or second mode for a given combination of K and Re in the drag-inertia dominated regime.

The drag and inertia coefficients obtained with a D = 6.5 inch rough cylinder (k/D = 1/100) in 1976 are shown in Figs. 11 and 12. The data obtained with the same cylinder in 1981 and 1982 are shown in Figs. 13 through 16. Finally, a composite plot of the entire data is shown in Figs. 17 and 18. Evidently, all three sets of the data agree extremely well and show that tunnel blockage did not play any role on the data reported previously by Sarpkaya [Refs. 9 and 10] for smooth as well as rough cylinders.

The observations of the in-line and transverse force traces for the rough cylinder have shown that only the second flow mode occurred in the drag-inertia dominated regime. Evidently, roughness increases the coherence

length, giving rise to larger drag coefficients and smaller inerti coefficients in the drag-inertia dominated regime. Additional work is needed to delineate more clearly the role played by the coherence length and surface roughness in the variation of the force-transfer coefficients.

The drag and inertia coefficients obtained with a D = 6 inch nominal diameter smooth and rough cylinder are shown in Figs. 19 through 22. The results are quite similar to those presented earlier for the D = 6.5 inch smooth and rough cylinder.

B. CYLINDERS AT 60 DEGREE YAW ANGLE

The drag and inertia coefficients obtained with 6 inch, 4.5 inch, and 3 inch (nominal diameter) smooth and rough cylinders (k/D = 1/100) are shown in Figs. 23 through 34 as a function of K ($K = U_{mn}T/D$). Two facts are immediately apparent. First, the drag coefficient does not exhibit multiple values in the drag-inertia dominated regime. In general, the drag coefficient increases to a peak and then decreases gradually with increasing K and Re. In fact, the observations of flow about the cylinder with tracer particles have shown that the vortices are far from coherent. Secondly, the inertia coefficient is larger than 2.0 for small values of K, giving the first indication that the independence principle is not probably valid.

C. CYLINDERS AT 45 DEGREE YAW ANGLE

The drag and inertia coefficients obtained with 6 inch, 4.5 inch, and 3 inch (nominal diameter) smooth and rough cylinders (k/D = 1/100) are shown in Figs. 35 through 46 as a function of K. Aside from a relatively larger scatter, the overall characteristics of the data are quite similar to those for the 60 degree yaw angle.

D. COMPARISON OF THE DRAG AND INERTIA COEFFICIENTS

The drag coefficient for three smooth cylinders at yaw angles of 90, 60, and 45 degree are shown in Figs. 47 through 49. Evidently, had the independence principle been valid, the three sets of data corresponding to three yaw angles would have collapsed into a single set, thus rendering C_d versus K relationship independent of the yaw angle (at least within the range of the test parameters and experimental errors).

The inertia coefficient for the three smooth cylinders at yaw angles of 90, 60, and 45 degree are shown in Figs. 50 through 52. Evidently, C_m varies significantly with the yaw angle and the independence principle is not valid within the range of test parameters. The inertia coefficients based on the normal component of acceleration are significantly larger than those for the normal cylinder (yaw angle = 90 degrees) at the corresponding Reynolds numbers and Keulegan-Carpenter numbers. Finally, the inertia coefficient for the yawed cylinders does not exhibit the usual "inertia crisis" associated with the normal cylinder. In fact, the inertia coefficient for the yawed cylinders varies gradually with K and remains 25 percent to 50 percent larger than that for the normal cylinder. Thus, it is clear from the foregoing that the normal force acting on a yawed cylinder is significantly underestimated through the use of Morison's equation, independence principle, and the drag and inertia coefficients appropriate to the normal cylinder.

The drag and inertia coefficients for the three rough cylinders at yaw angles of 90, 60, and 45 degree are shown in Figs. 53 through 58. Evidently, roughness plays an important and, oddly enough, a unifying role on the drag coefficient. This is somewhat anticipated on the basis of the fact that roughness precipitates earlier transition and greater incoherence in the

flow about a yawed cylinder, thereby creating conditions more favorable to the independence principle. Figures 53 through 55 show that the independence principle for rough cylinders is almost valid with the exception of the drag-inertia dominated regime. However, the inertia coefficient for rough cylinders depends strongly on the yaw angle (see Figs. 56 through 58). Thus, it appears that the independence principle or the cosine law, as it is sometimes called, is a gross simplification of the behavior of flow in the near wake. One may, therefore, conclude that the Fourier-averaged drag and inertia coefficients, based on Morison's equation, are unique for each angle of yaw, Reynolds number, Keulegan-Carpenter number, and the relative roughness.

E. EVALUATION OF MORISON'S EQUATION FOR YAWED CYLINDERS

Since the independence principle cannot be applied to yawed cylinders in sinusoidally oscillating planar flow, it is necessary to determine if the Fourier-averaged coefficients calculated from the normal forces will predict the forces exerted on the cylinder when Morison's equation is used together with the experimentally determined C_d and C_m values, appropriate to each yaw angle. In general it was found that the Morison equation predicts the forces on the yawed cylinder with the same degree of accuracy as the 90 degree case. Figures 59 through 63 show comparisons of the measured and calculated forces for the 90 degree 6-inch rough cylinder at K values of 6.86, 10.18, 11.88, 16.15, and 22.56. Examples for the 60 degree case are shown in Figs. 64 through 66 for K values of 6.89, 16.83, and 23.94. Finally, Figs. 67 through 71 show the comparison of the measured and calculated forces for the 45-degree case for K values of 7.90, 10.05, 12.50, 16.35, and 24.04. It is clear from these comparisons that when C_m and C_d are known for a given angle of yaw,

Morison's equation will predict the normal forces on cylinders at angles of yaw as well as the normal cylinder case.

F. TRANSVERSE (LIFT) FORCES

The lift force data are presented in terms of the normalized rms value of the measured lift force. Figures 72 and 73 show the lift coefficients for the 6-inch smooth and rough cylinder, respectively, for the three yaw angles. The lift coefficient for the 60 degree and 45 degree yaw angles is considerably smaller than that for the normal smooth cylinder. Furthermore, the data for the 60-degree and the 45-degree cases exhibit great deal of scatter. This is primarily due to the fact that the coherence length is considerably smaller and the flow exhibits numerous modes, leading to a non-stationary random process as far as the vortex shedding is concerned.

For the rough cylinder, the lift coefficients are relatively larger for all values of K. However, the lift coefficient for the 60-degree and 45-degree cases is about half of that for the normal cylinder for values of K larger than about 15. The data for all other smooth and rough cylinders showed similar trends and will not be discussed here further.

G. FOURIER ANALYSIS OF THE LIFT FORCE

Calculation of the first fifteen Fourier coefficients, magnitudes, and phase angles of the lift force only reinforced the fact that the lift force is a highly random process. Except for low values of K (where second harmonic was dominant) there was no clear dominance of any particular harmonic. In fact, it showed that a number of harmonics were present. Neither was any trend visible in the phase angle variation. Figures 74 through 93 show sample data plots, and harmonics for the 45-degree 6-inch rough and smooth cylinders

at various K values. The existence of a large number of harmonics in the lift force accounts for most of the scatter in $C_{l_{rms}}$.

VI. CONCLUSIONS

The forces acting on yawed smooth and rough circular cylinders in sinusoidally oscillating planar flow have been investigated extensively and the following conclusions have been reached:

1. The independence principle does not apply over the range of K and Re values investigated. The drag and inertia coefficients for the 45-degree and 60-degree smooth and rough yawed cylinders differ significantly from those for the 90-degree normal cylinder.

2. The Fourier-averaged drag and inertia coefficients, based on Morison's equation, and the rms value of the lift coefficient are unique for each yaw angle, Reynolds number, Keulegan-Carpenter number, and the relative roughness.

3. When the drag and inertia coefficients are calculated from the measured force for the yawed cylinder, in a manner similar to that used for the 90-degree cylinder, Morison's equation predicts the measured force with the same accuracy as that for the 90-degree cylinder.

4. The normal force acting on a smooth or rough yawed cylinder is significantly underestimated through the use of the independence principle and the drag and inertia coefficients appropriate to the normal cylinder.

5. Extensive flow visualization about normal and yawed cylinders has shown that the cylinder inclination significantly decreases the spanwise coherence and the kinematics of flow about yawed cylinders are considerably more complex than those for a normal cylinder.

6. The lift force is a non-stationary random process and contains a large number of harmonics. In general, $C_{l_{rms}}$ for yawed cylinders is considerably smaller than that for the normal cylinder.

7. The data presented herein should form the basis of future calculations for the forces acting on yawed cylinders. Additional data at higher Reynolds numbers and the understanding of the role played by the coherence length will add significantly to the quantitative and qualitative understanding of flow about yawed cylinders.

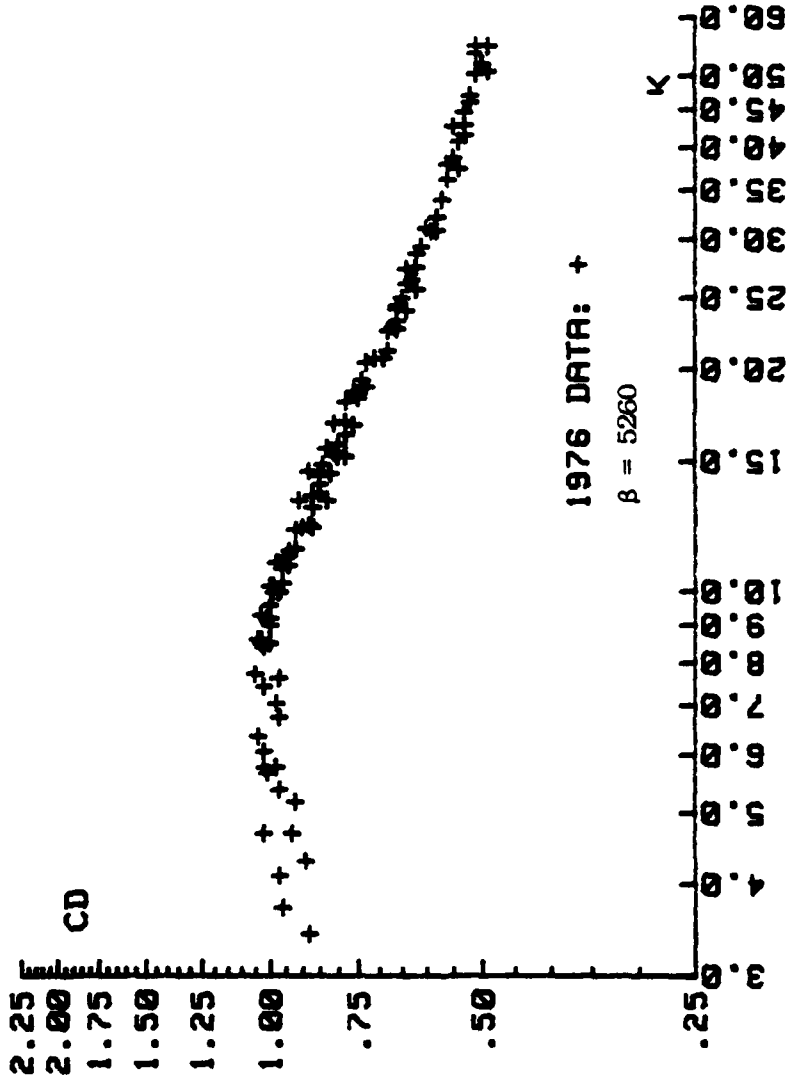

Figure 2. C_d versus K (1976 data)

Figure 3. C_m versus K (1976 data)

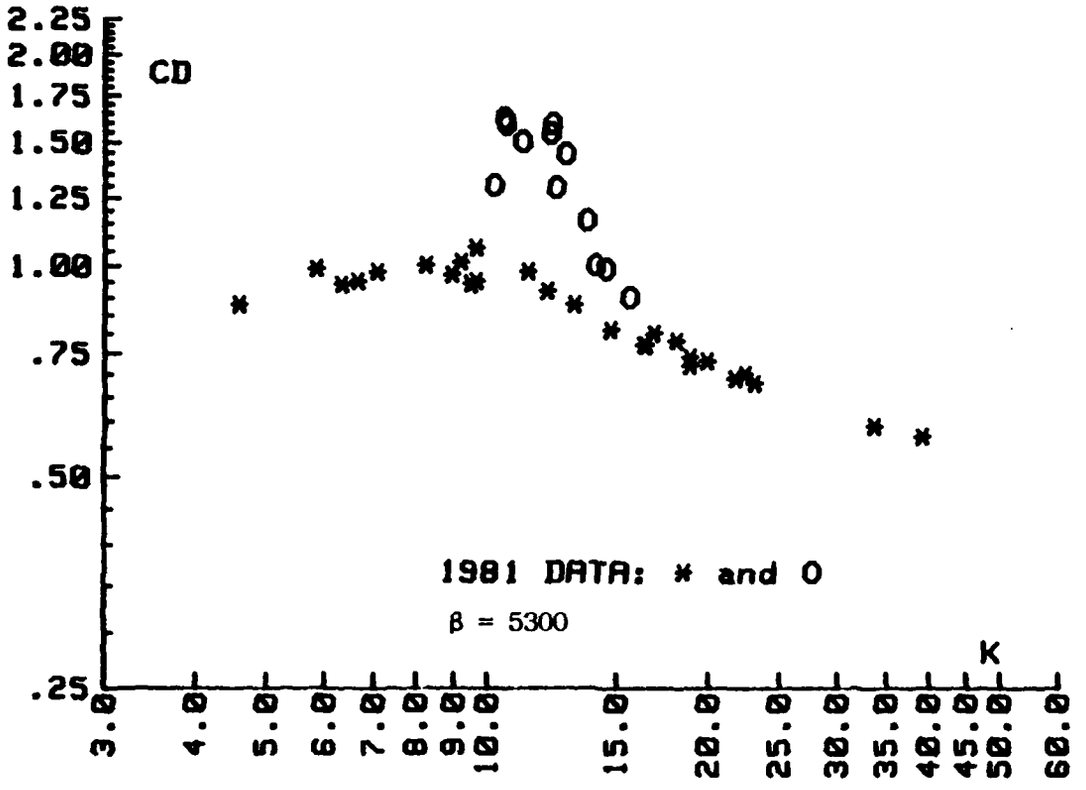

Figure 4. C_d versus K (1981 data)

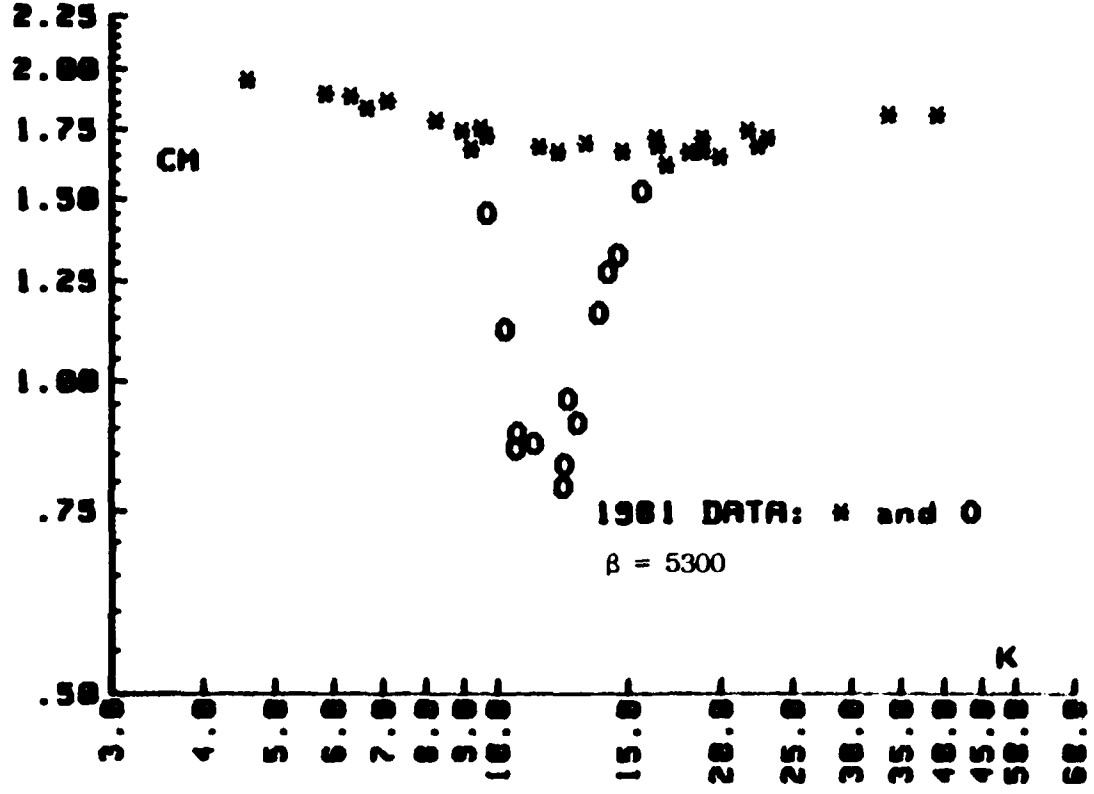

Figure 5. C_m versus K (1981 data)

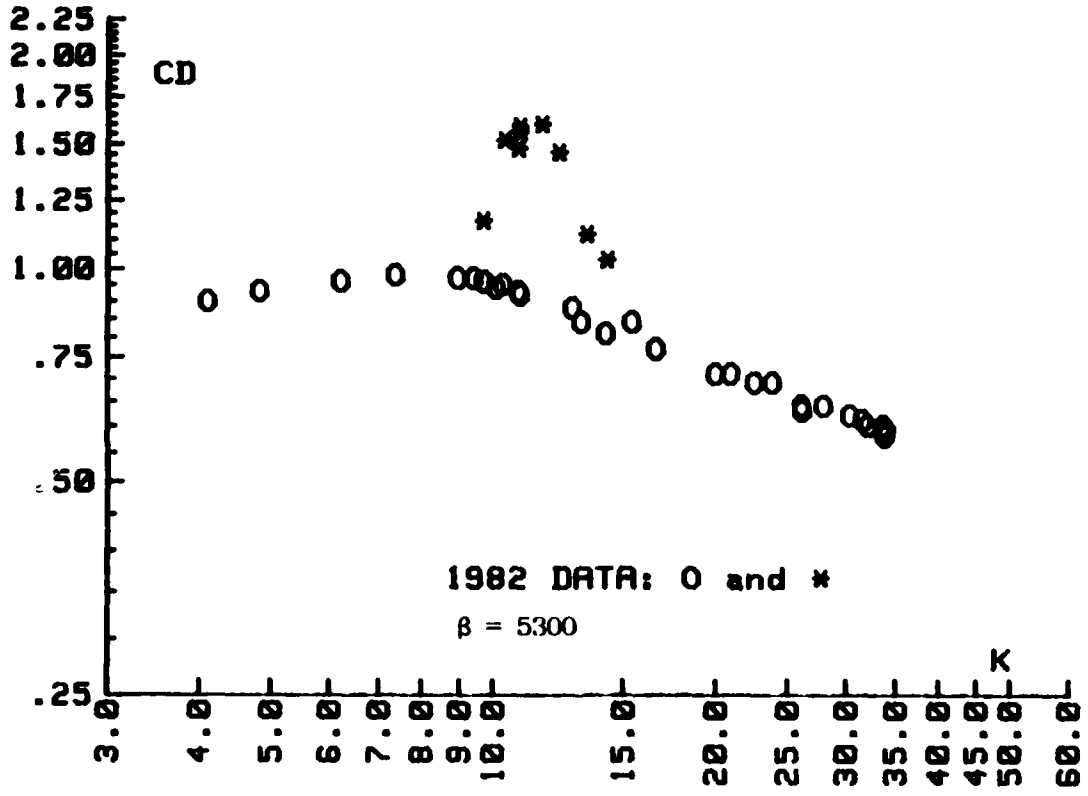

Figure 6. C_d versus K (1982 data)

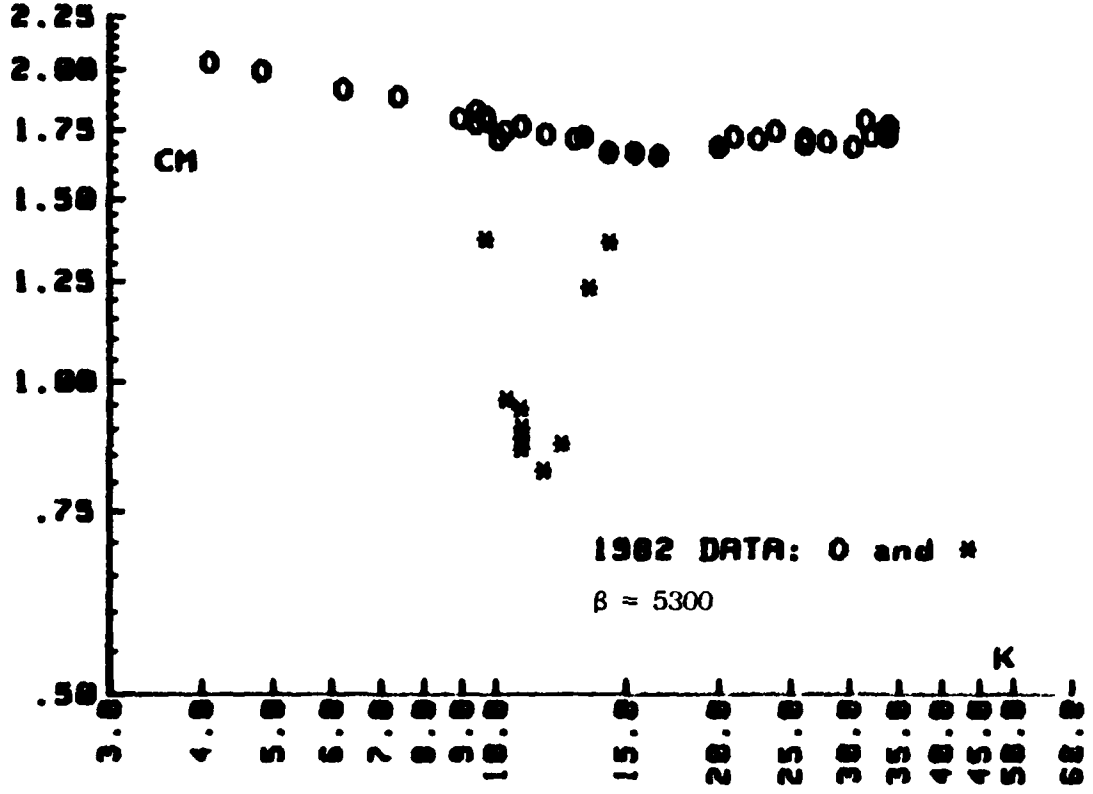

Figure 7. C_m versus K (1982 data)

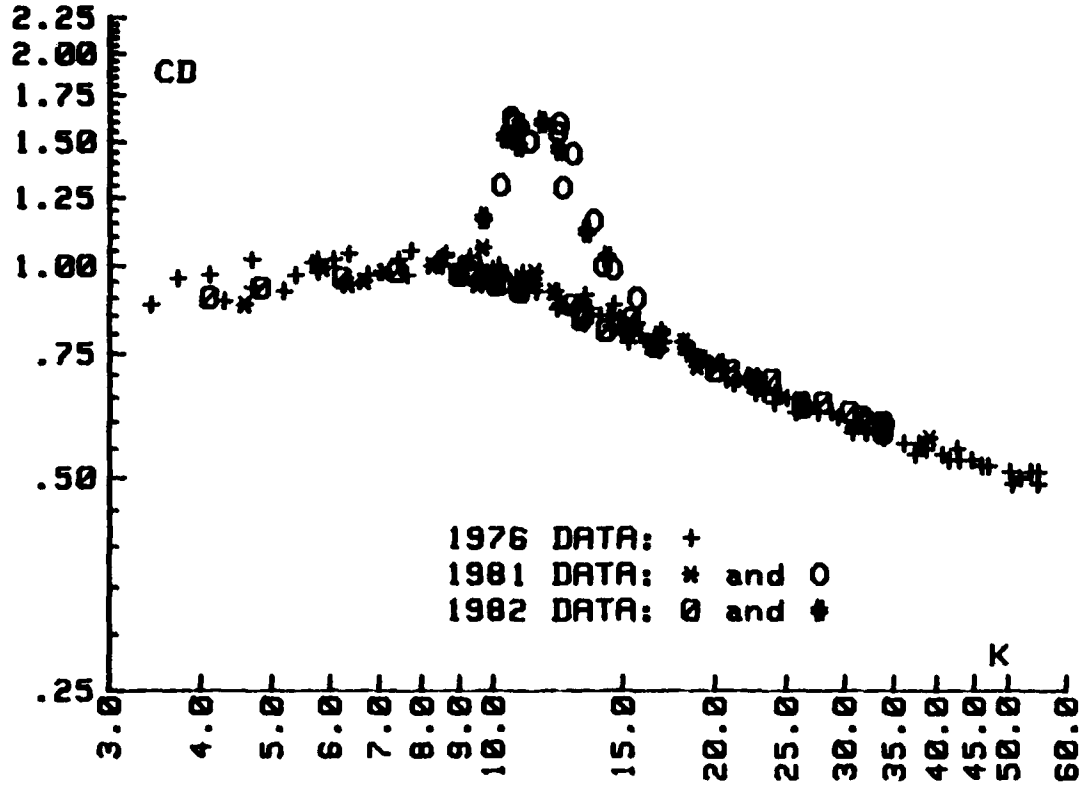

Figure 8. C_d versus K (1976, 1981, and 1982 data)

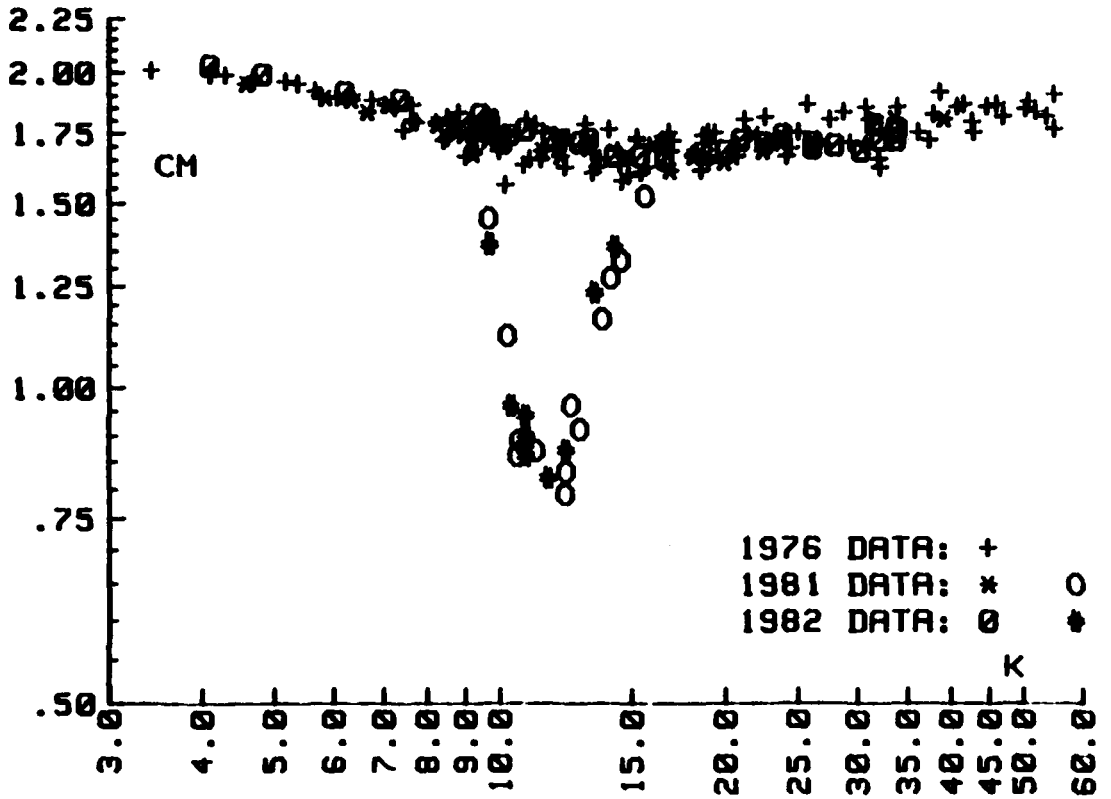

Figure 9. C_m versus K (1976, 1981, and 1982 data)

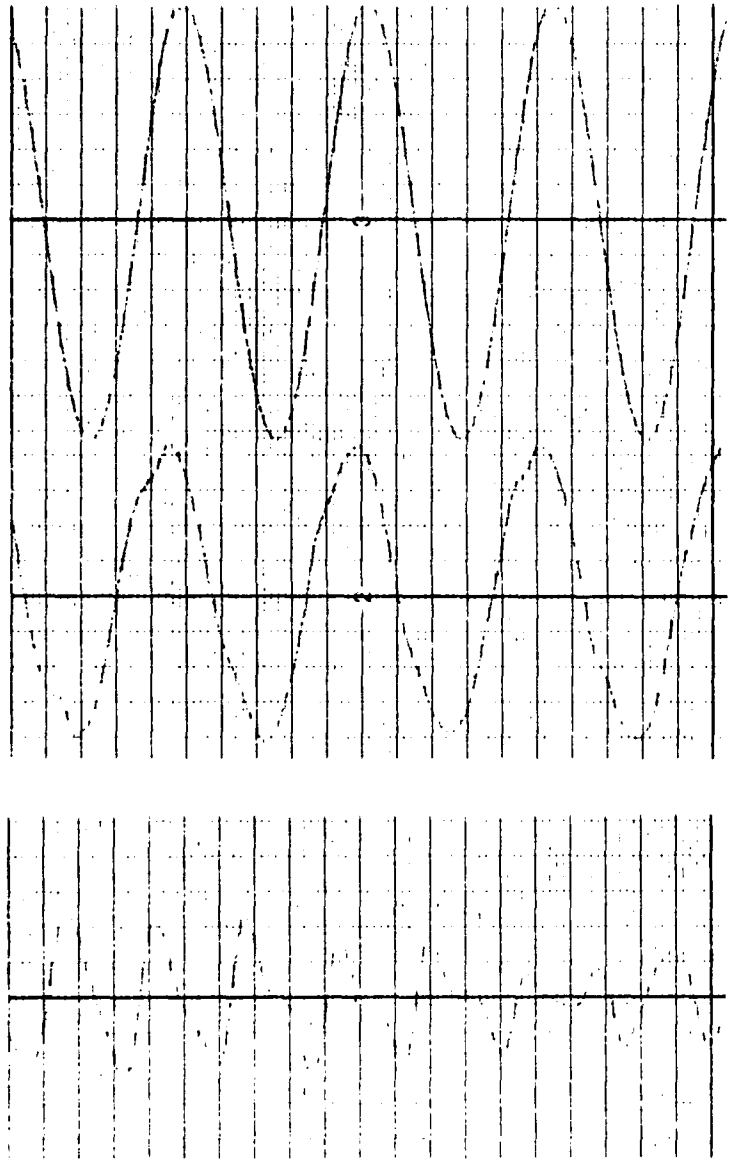

Figure 10a. First mode of vortex shedding

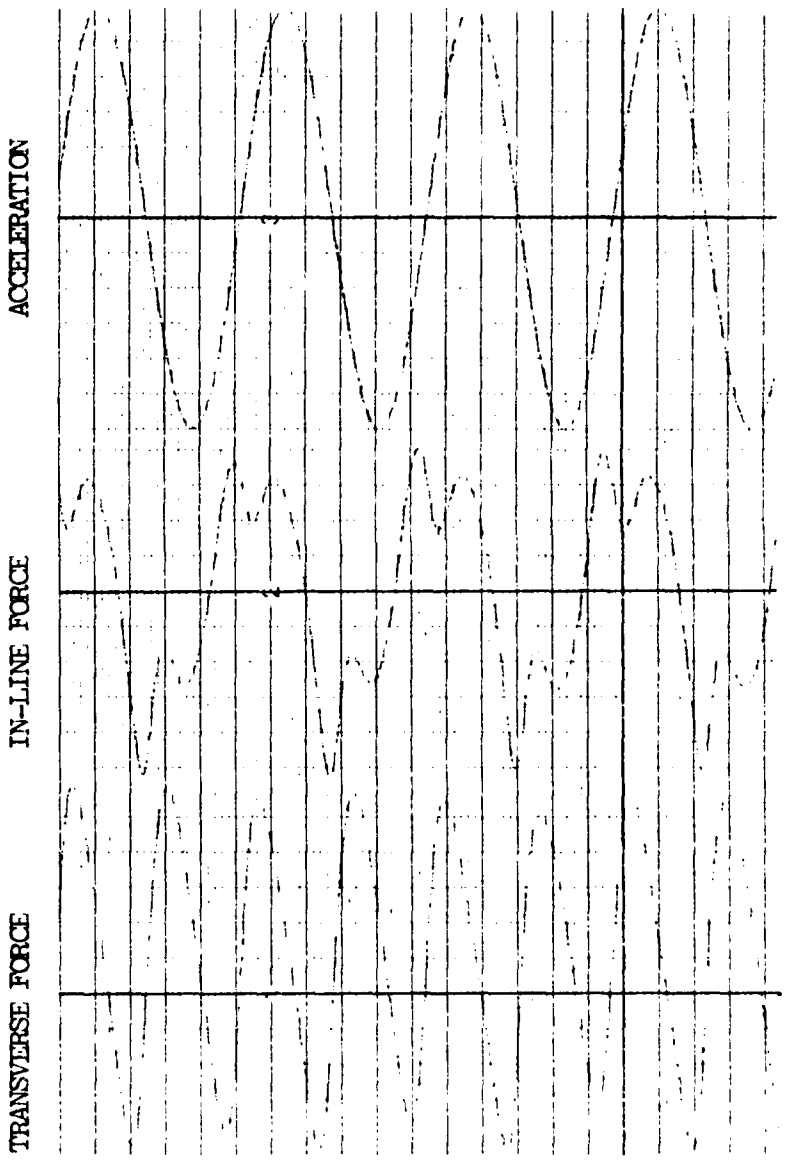

Figure 10b. Second mode of vortex shedding

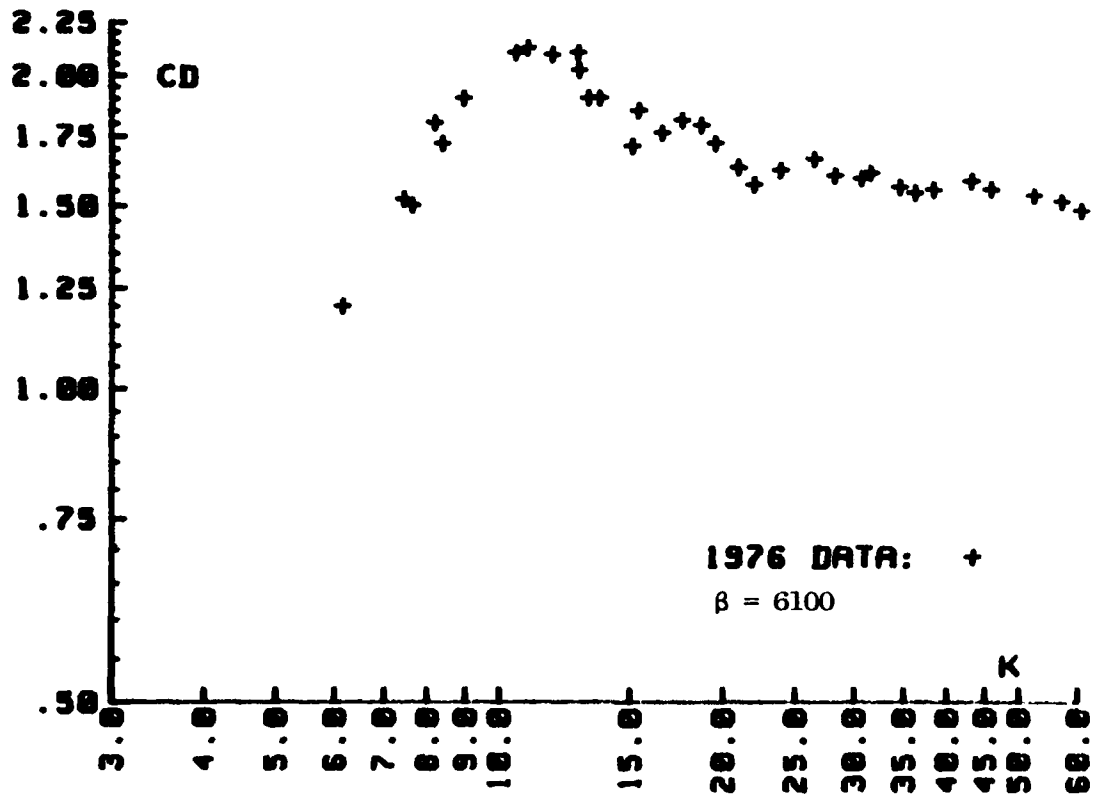

Figure 11. C_d versus K for a 6.5 inch rough cylinder (1976 data)

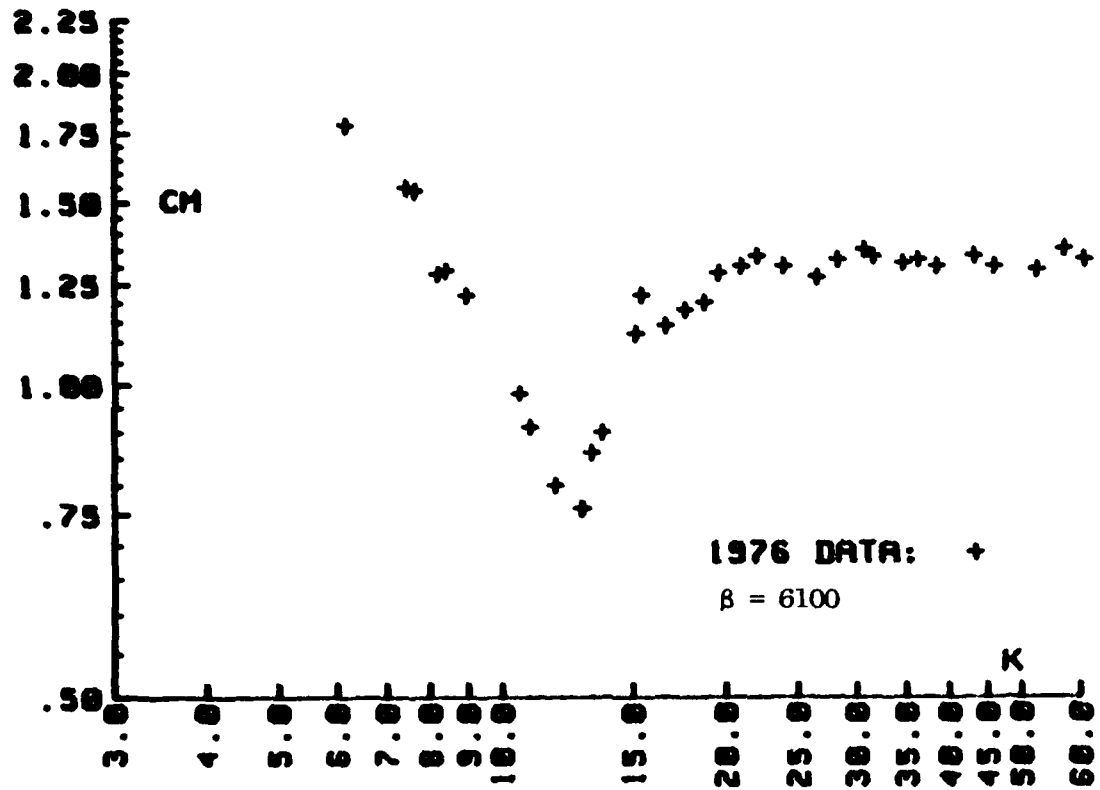

Figure 12. C_m versus K for a 6.5 inch rough cylinder (1976 data)

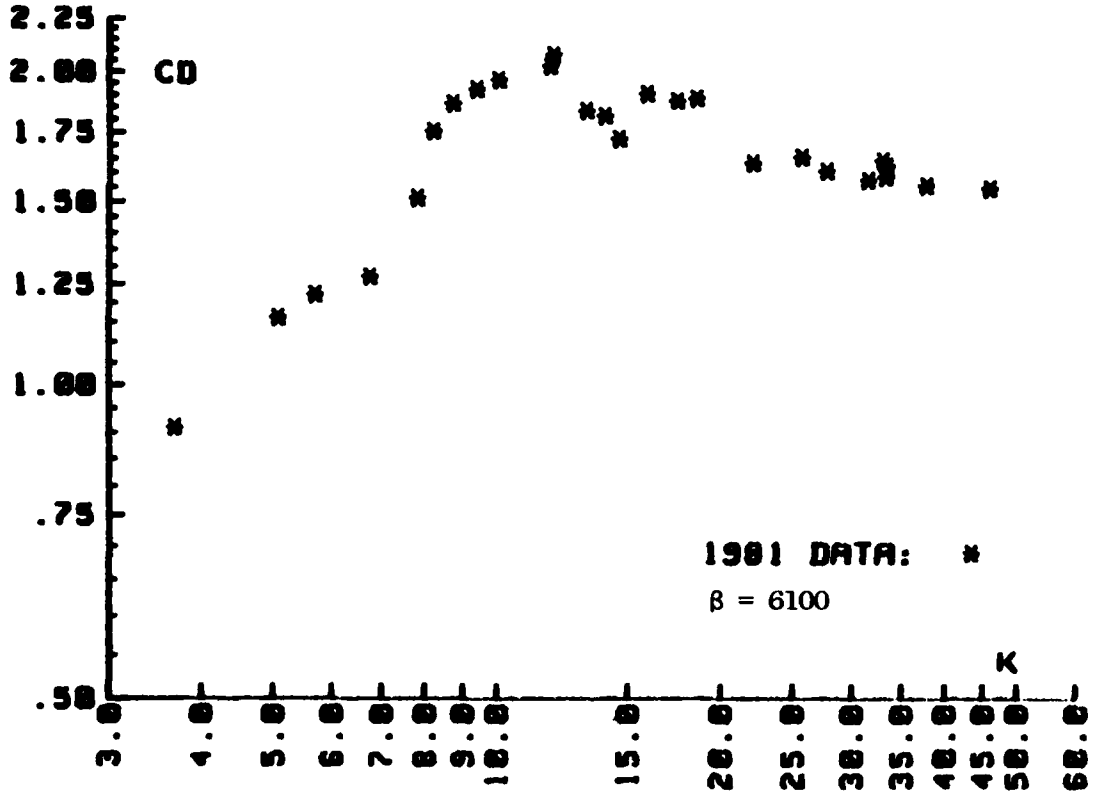

Figure 13. C_d versus K for a 6.5 inch rough cylinder (1981 data)

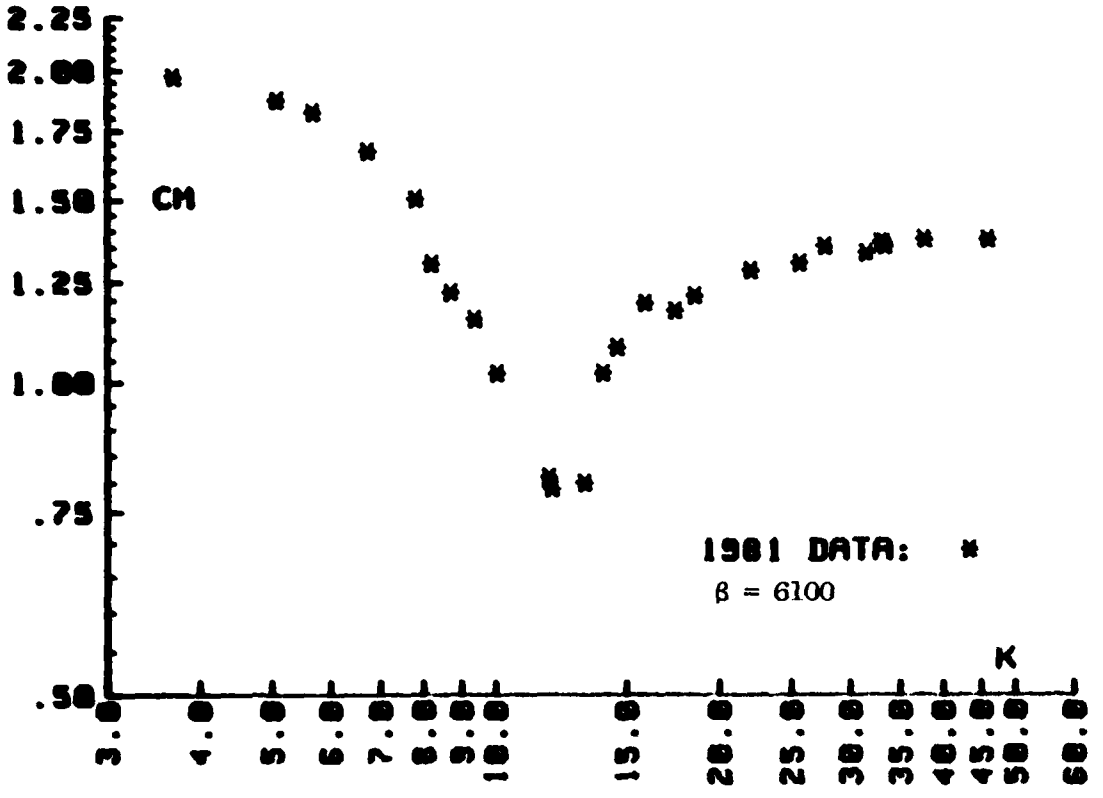

Figure 14. C_m versus K for a 6.5 inch rough cylinder (1981 data)

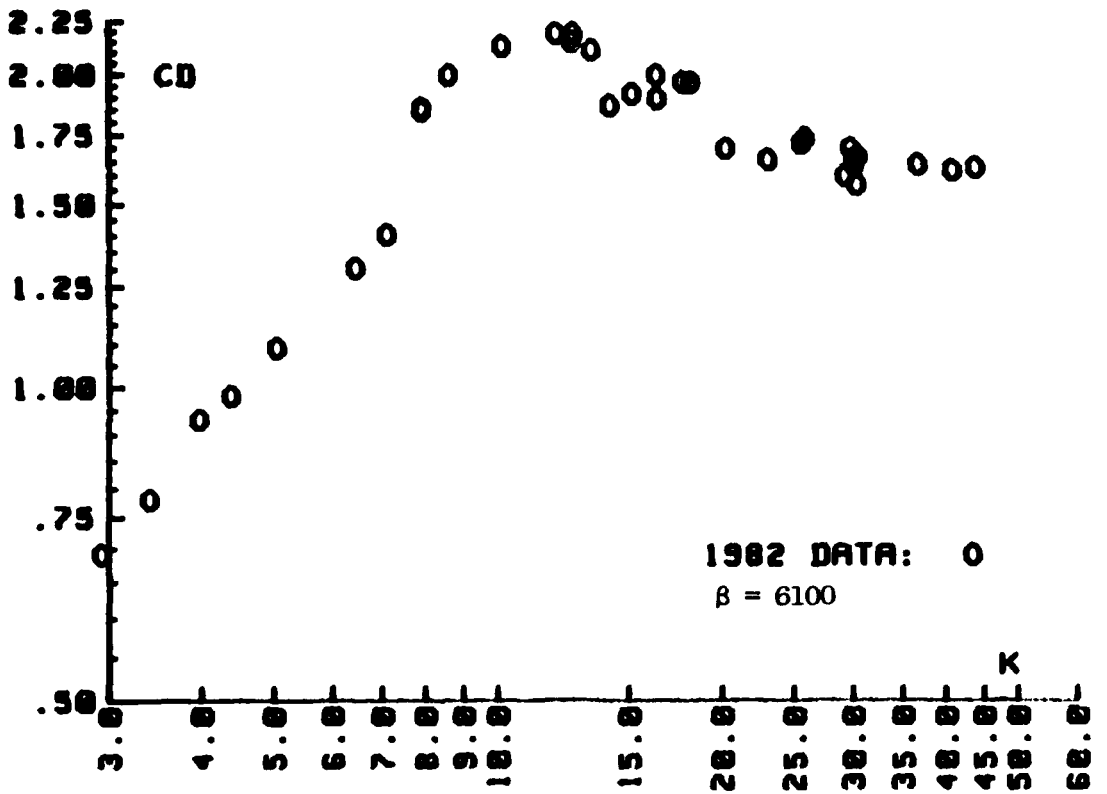

Figure 15. C_d versus K for a 6.5 inch rough cylinder (1982 data)

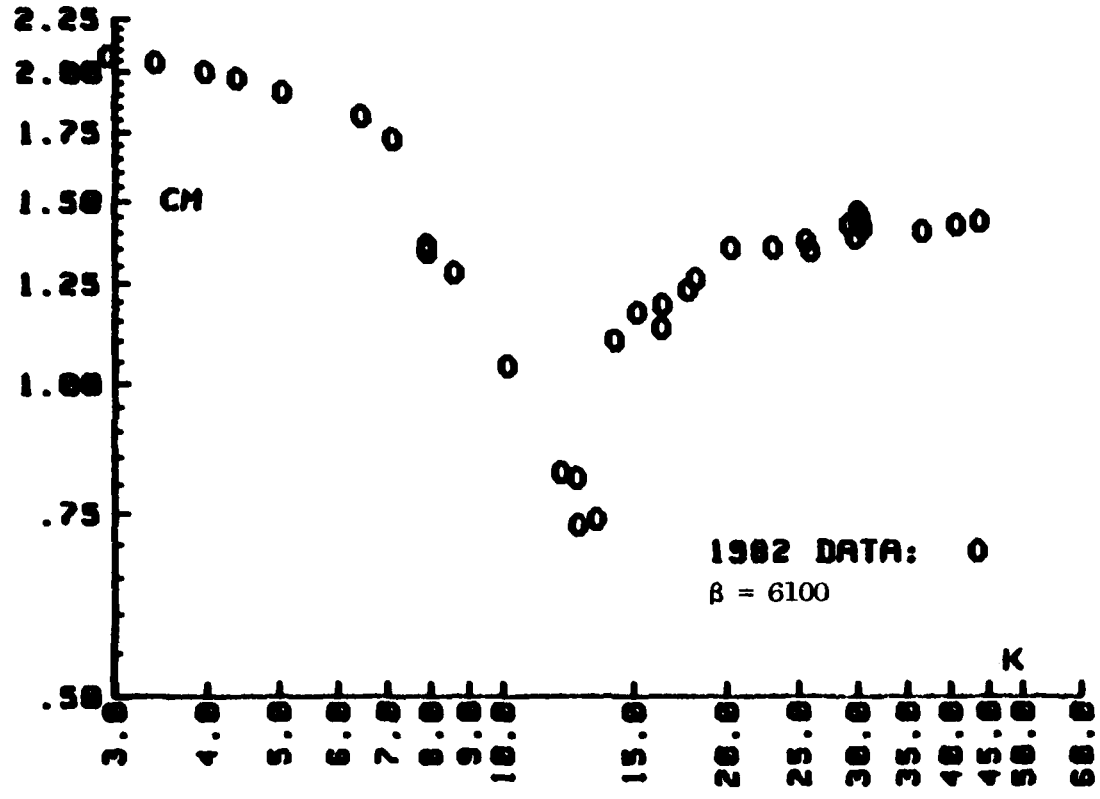

Figure 16. C_m versus K for a 6.5 inch rough cylinder (1982 data)

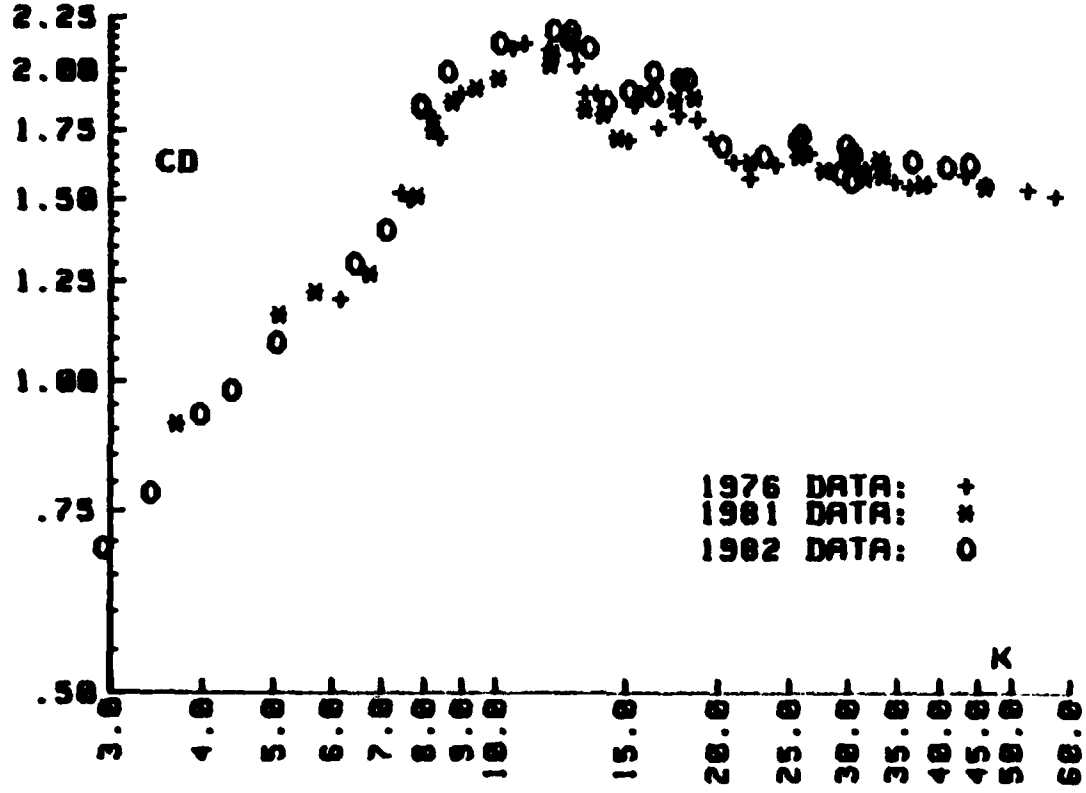

Figure 17. C_d versus K for a 6.5 inch rough cylinder (1976, 1981, and 1982 data)

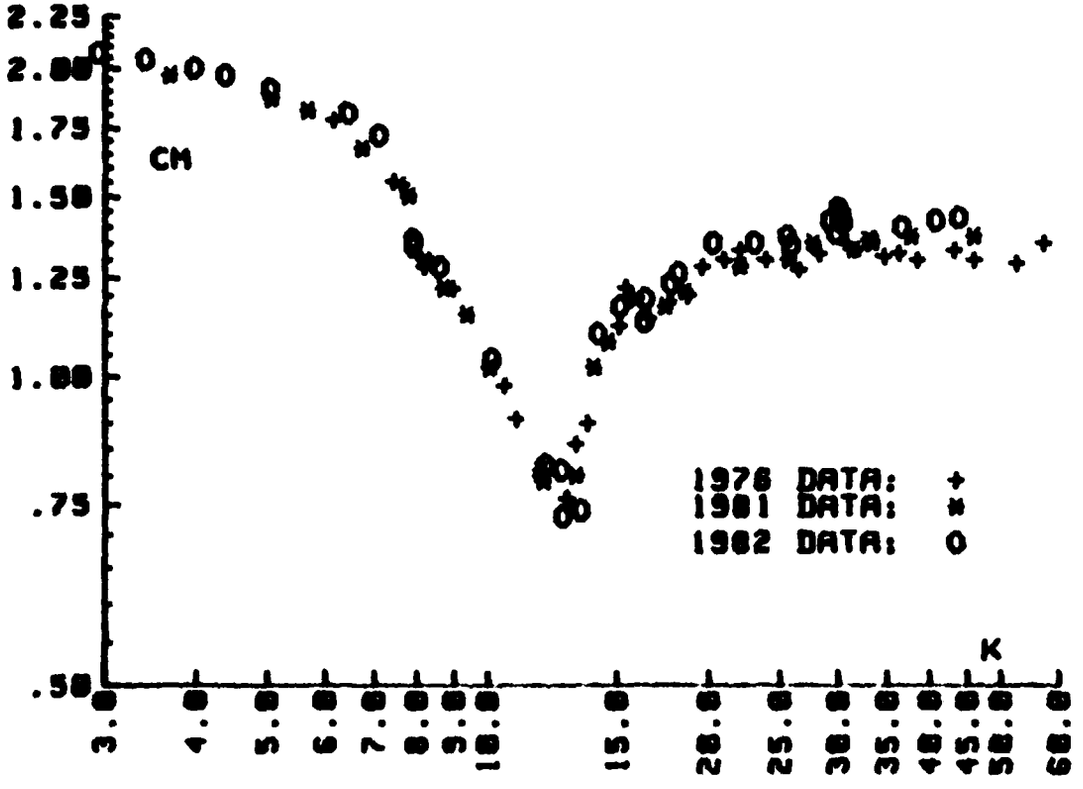

Figure 18. C_m versus K for a 6.5 inch rough cylinder (1976, 1981, and 1982 data)

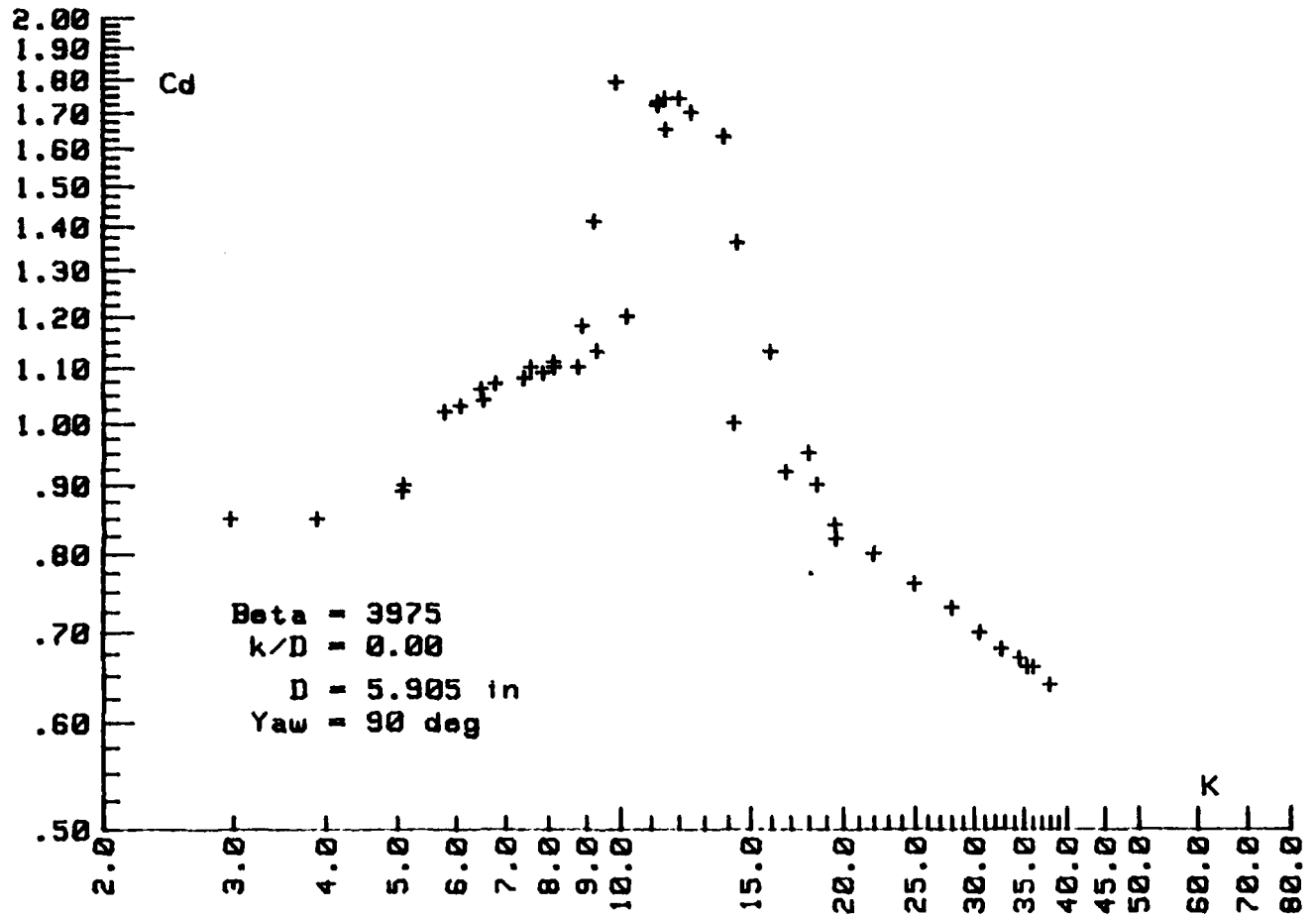

Figure 19. C_d Versus K for β= 3975, α= 90 Deg., k/D = 0.00

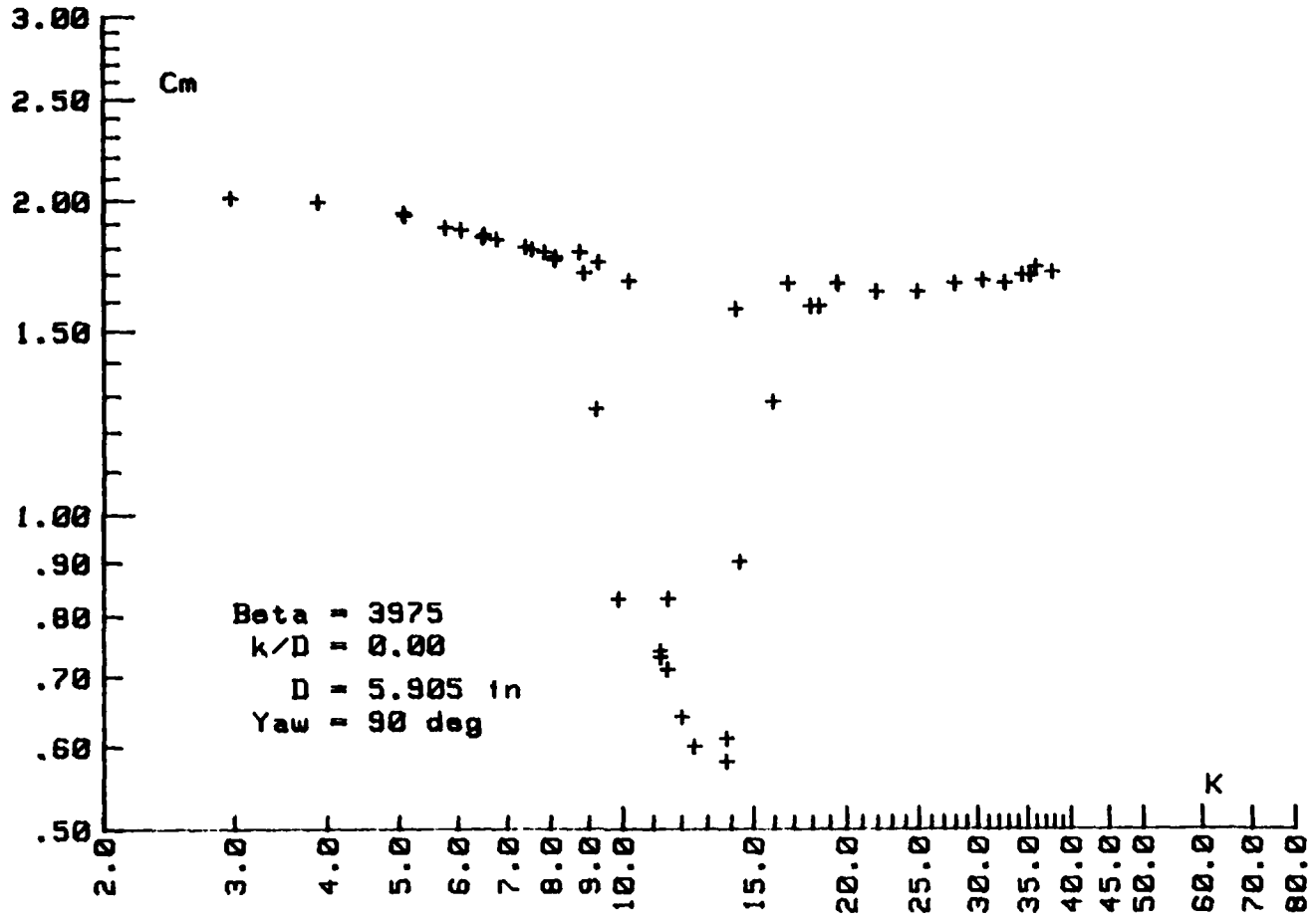

Figure 20. C_m Versus K for β = 3975, α = 90 Deg., k/D = 0.00

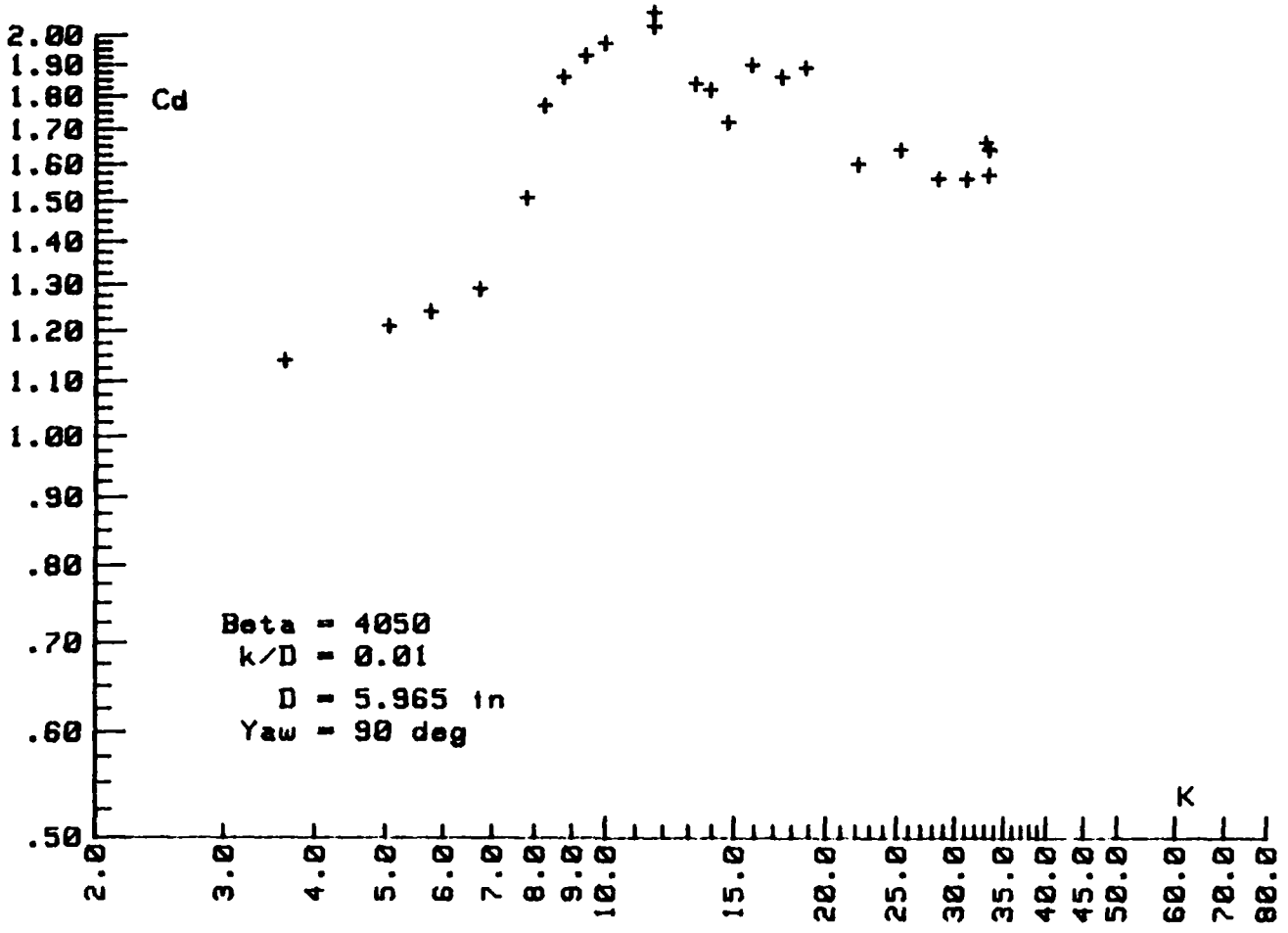

Figure 21. C_d Versus K for β = 4050, α = 90 Deg., k/D = 0.01

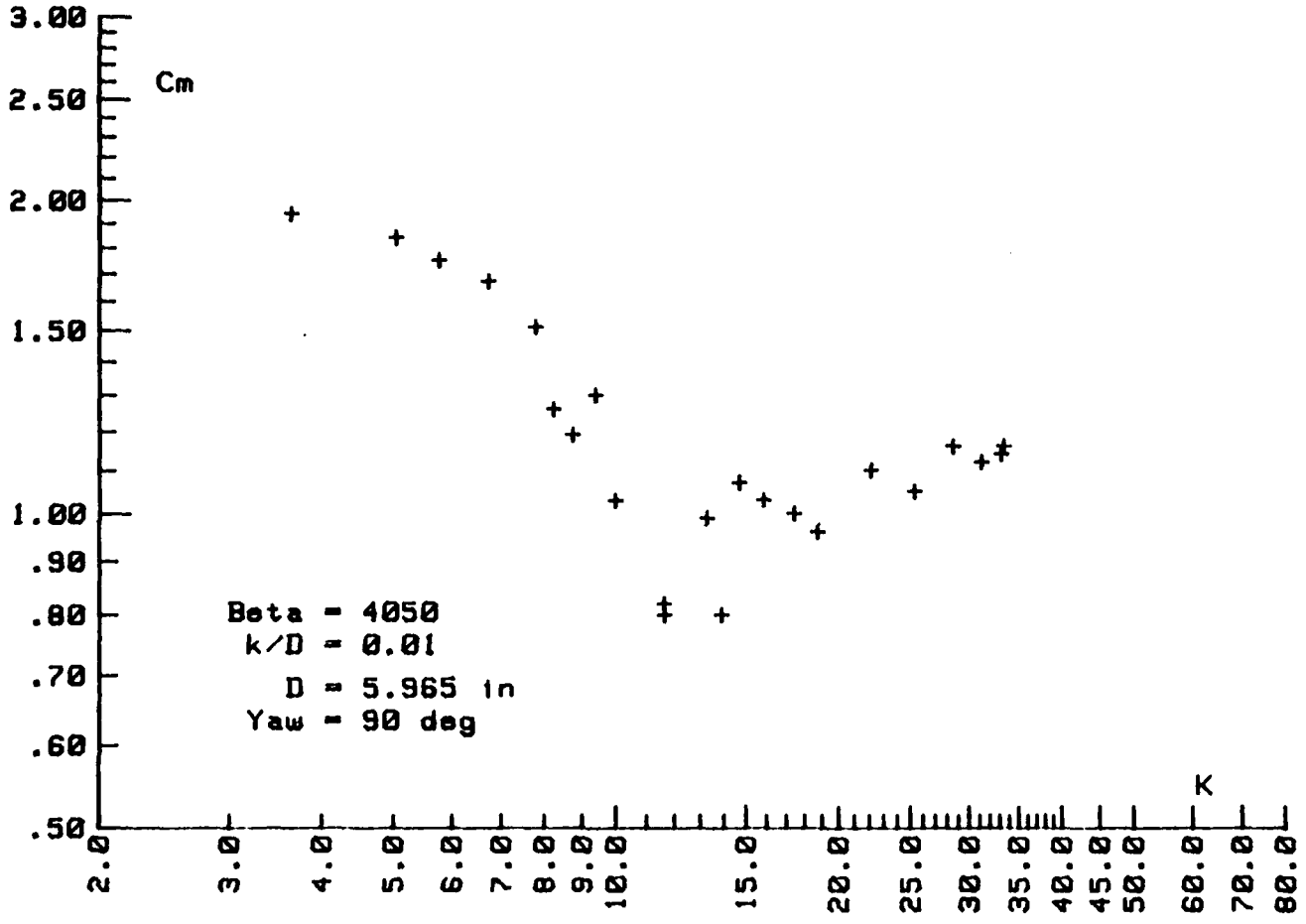

Figure 22. C_m Versus K for β= 4050, α= 90 Dec., k/D = 0.01

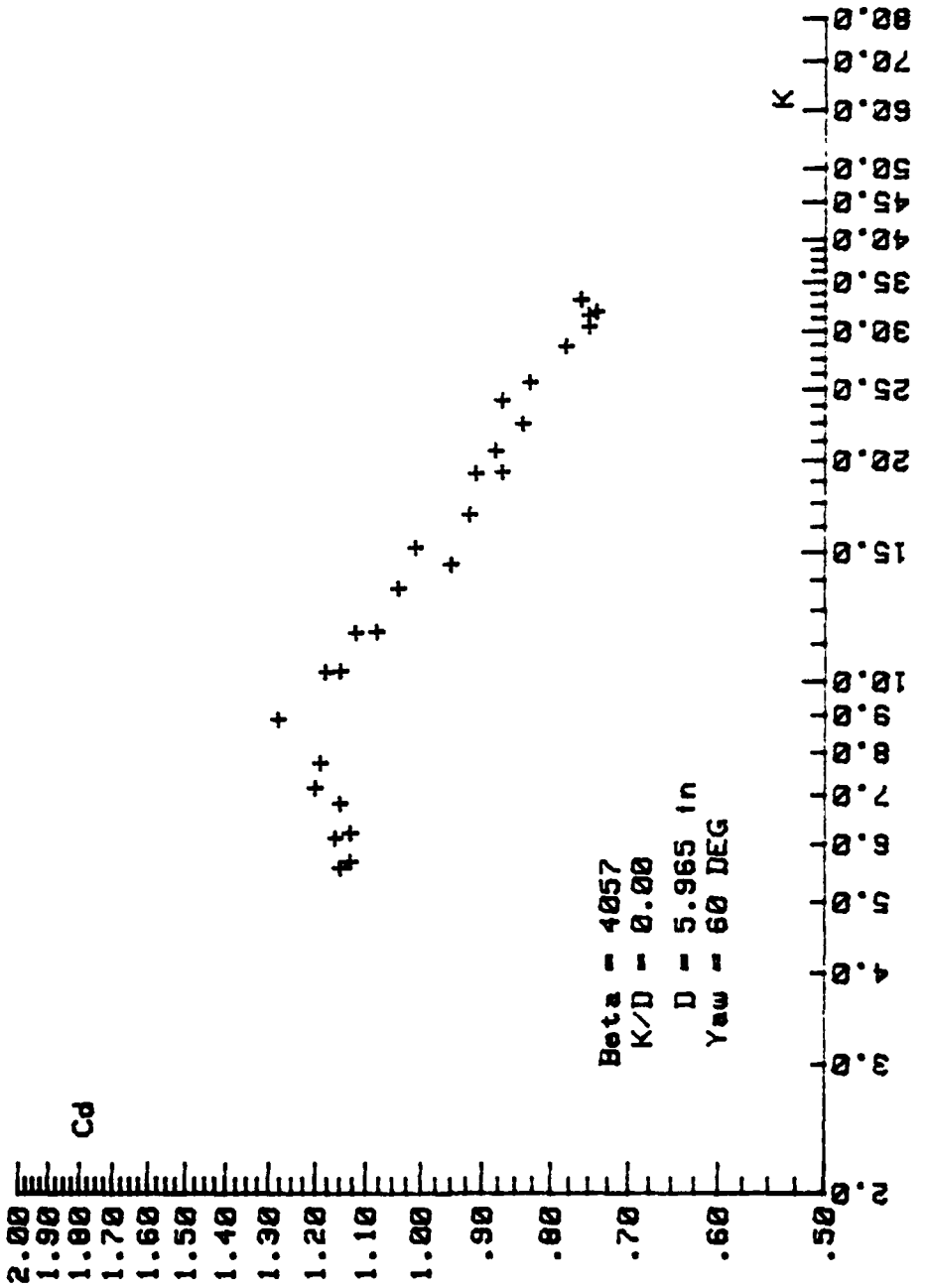

Figure 23. C_d Versus K for β = 4057, α = 60 Deg., k/D = 0.00.

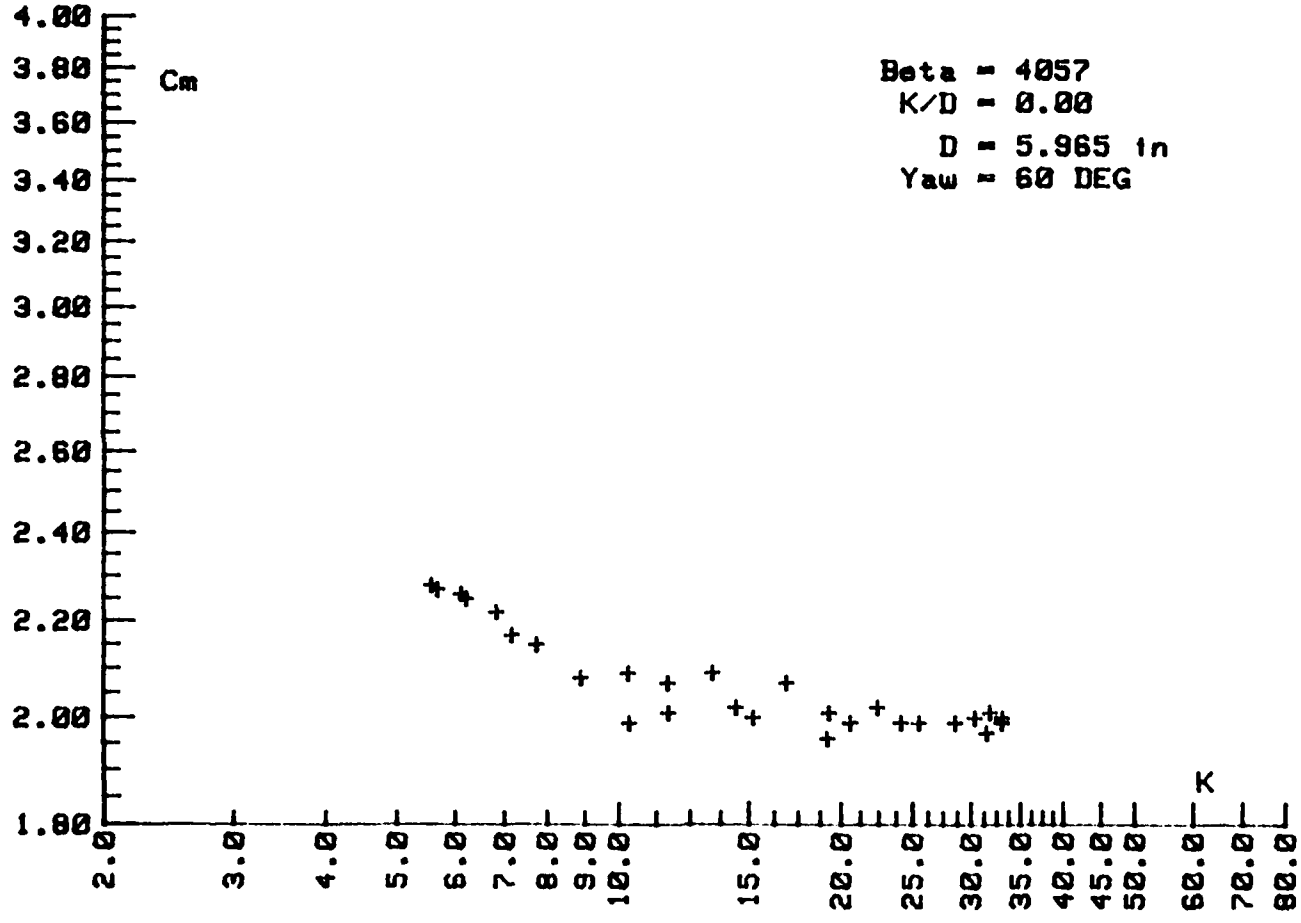

Figure 24. C_m Versus K for β = 4057, α = 60 Deg., k/D = 0.00.

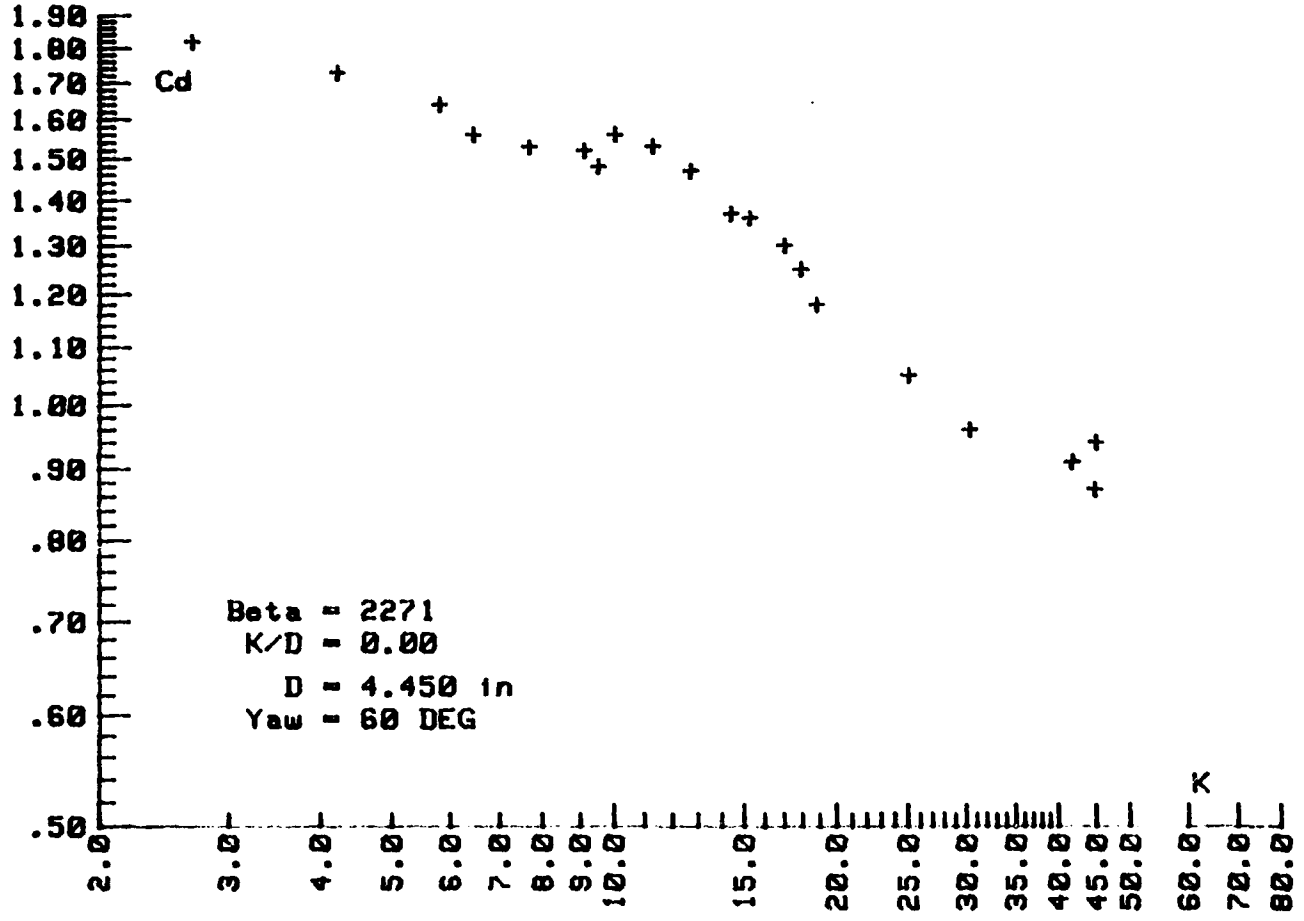

Figure 25. C_d Versus K for β = 2271, α = 60 Deg., k/D = 0.00.

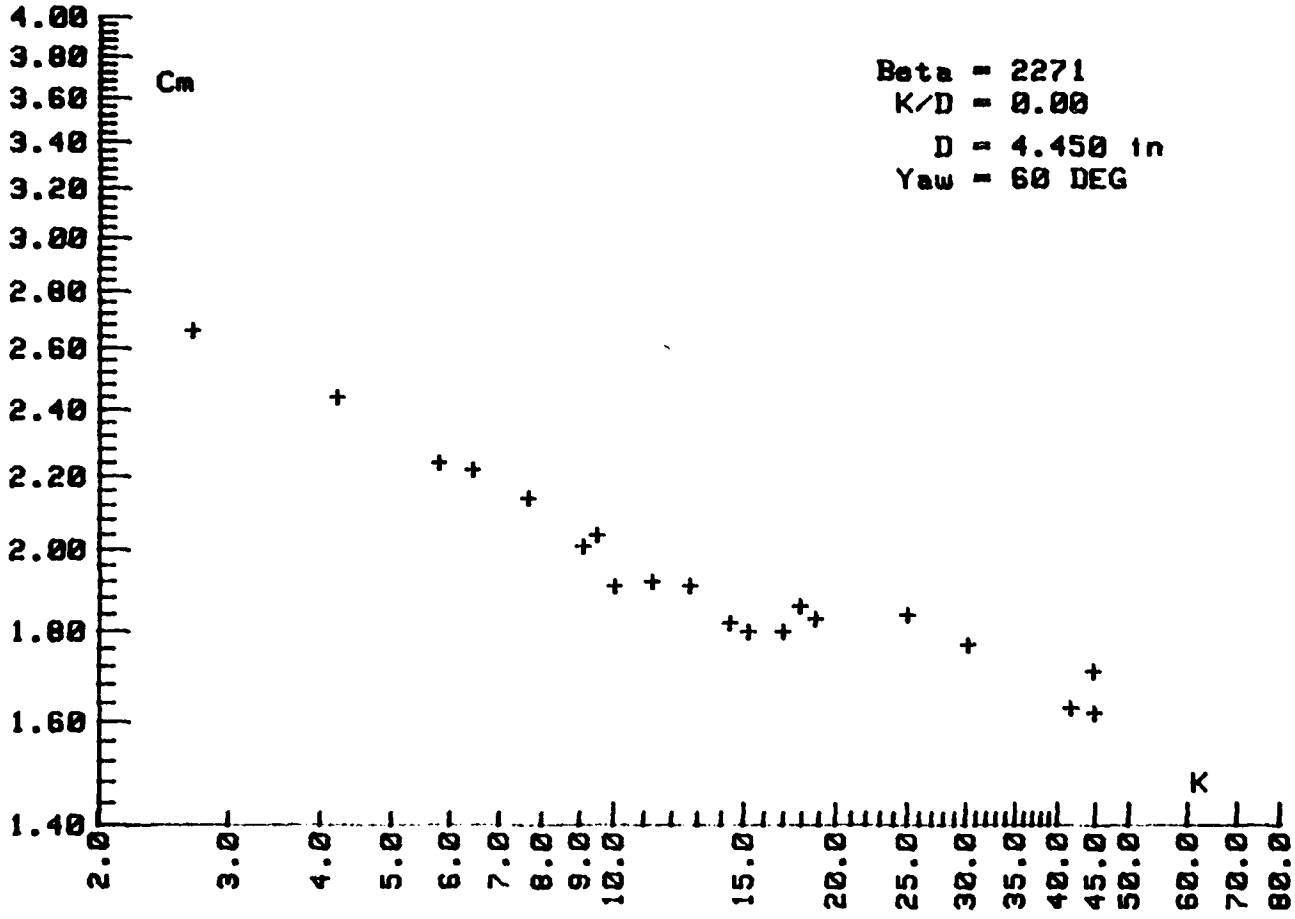

Figure 26. C_m Versus K for β = 2271, α = 60 Deg., k/D = 0.00.

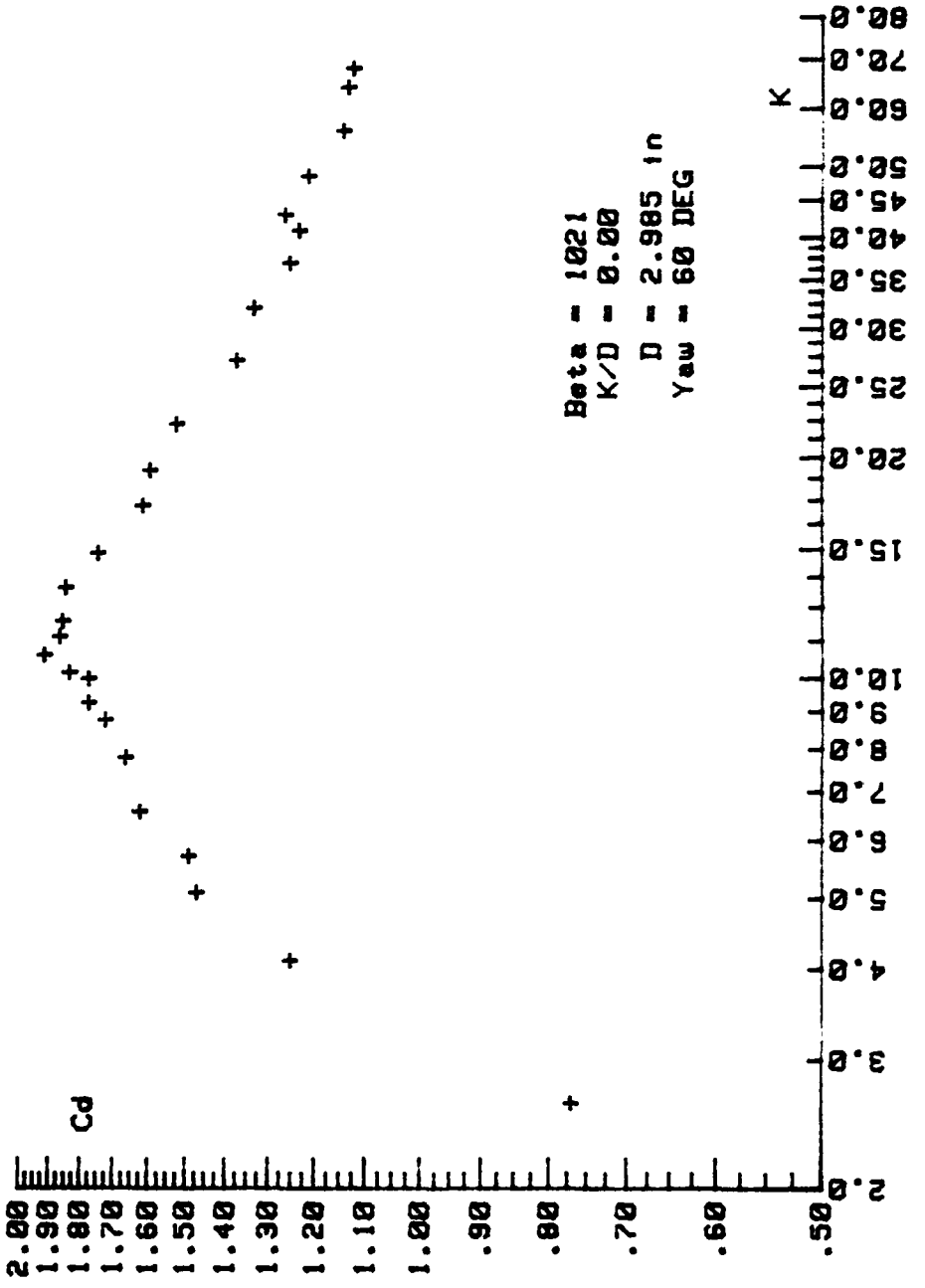

Figure 27. C_d Versus K for β = 1021, α = 60 Deg., k/D = 0.00.

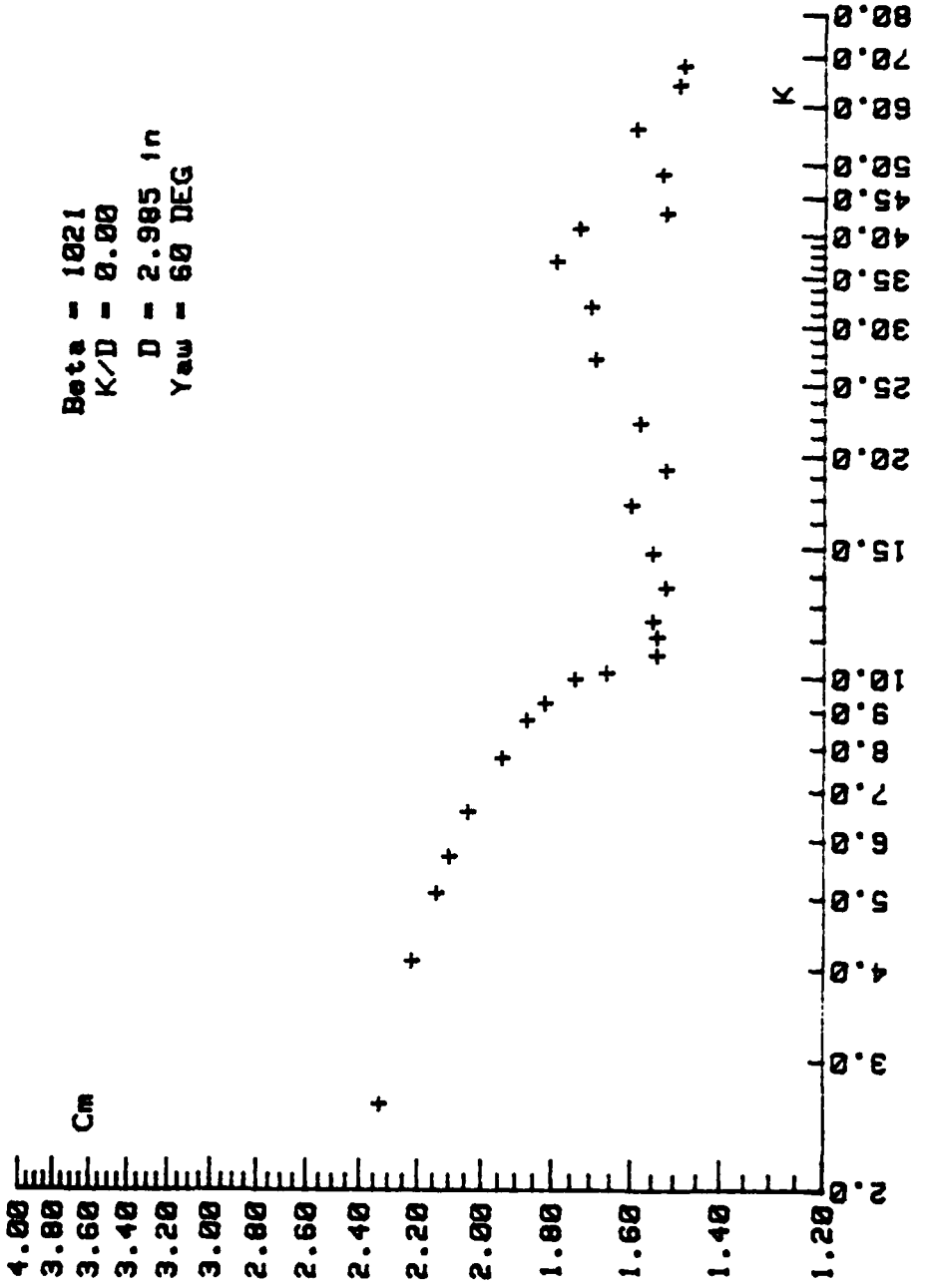

Figure 28. C_m Versus K for β = 1021, α = 60 Deg., k/D = 0.00.

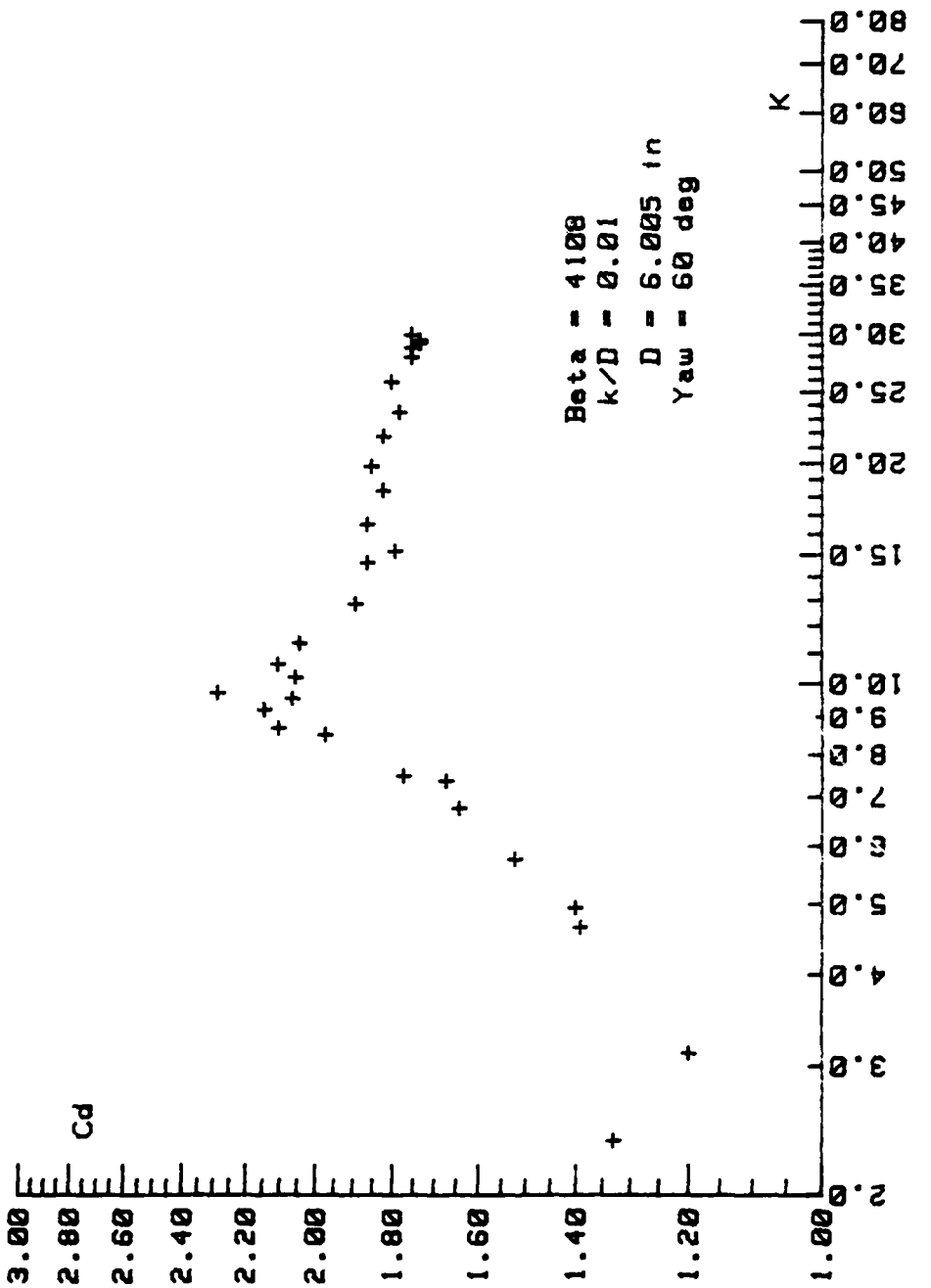

Figure 29. C_d Versus K for β= 4108, α= 60 Deg., k/D = 0.01

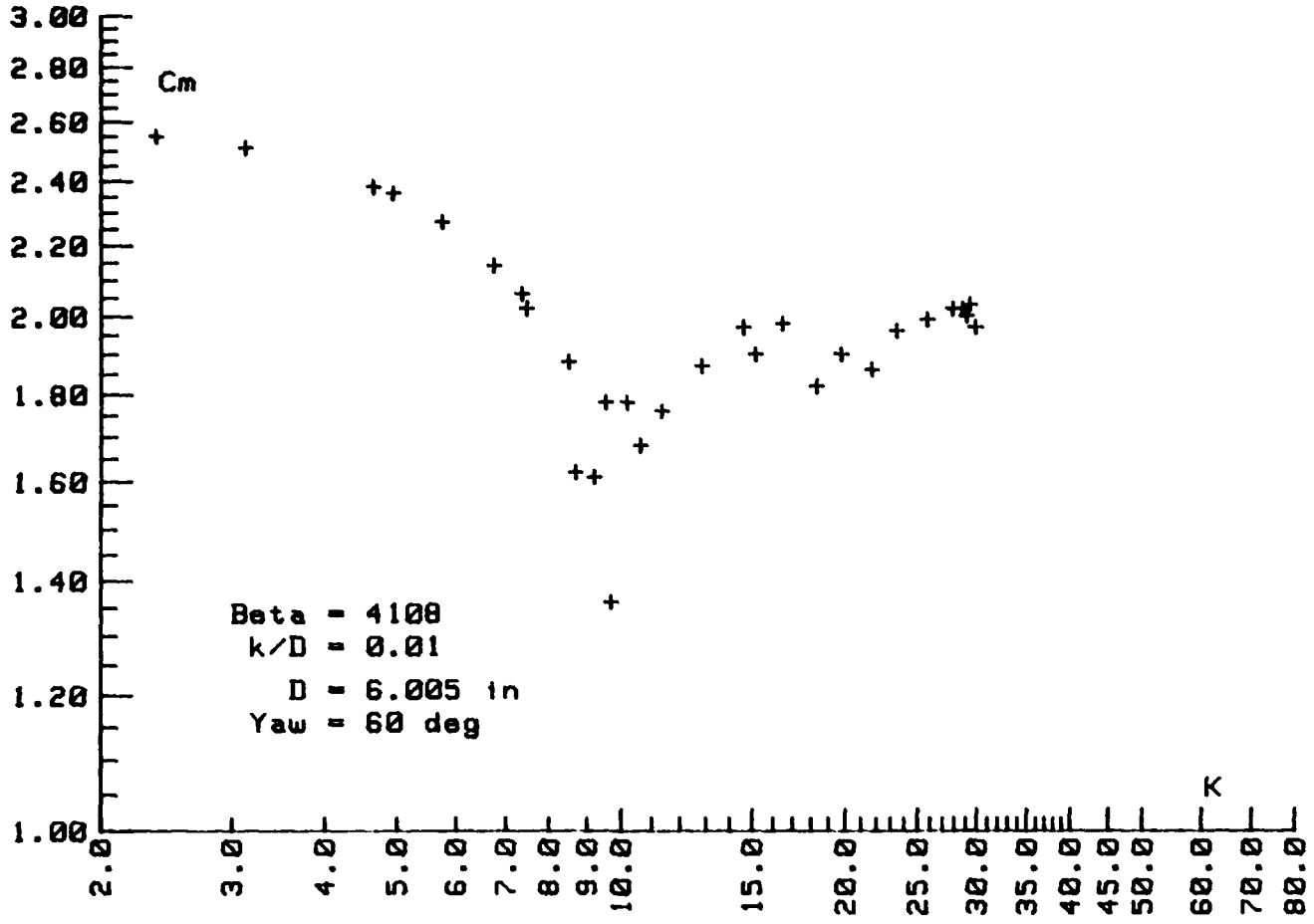

Figure 30. C_m Versus K for β= 4108, α= 60 Deg., k/D = 0.01

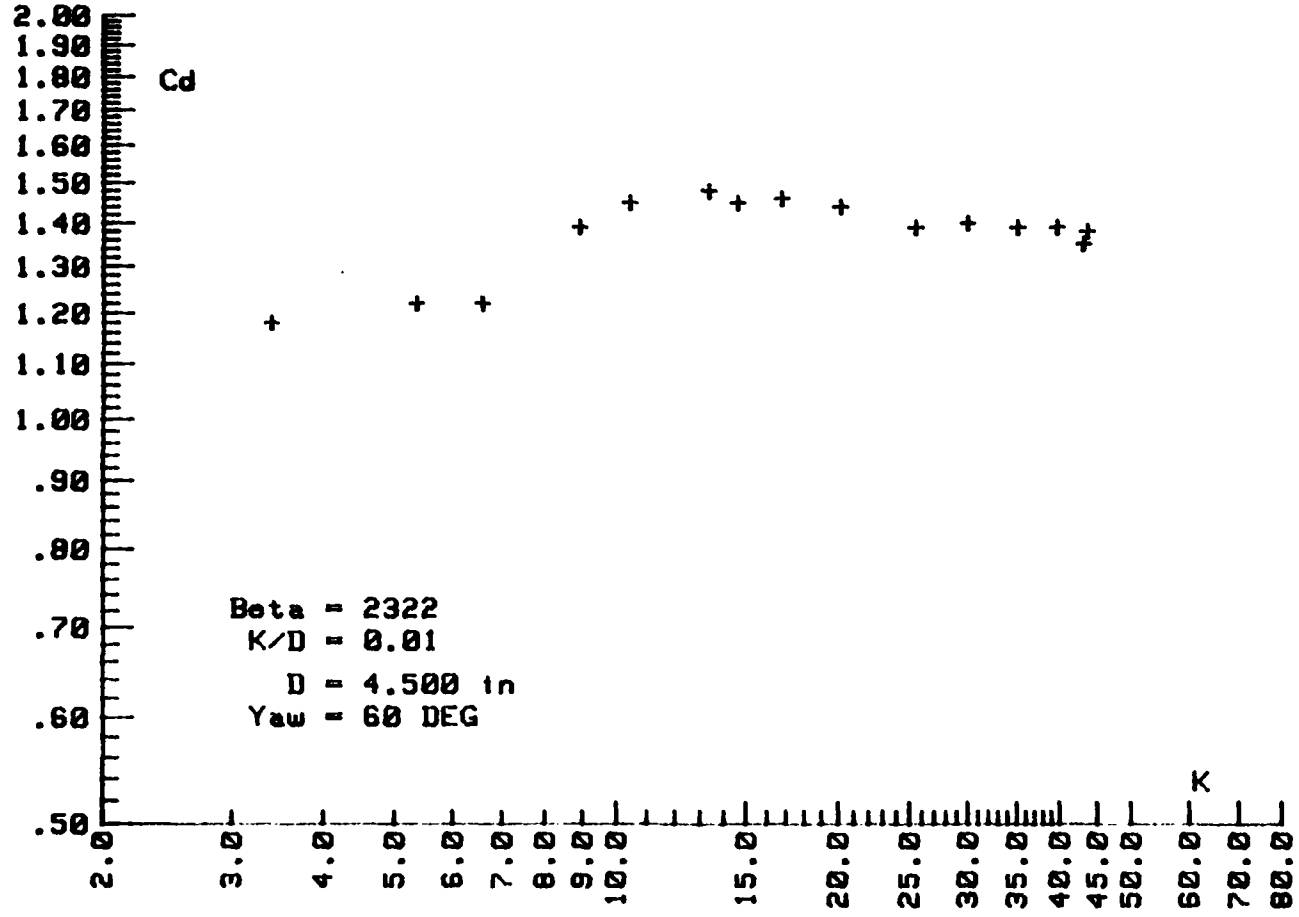

Figure 31. C_d Versus K for β = 2322, α = 60 Deg., k/D = 0.01.

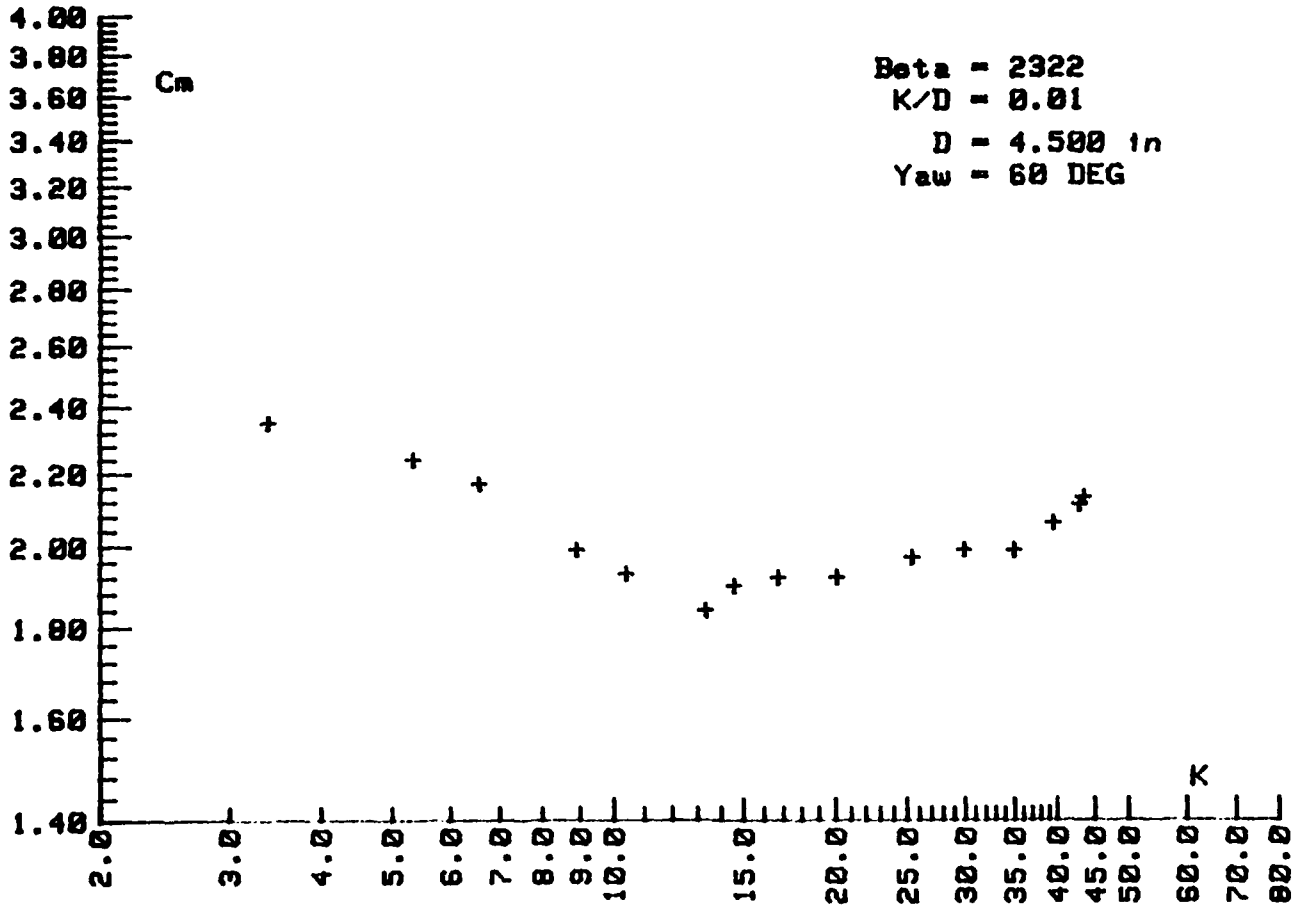

Figure 32. C_m Versus K for β = 2322, α = 60 Deg., k/D = 0.01.

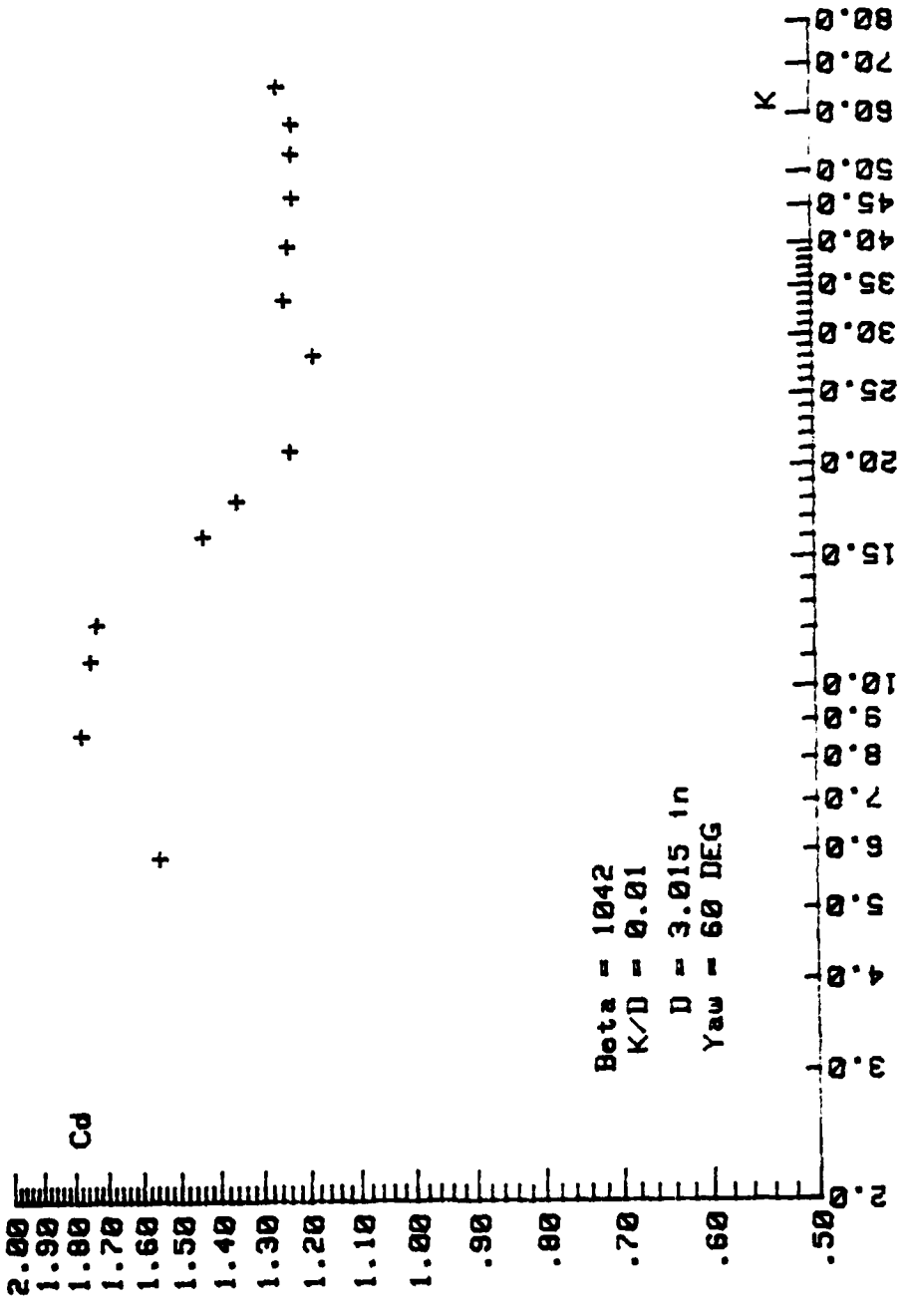

Figure 33. C_d Versus K for β = 1042, α = 60 Deg., k/D = 0.01.

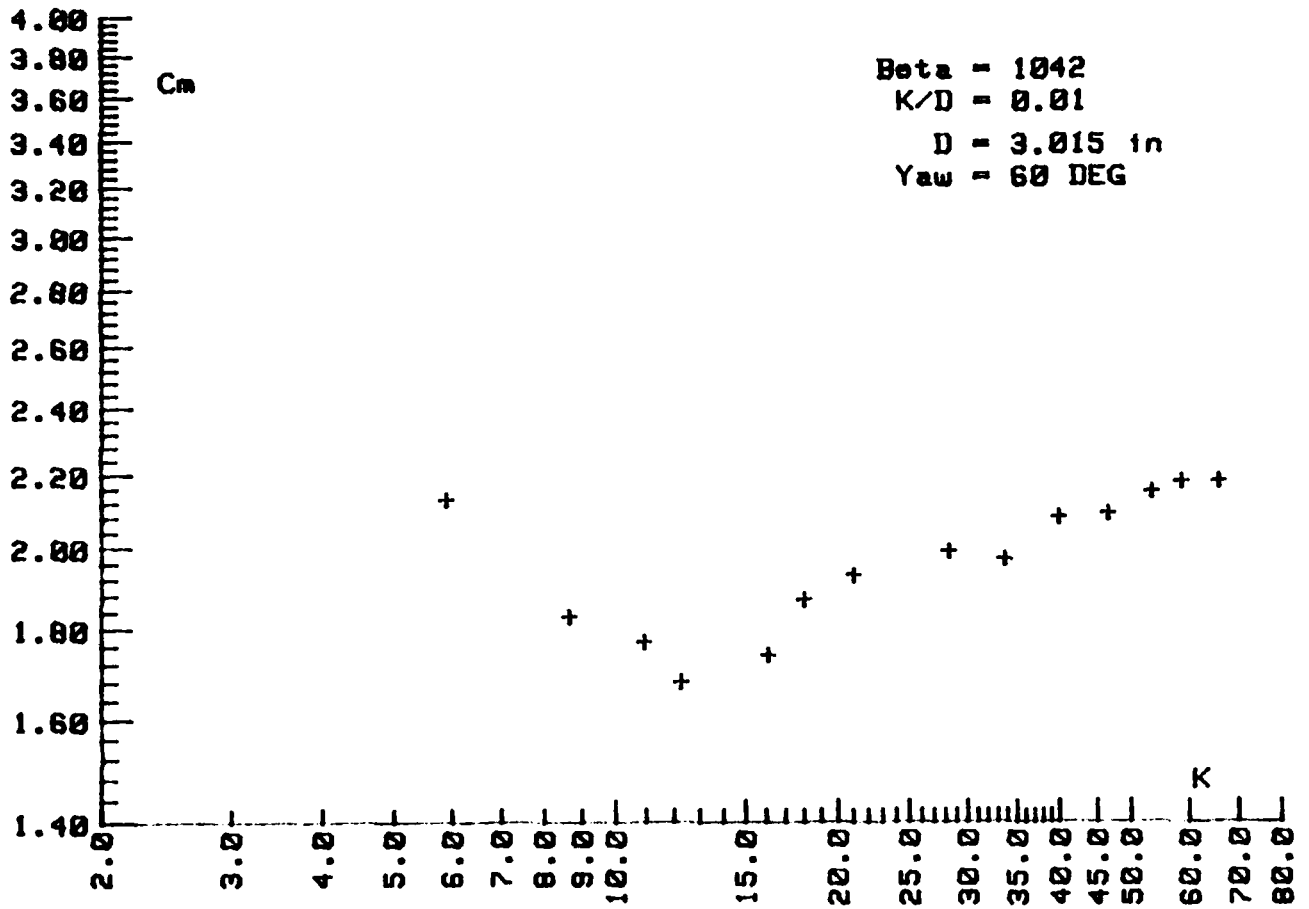

Figure 34. C_m Versus K for β = 1042, α = 60 Deg., k/D = 0.01.

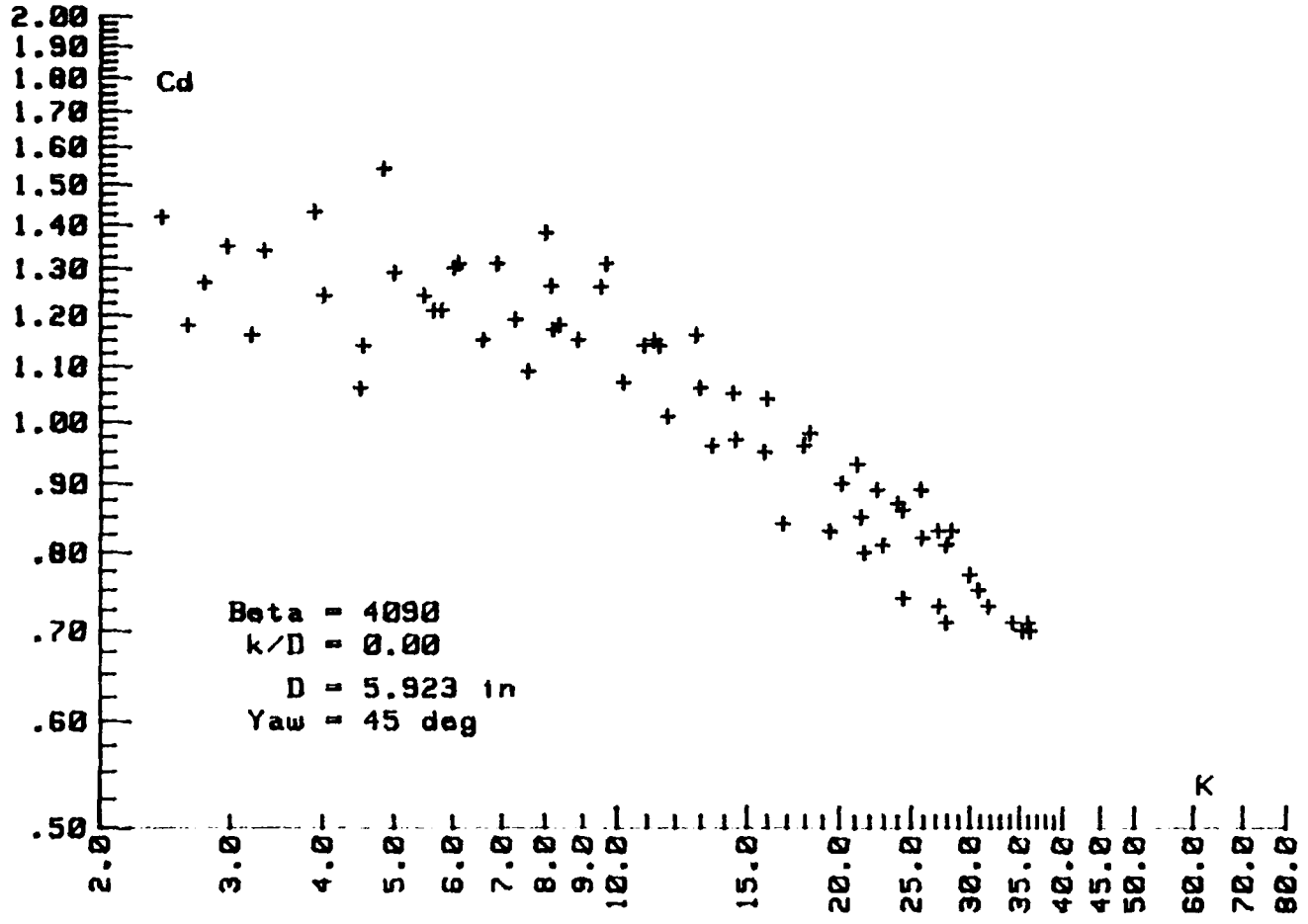

Figure 35. C_d Versus K for β= 4090, α= 45 Deg., k/D = 0.00

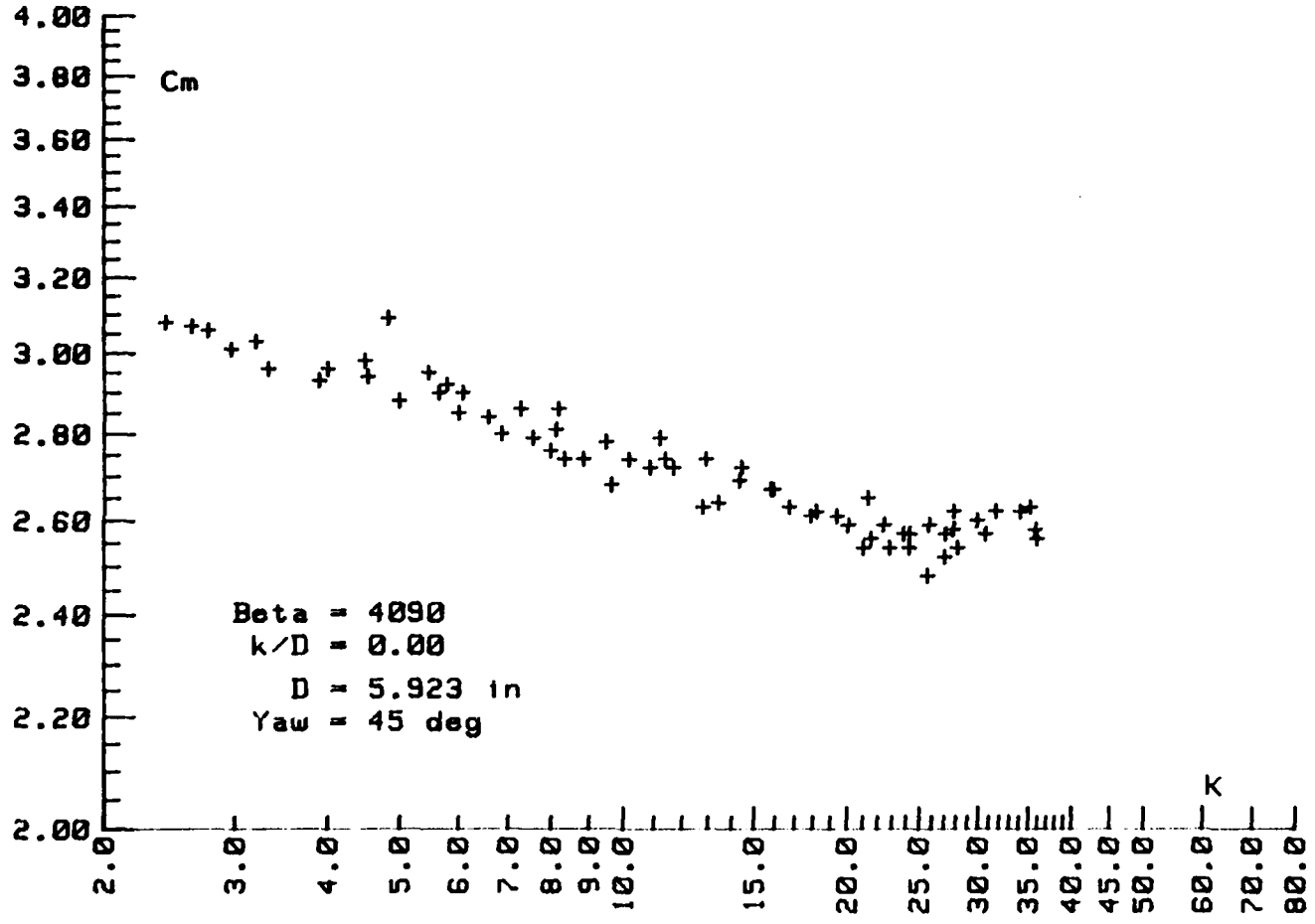

Figure 36. C_m Versus K for β = 4090, α = 45 Deg., k/D = 0.00

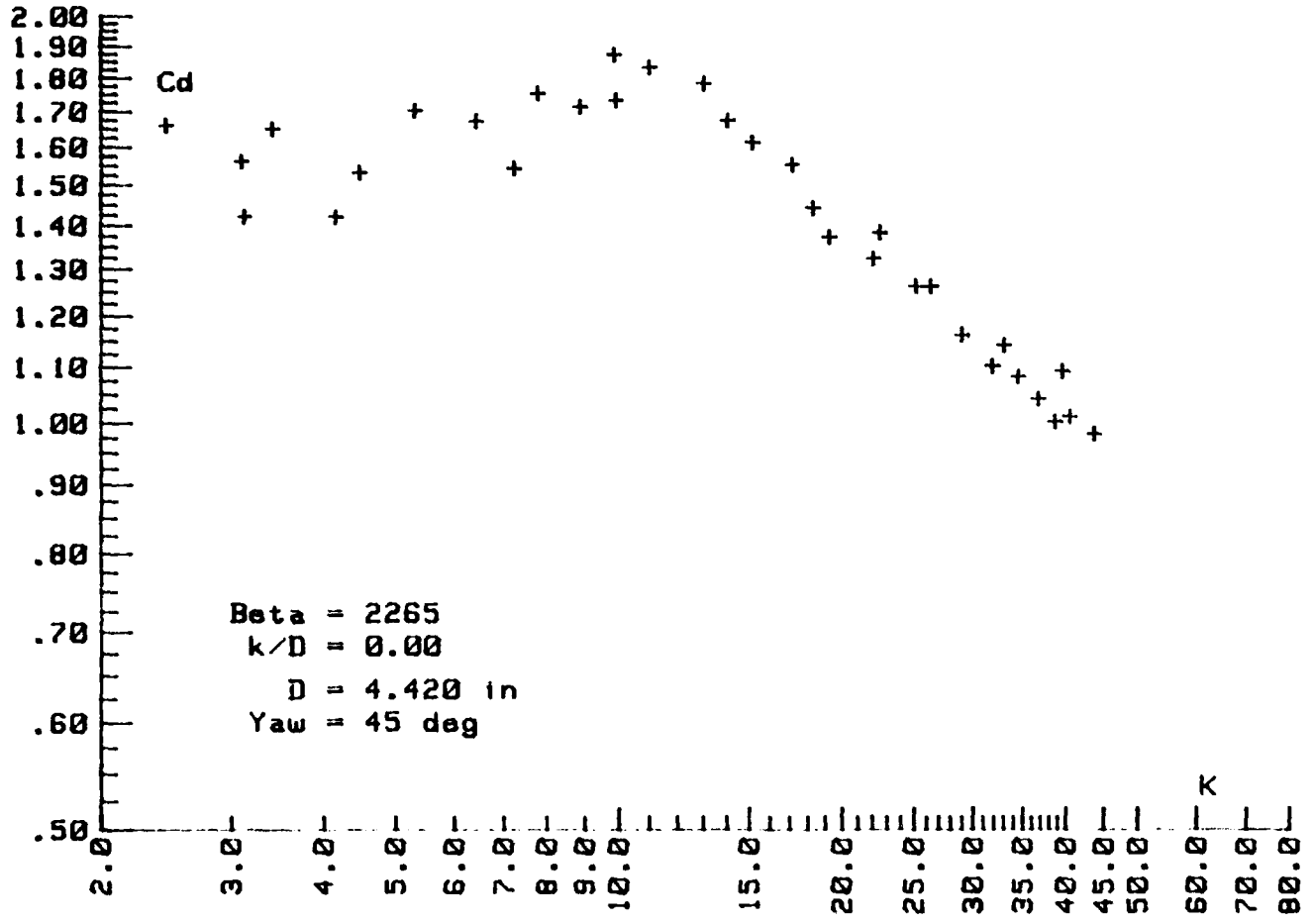

Figure 37. C_d Versus K for β= 2265, α= 45 Deg., k/D = 0.00

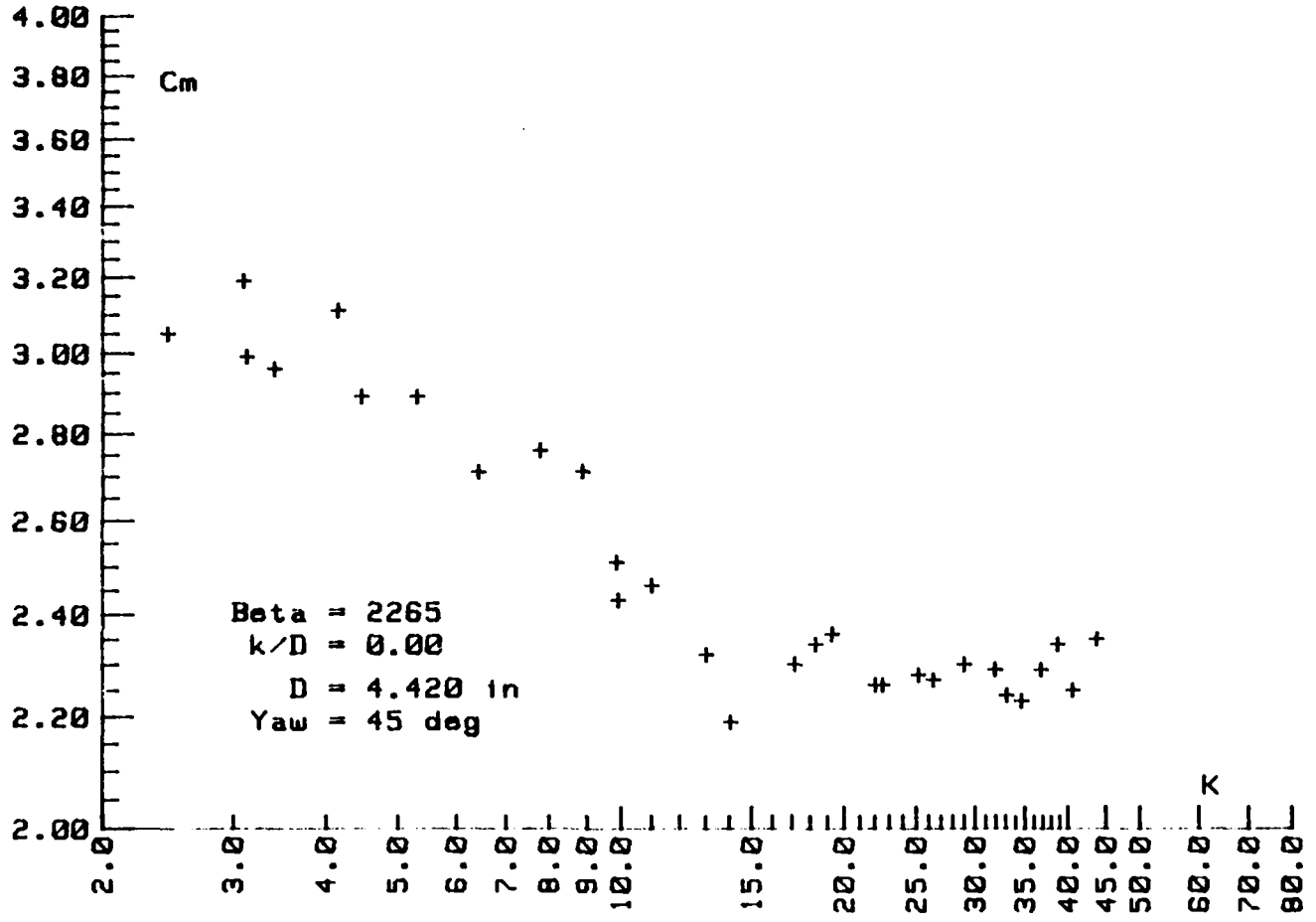

Figure 38. C_m Versus K for β = 2265, α = 45 Deg., k/D = 0.00

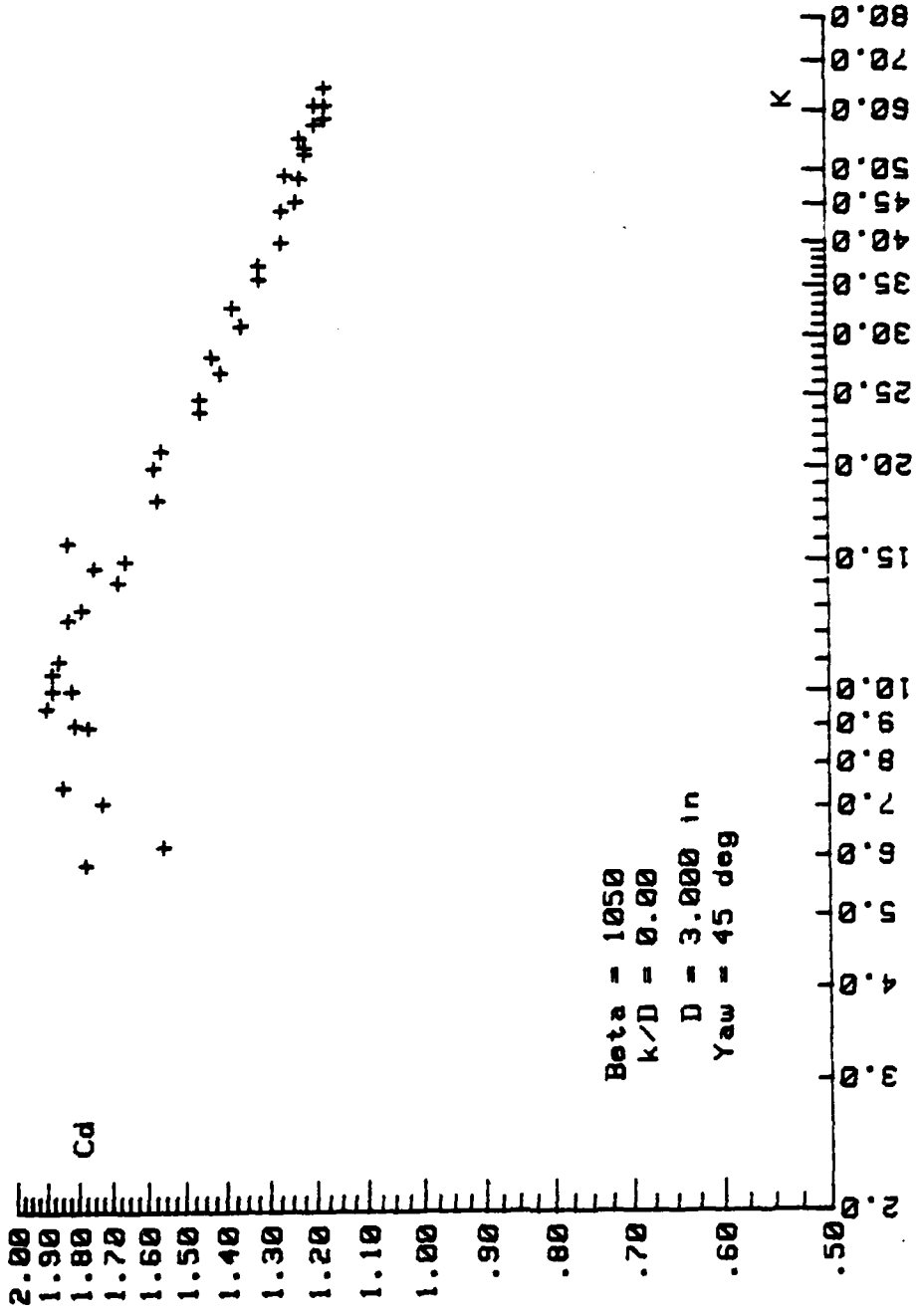

Figure 39. C_d Versus K for β = 1050, α = 45 Deg., k/D = 0.00

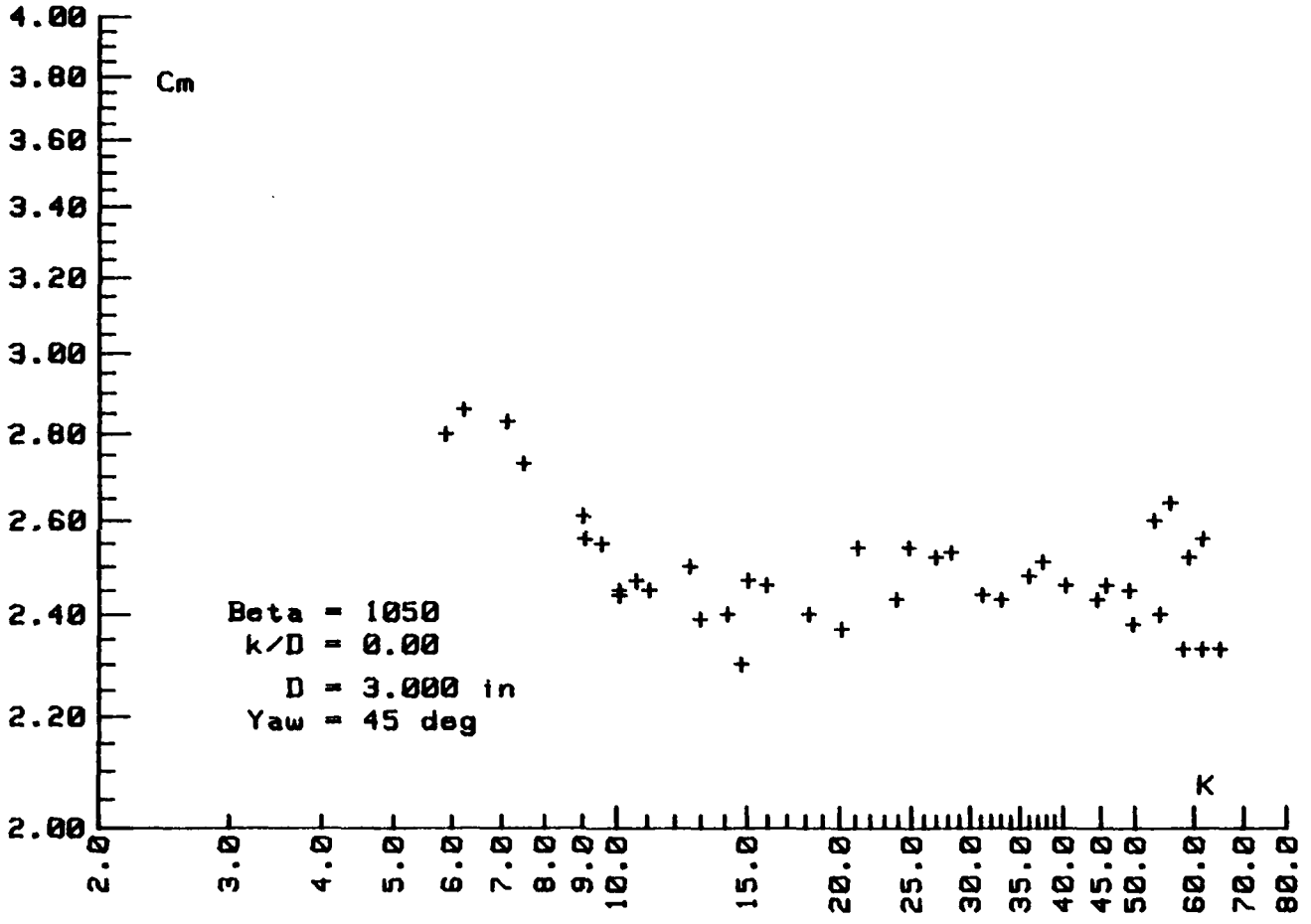

Figure 40. C_m Versus K for β= 1050, α= 45 Deg., k/D = 0.00

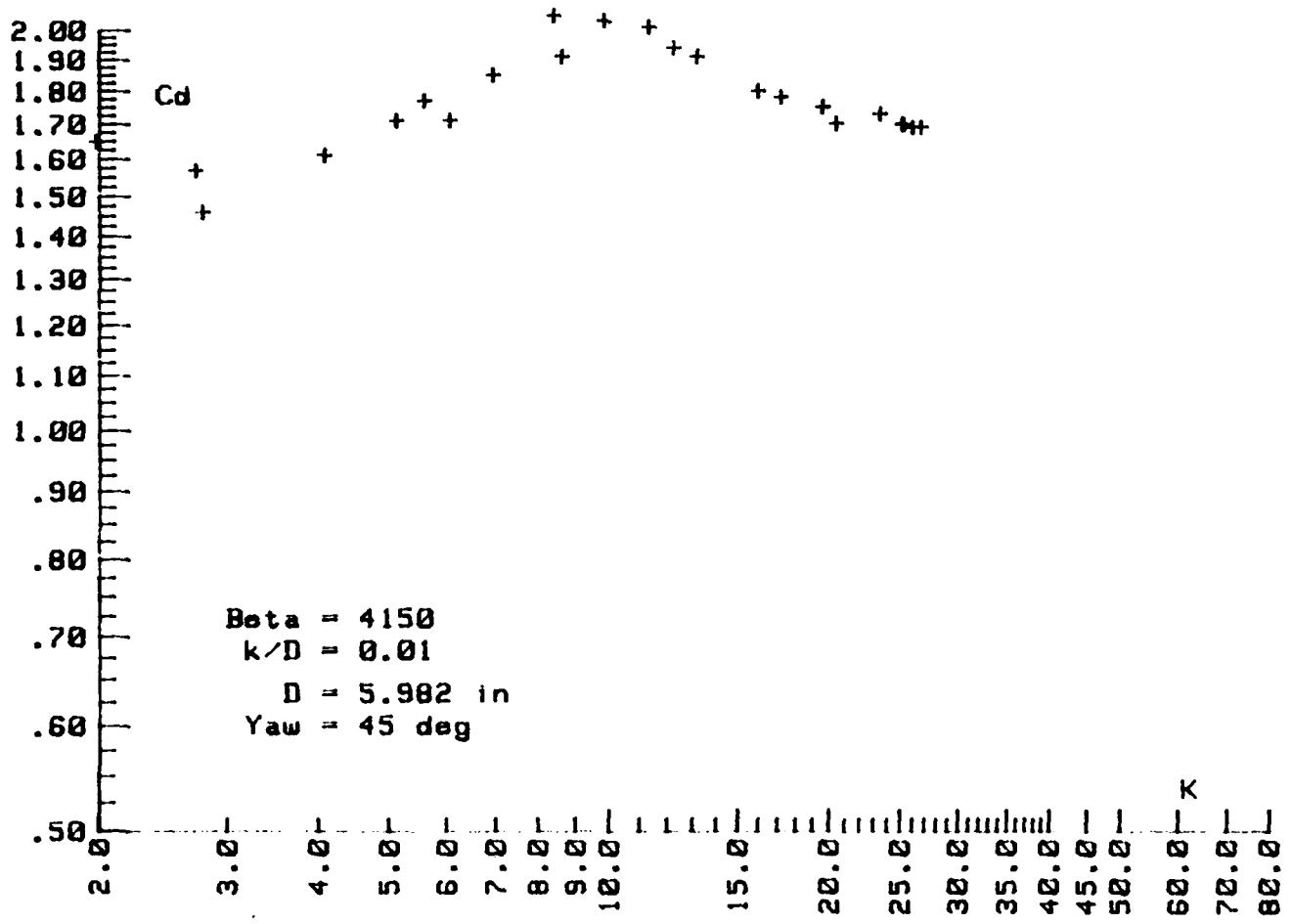

Figure 41. C_d Versus K for β= 4150, α= 45 Deg., k/D = 0.01

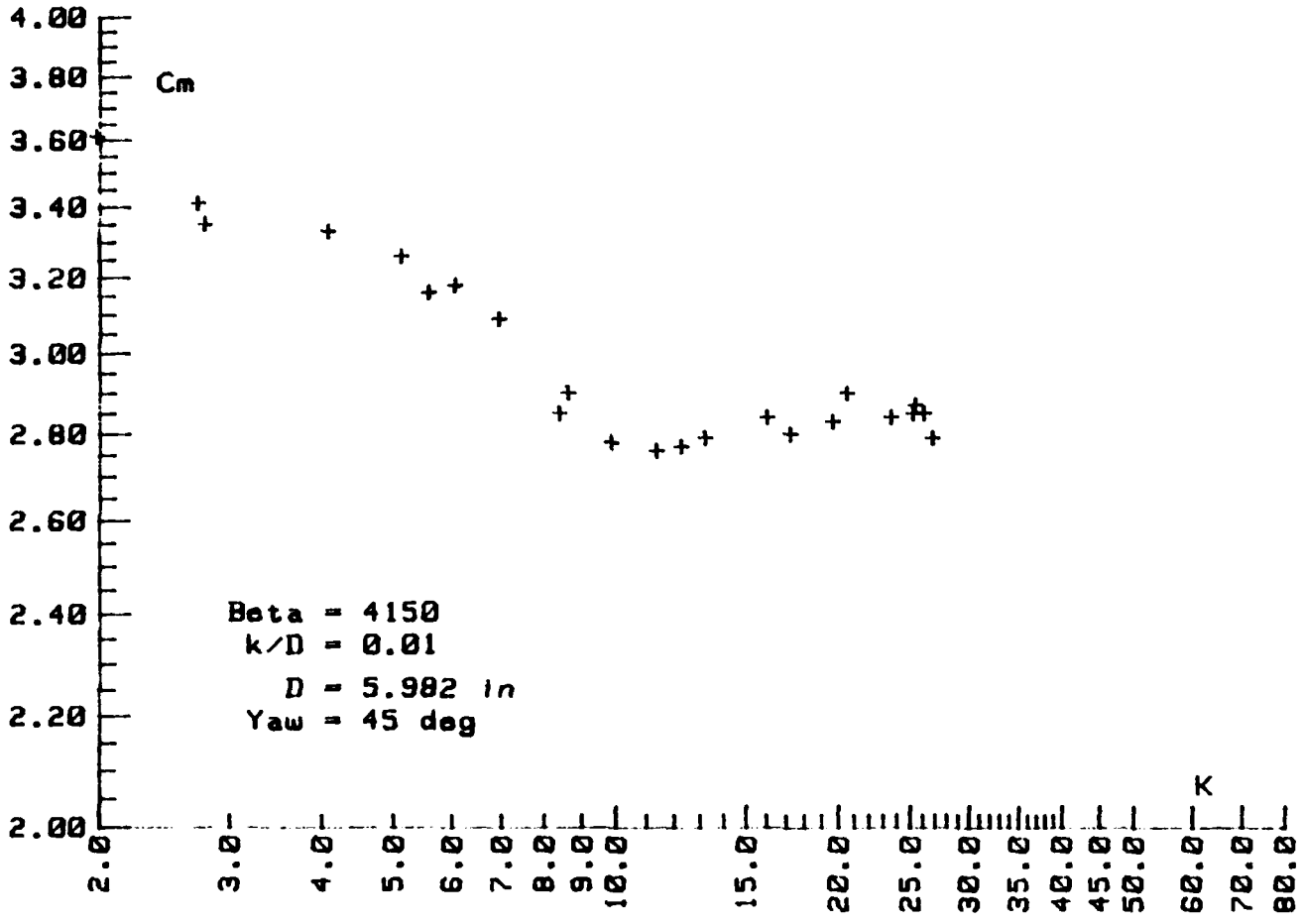

Figure 42. C_m Versus K for β= 4150, α= 45 Deg., k/D = 0.01

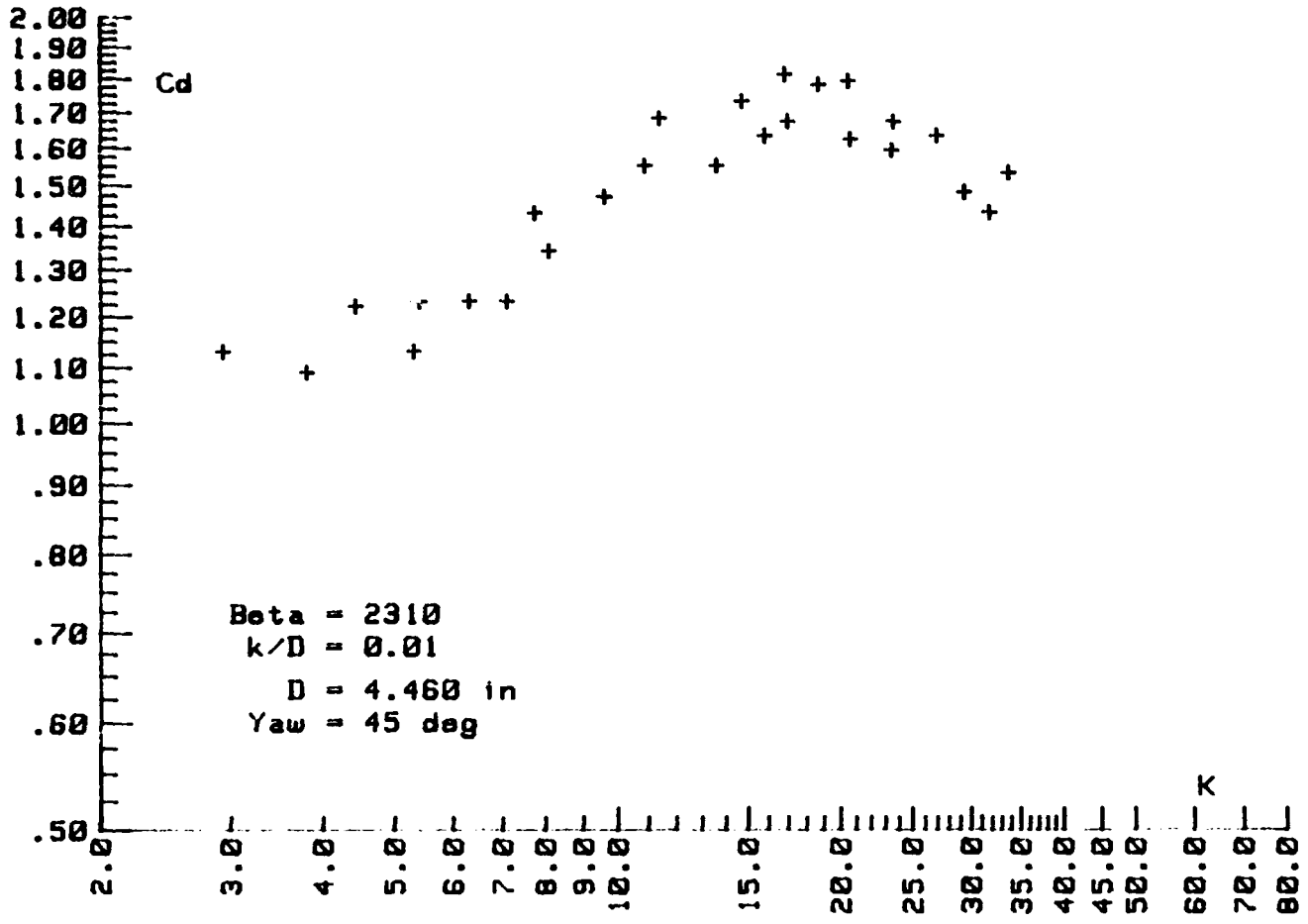

Figure 43. C_d Versus K for β= 2310, α= 45 Deg., k/D = 0.01

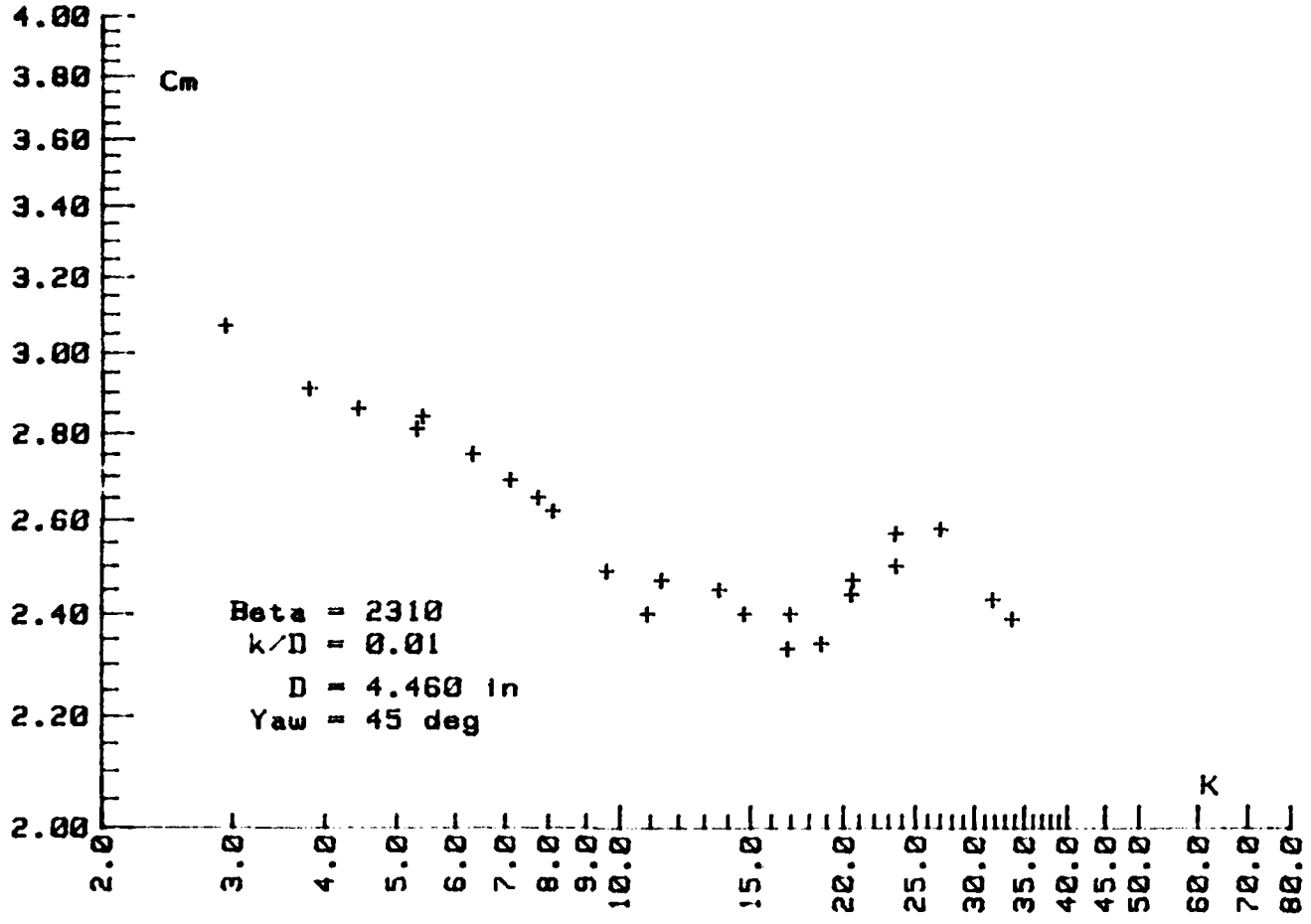

Figure 44. C_m Versus K for β= 2310, α= 45 Deg., k/D = 0.01

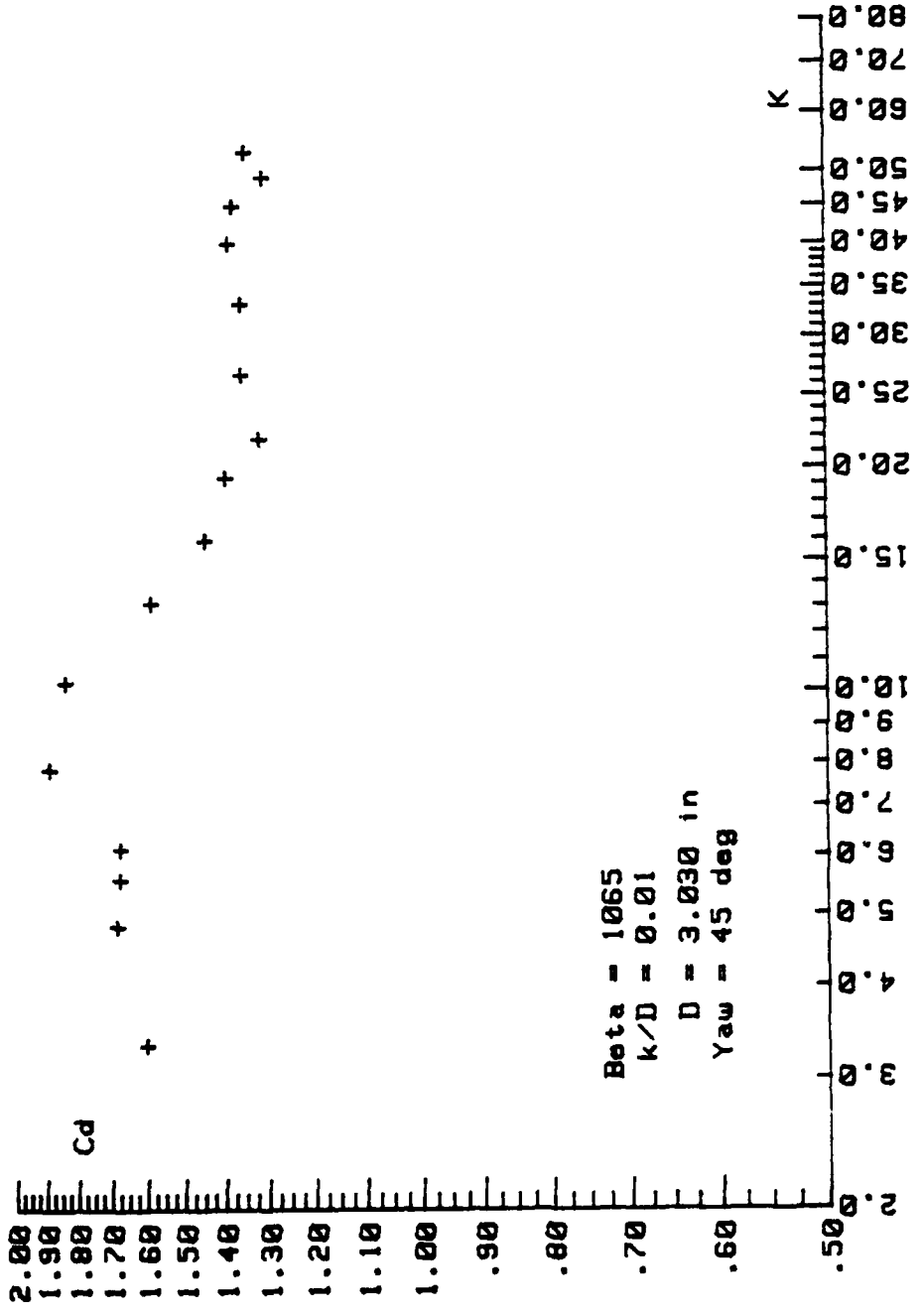

Figure 45. C_d Versus K for β= 1065, α= 45 Deg., k/D = 0.01

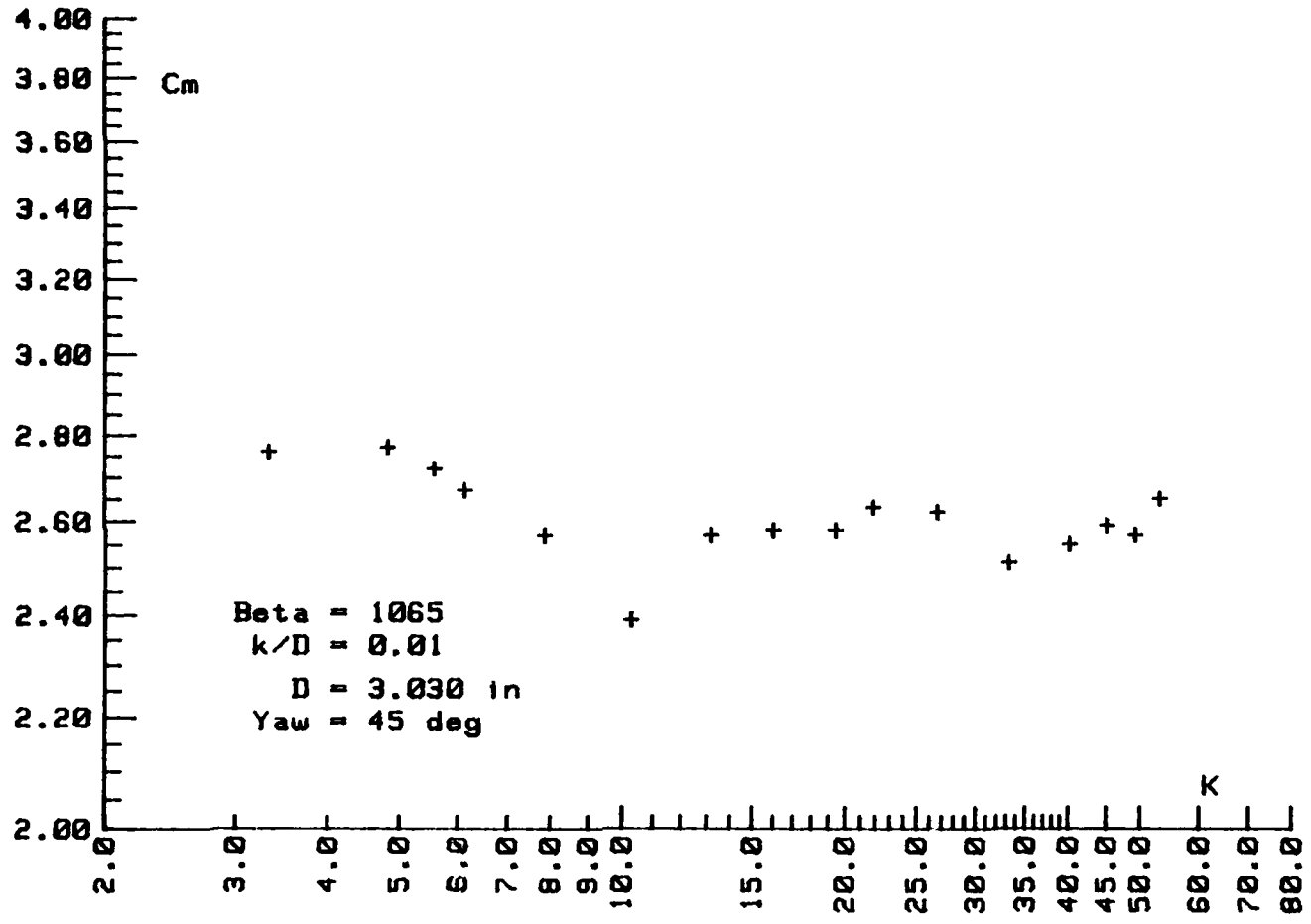

Figure 46. C_m Versus K for β= 1065, α= 45 Deg., k/D = 0.01

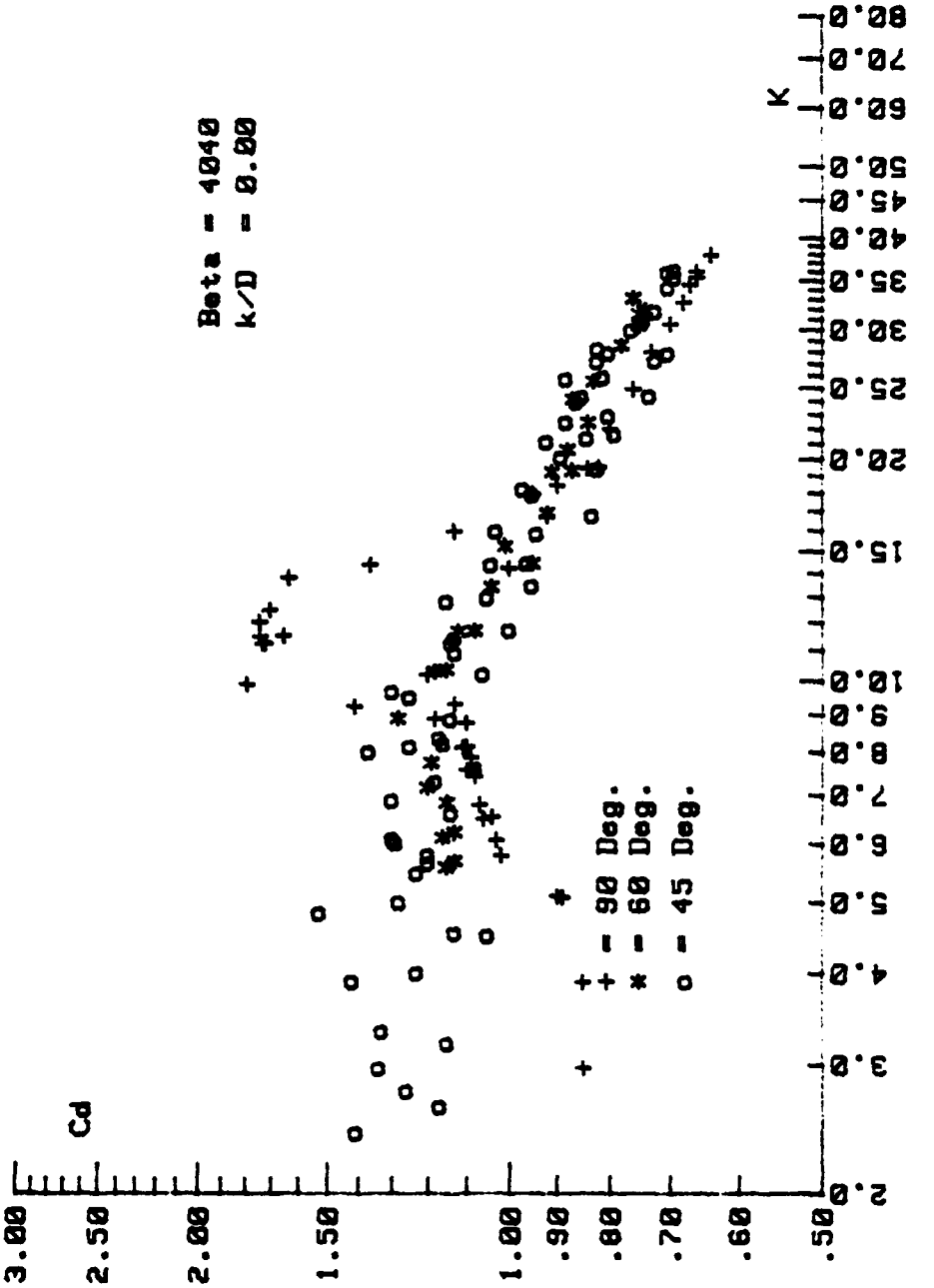

Figure 47. Comparison of C_d Versus K for β = 4040, k/D = 0.00, α = 90, 60, and 45 Deg.

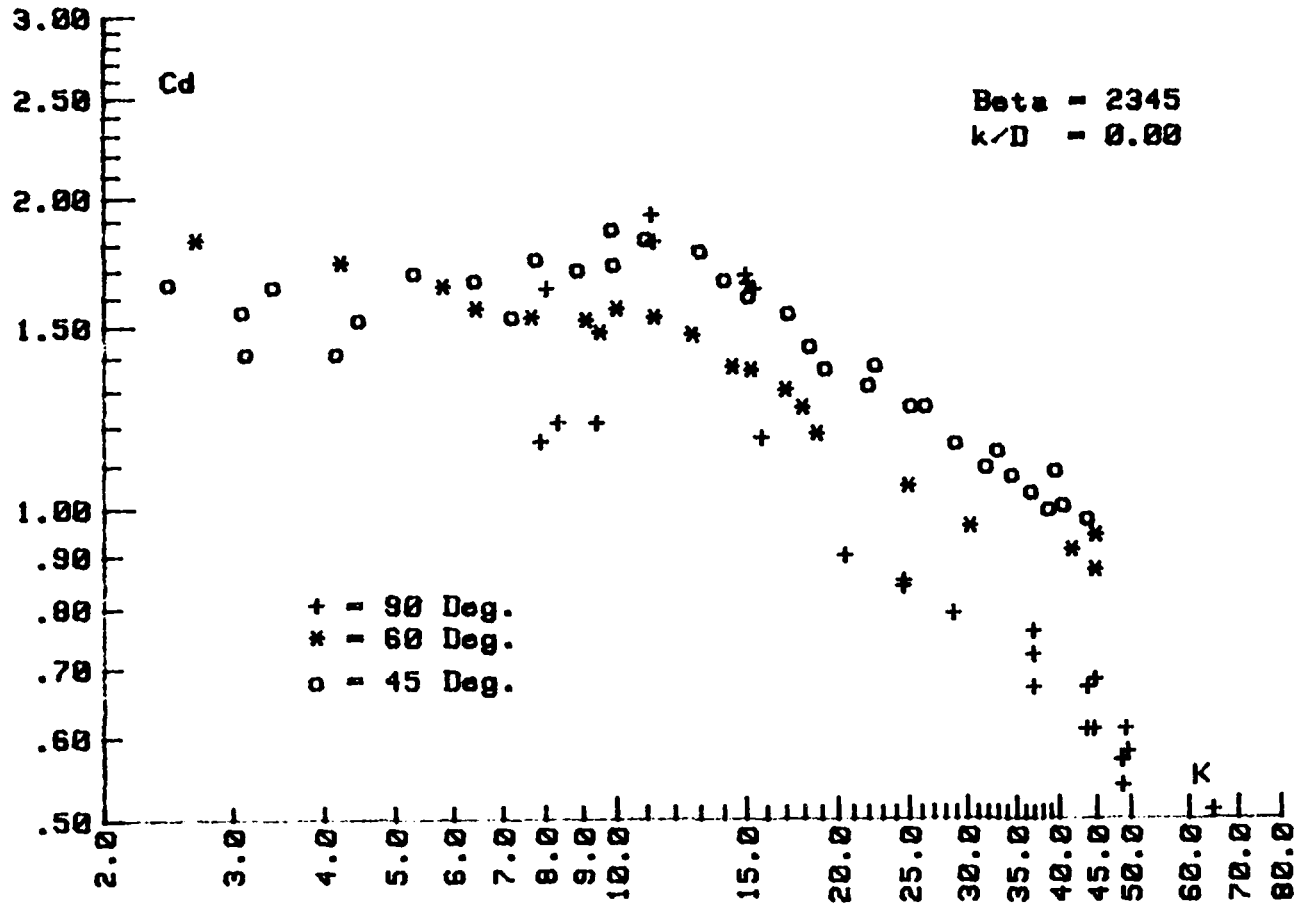

Figure 48. Comparison of C_d Versus K for β = 2345, k/D = 0.00, α = 90, 60, and 45 Deg.

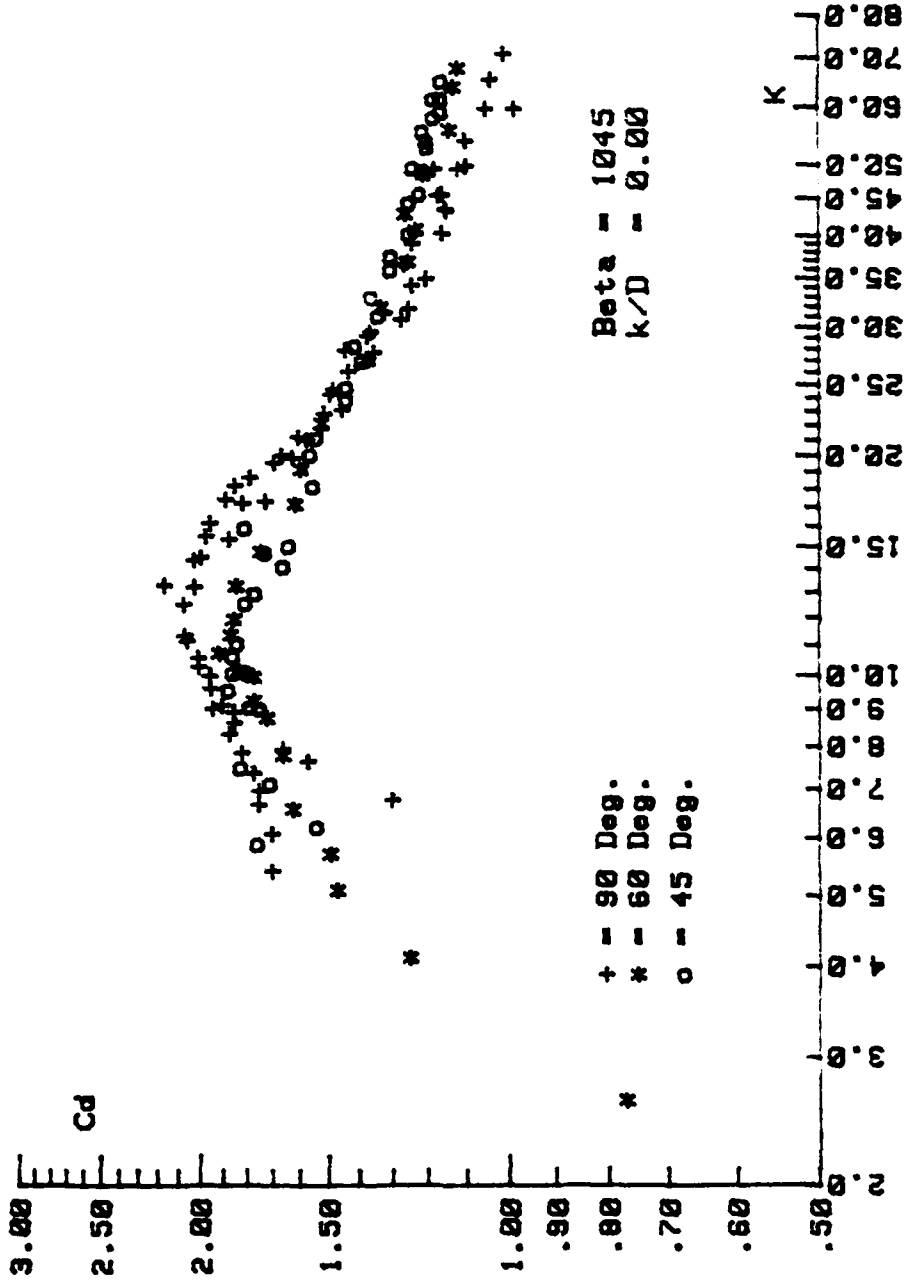

Figure 49. Comparison of C_d Versus K for β = 1045, k/D = 0.00, α = 90, 60, and 45 Deg.

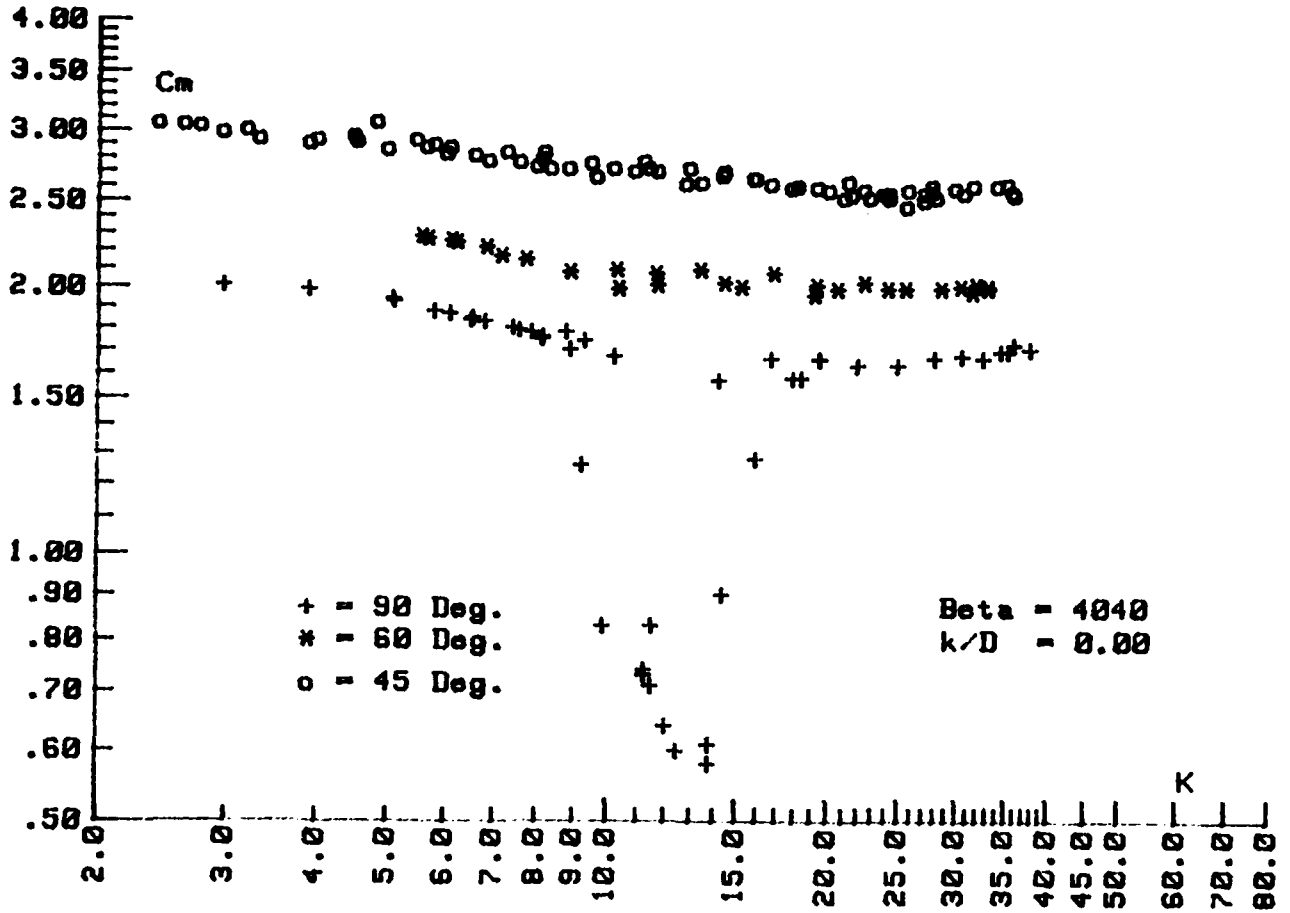

Figure 50. Comparison of C_m Versus K for β = 4040, k/D = 0.00, α = 90, 60, and 45 Deg.

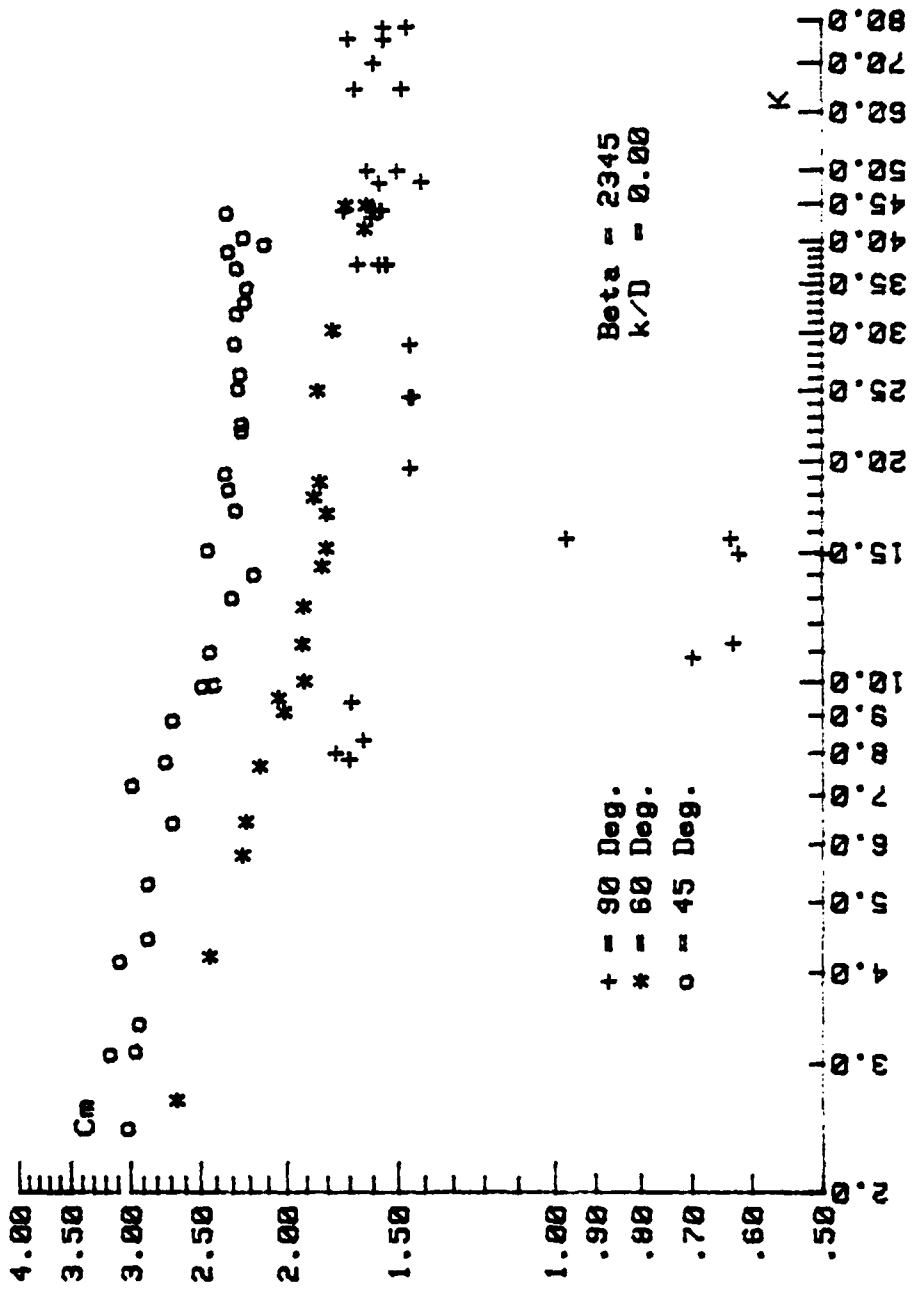

Figure 51. Comparison of C_m Versus K for β = 2345, k/D = 0.00, α = 90, 60, and 45 Deg.

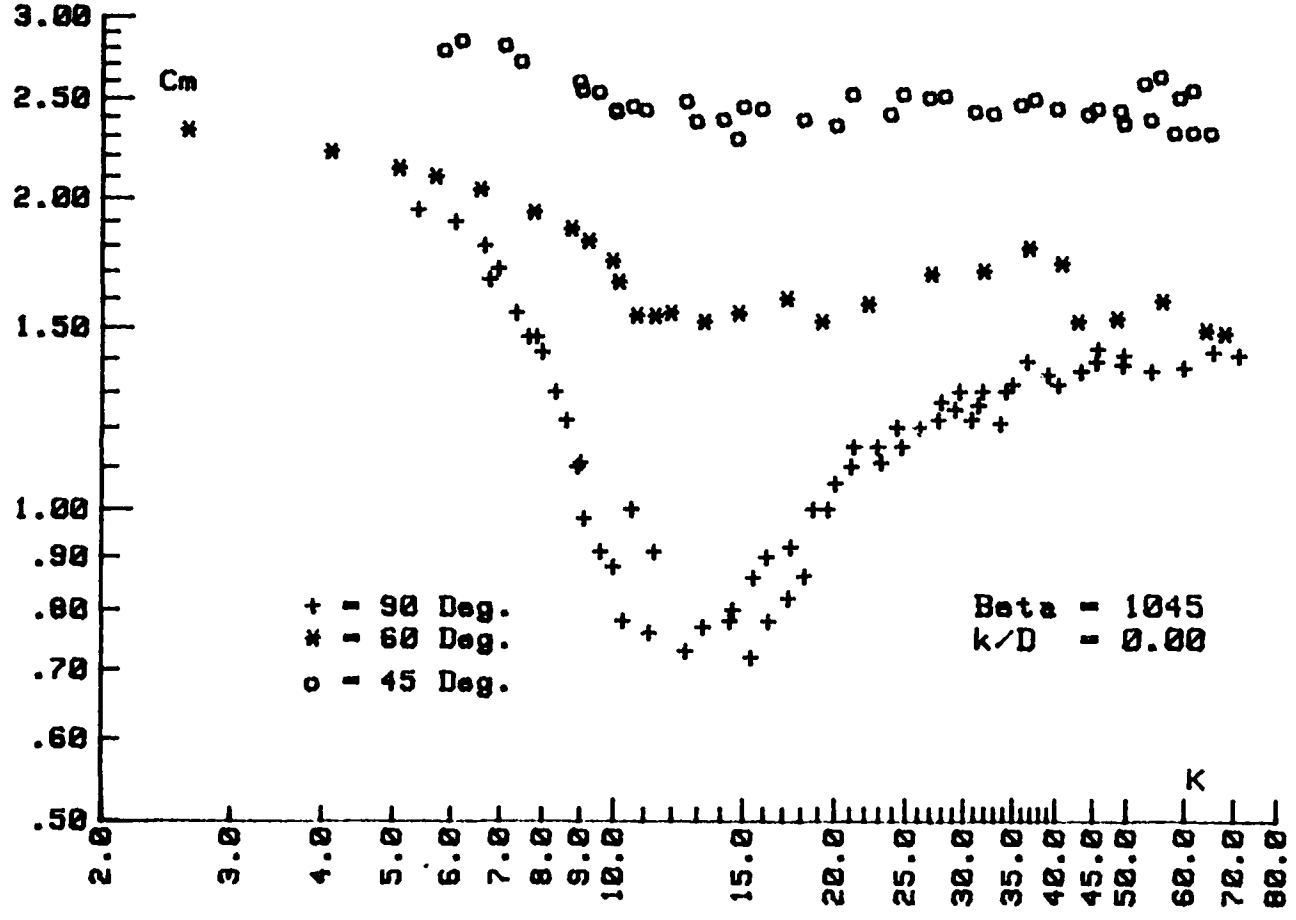

Figure 52. Comparison of C_m Versus K for β = 1045, k/D = 0.00, α = 90, 60, and 45 Deg.

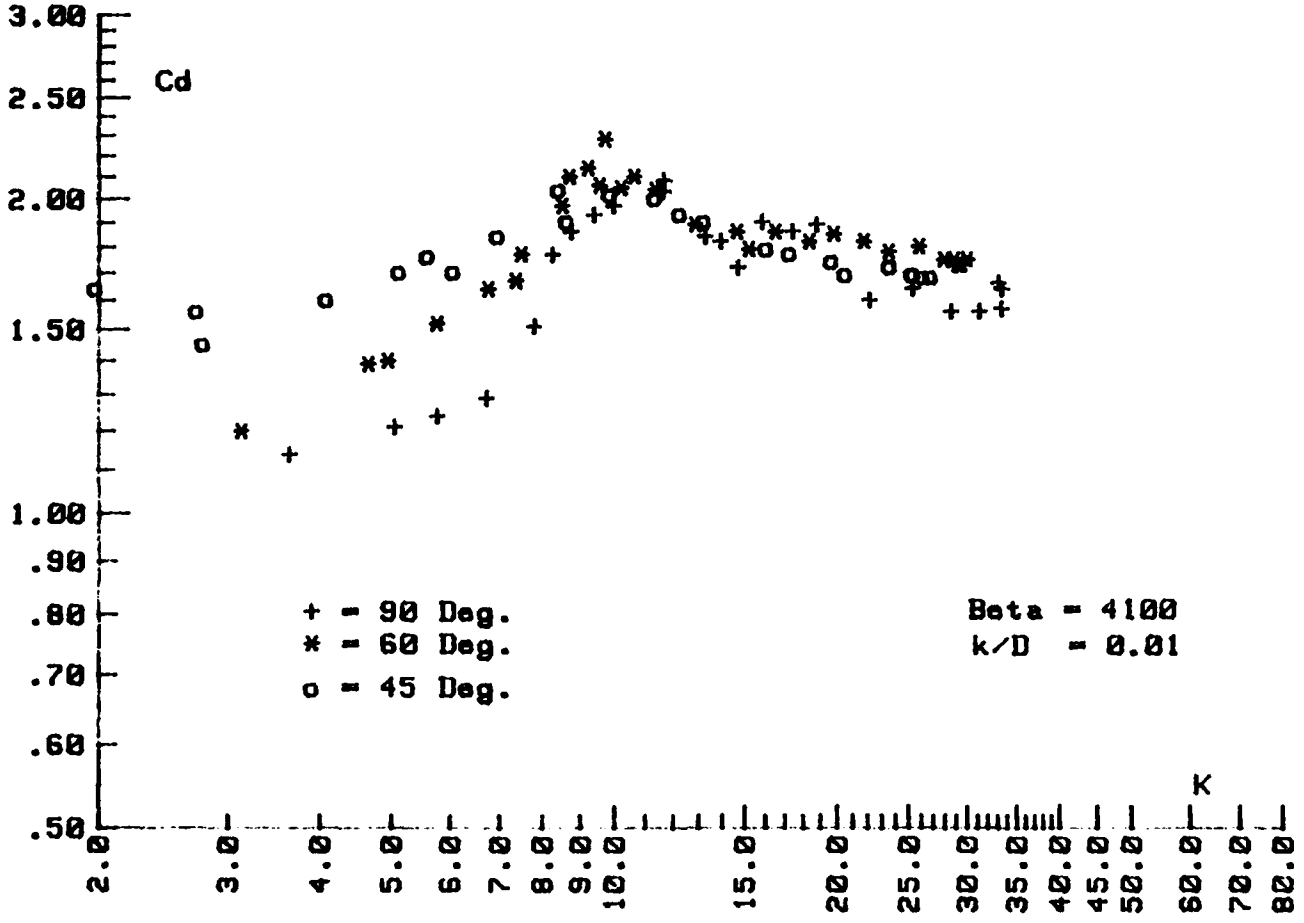

Figure 53. Comparison of C_d Versus K for β = 4100, k/D = 0.01, α = 90, 60, and 45 Deg.

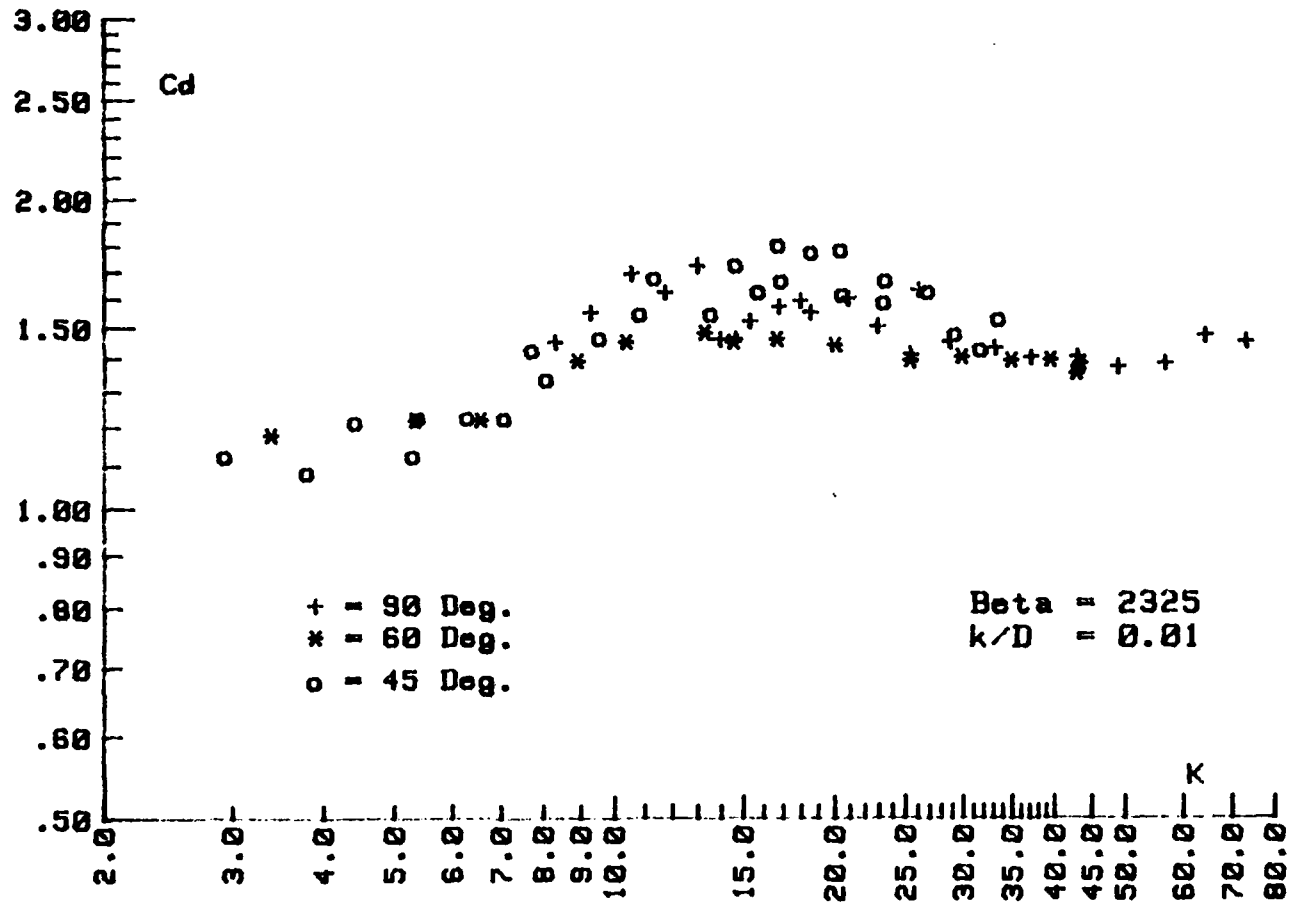

Figure 54. Comparison of C_d Versus K for β = 2325, k/D = 0.01, α = 90, 60, and 45 Deg.

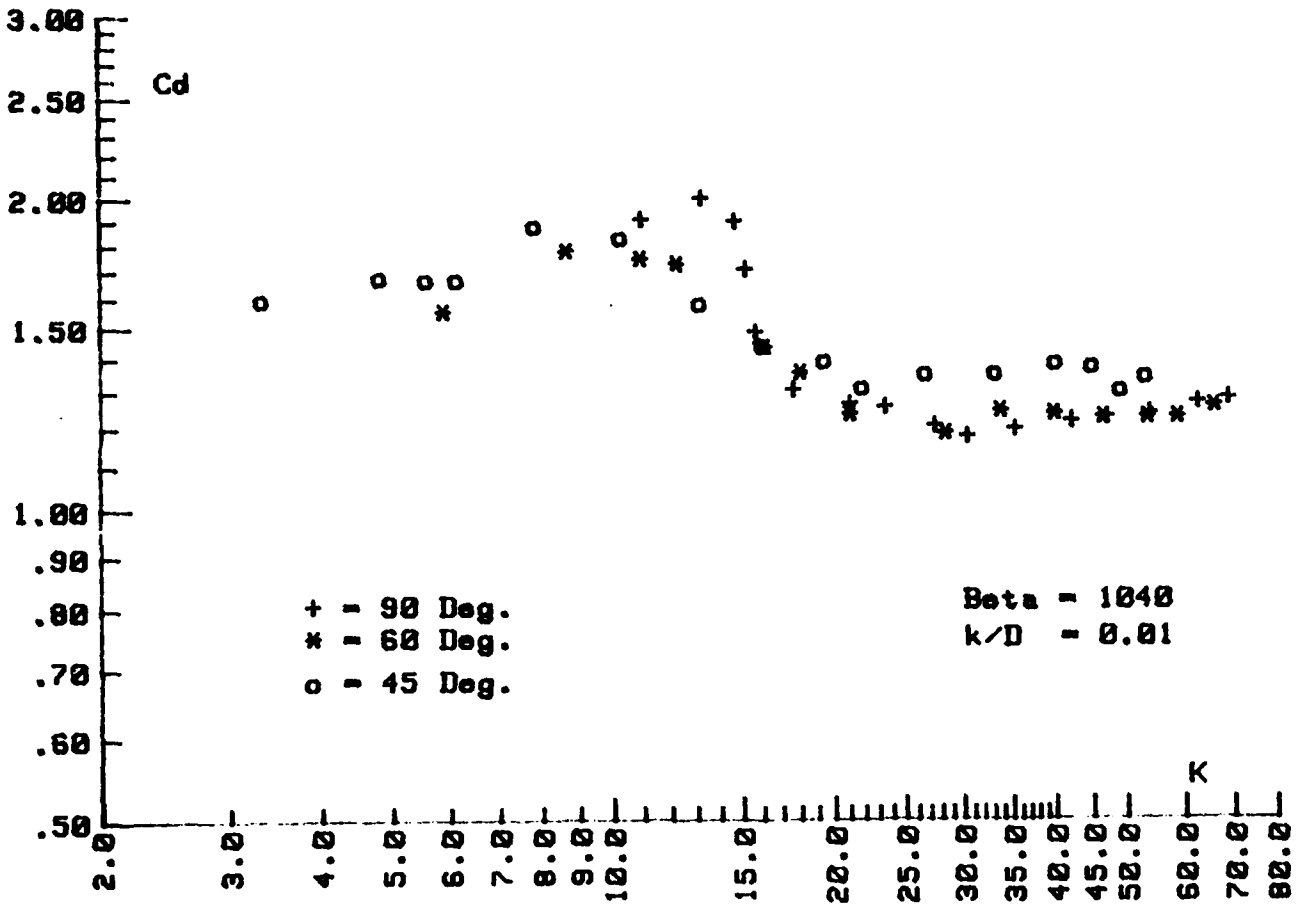

Figure 55. Comparison of C_d Versus K for β = 1040, k/D = 0.01, α = 90, 60, and 45 Deg.

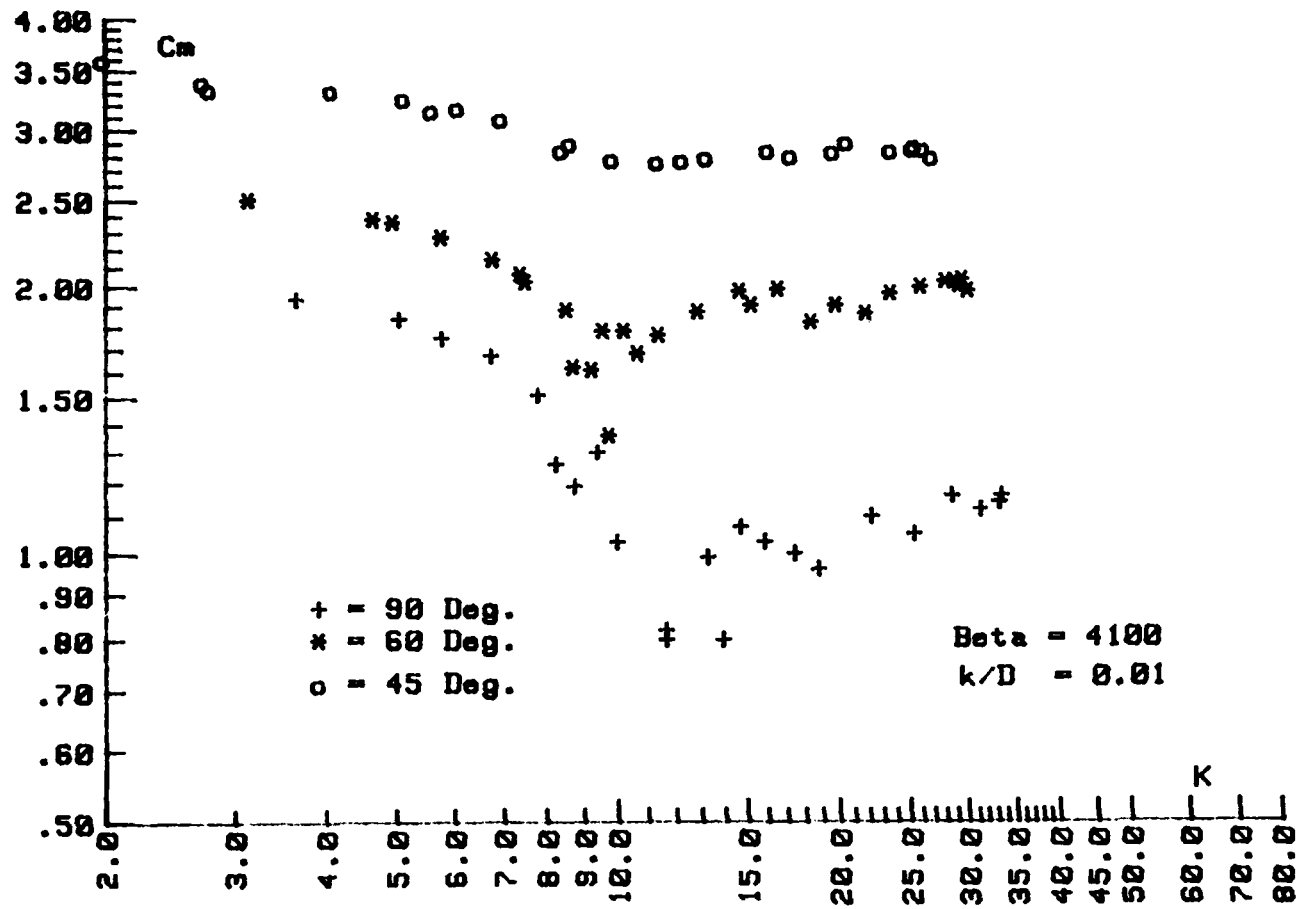

Figure 56. Comparison of C_m Versus K for β = 4100, k/D = 0.01, α = 90, 60, and 45 Deg.

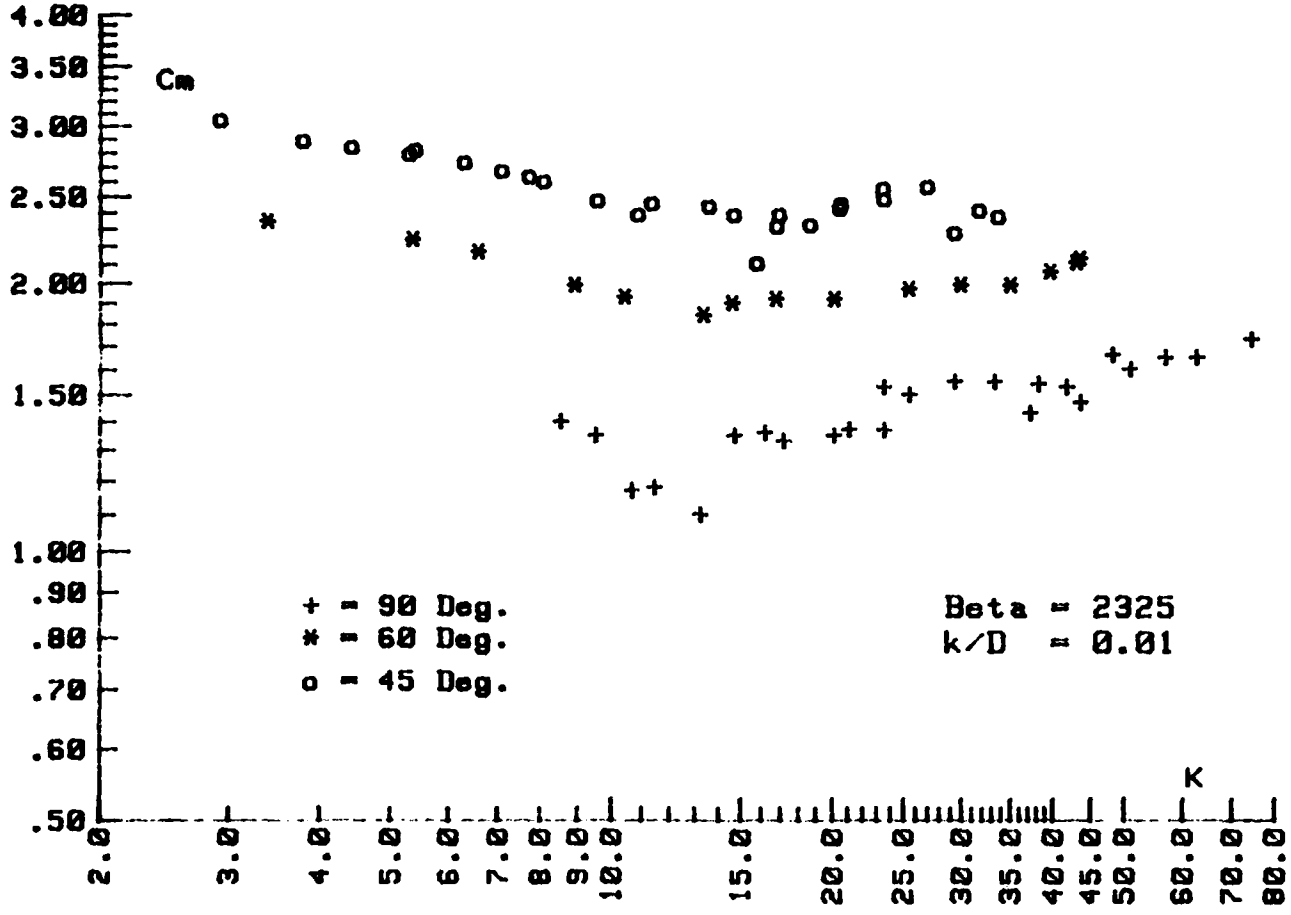

Figure 57. Comparison of C_m Versus K for β = 2325, k/D = 0.01, α = 90, 60, and 45 Deg.

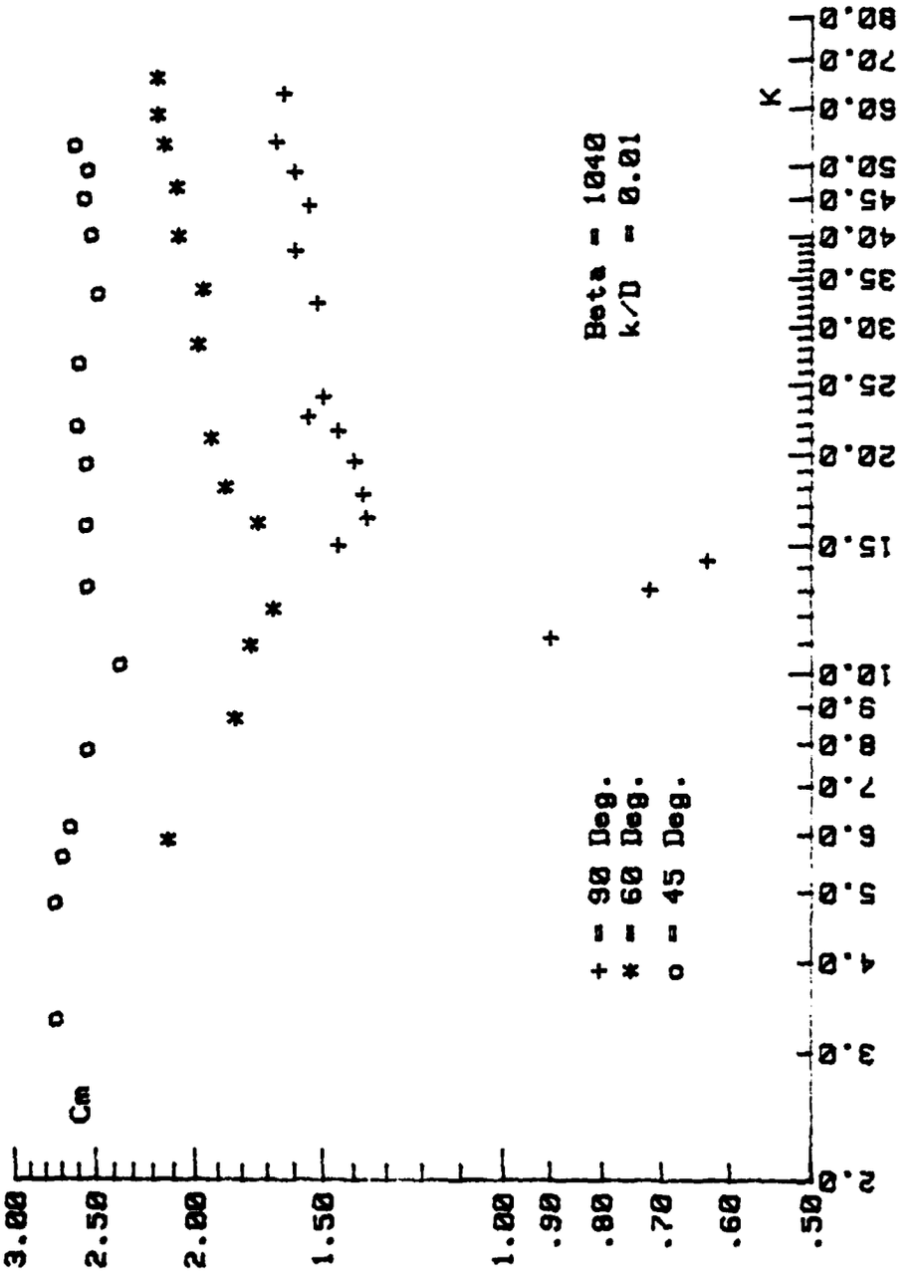

Figure 58. Comparison of C_m Versus K for β = 1040, k/D = 0.01, α = 90, 60, and 45 Deg.

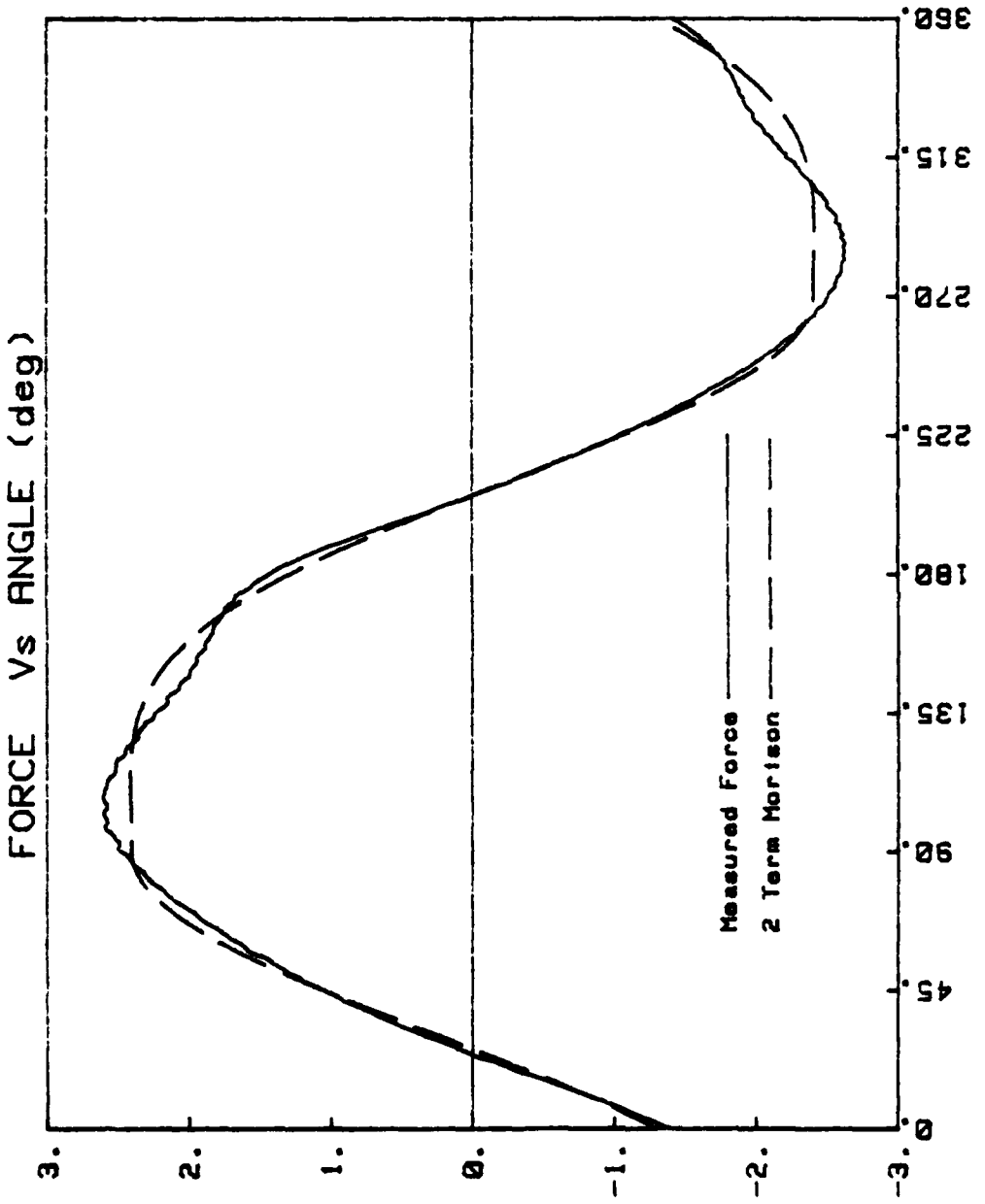

Figure 59. Comparison of Measured and Calculated Force (Two-Term Morison Equation) for K = 6.86, β = 4050, α = 90 Deg., k/D = 0.01

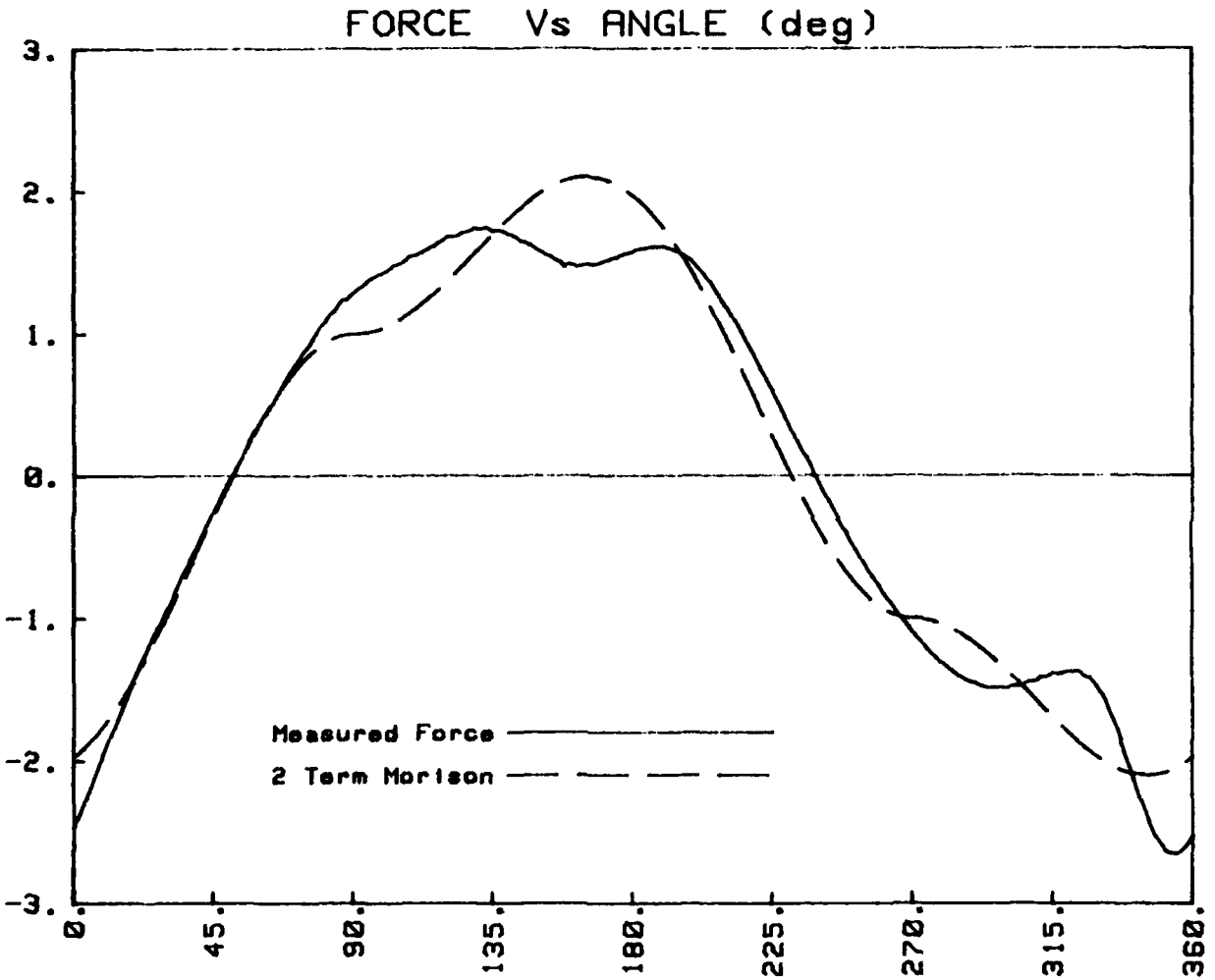

Figure 60. Comparison of Measured and Calculated Force (Two-Term Morison Equation) for K = 10.18, β = 4050, α = 90 Deg., k/D = 0.01

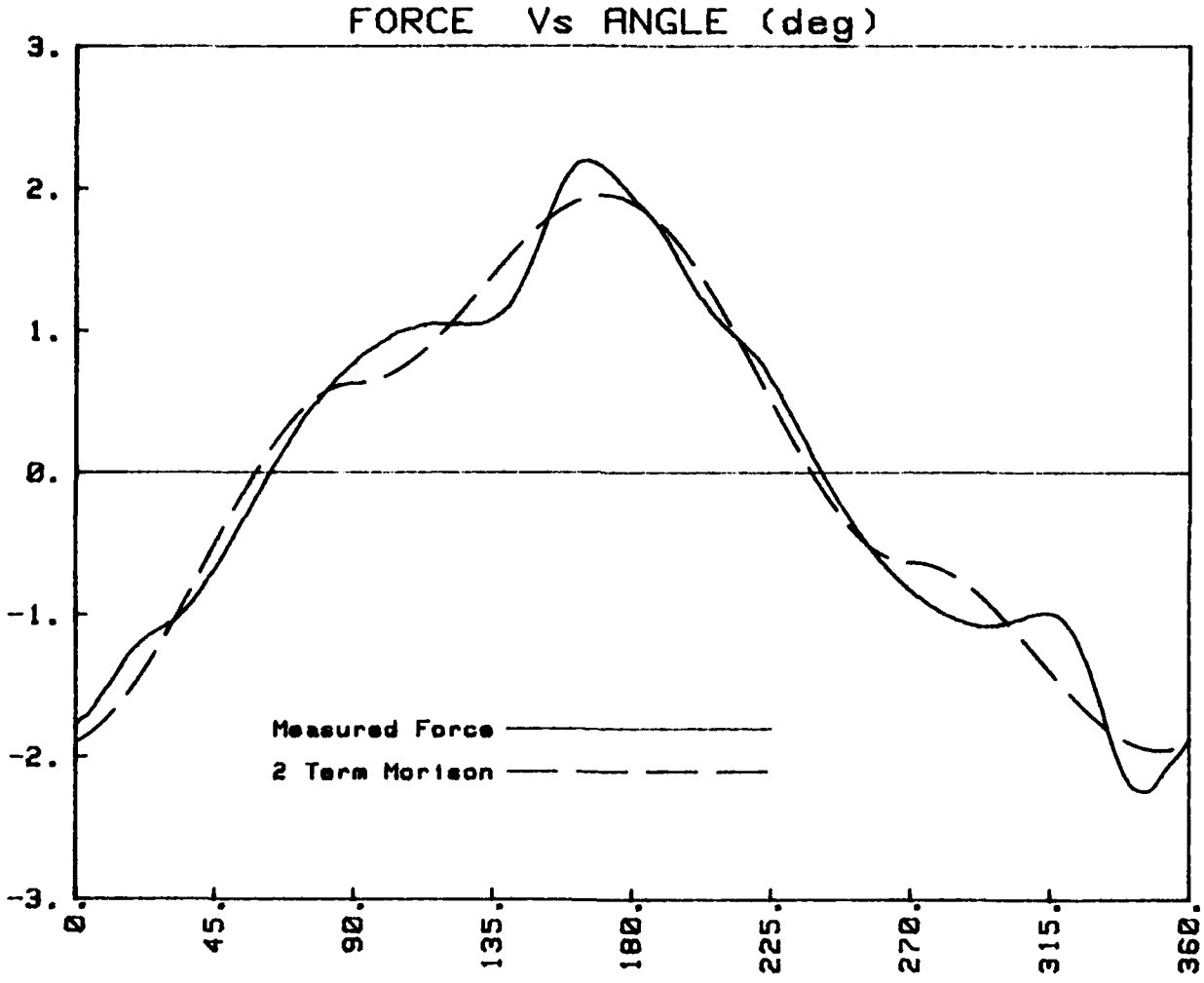

Figure 61. Comparison of Measured and Calculated Force (Two-Term Morison Equation) for K = 11.88, β = 4050, α = 90 Deg., k/D = 0.01

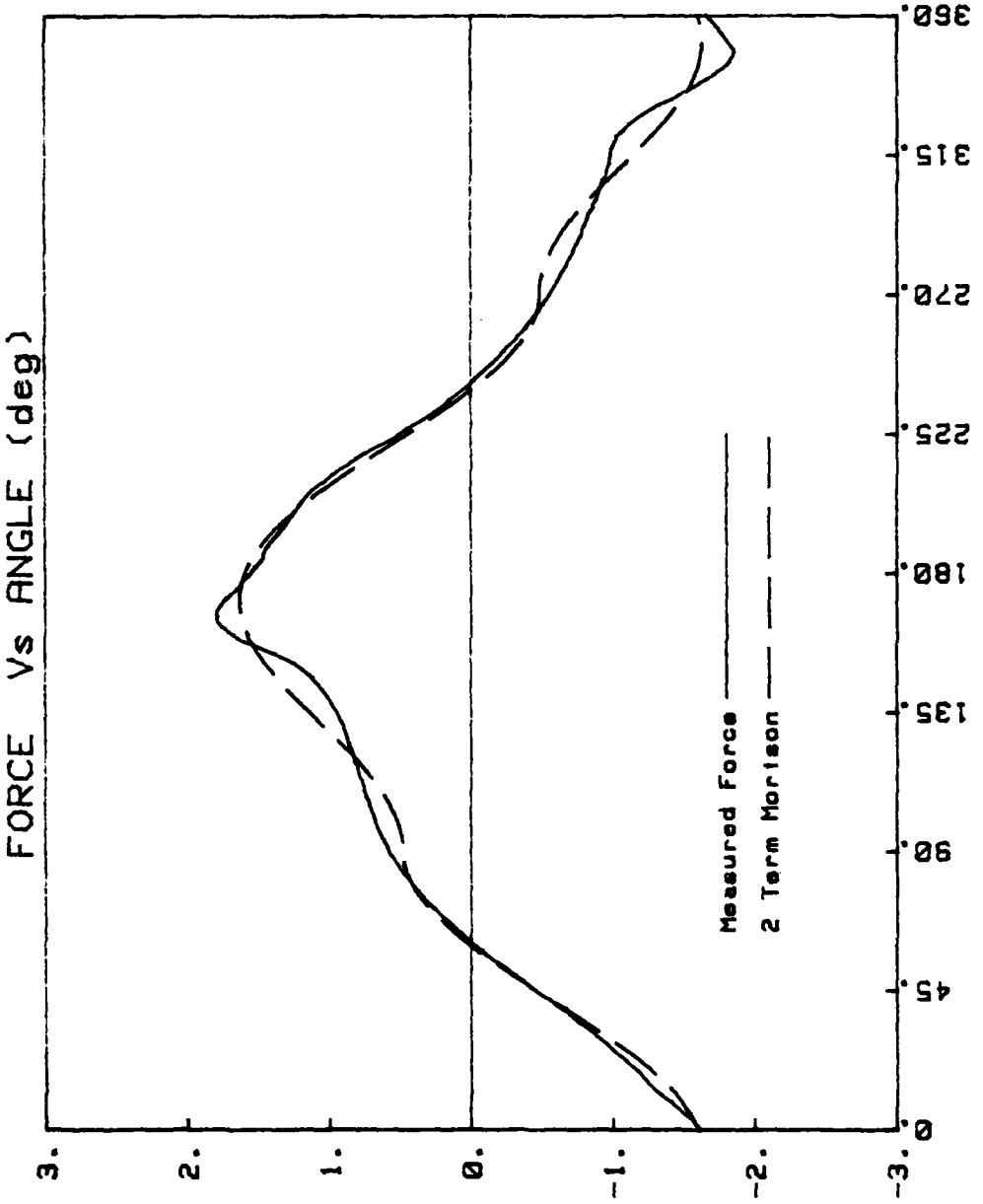

Figure 62. Comparison of Measured and Calculated Force (Two-Term Morison Equation) for K = 16.15, β = 4050, α = 90 Deg., k/D = 0.01

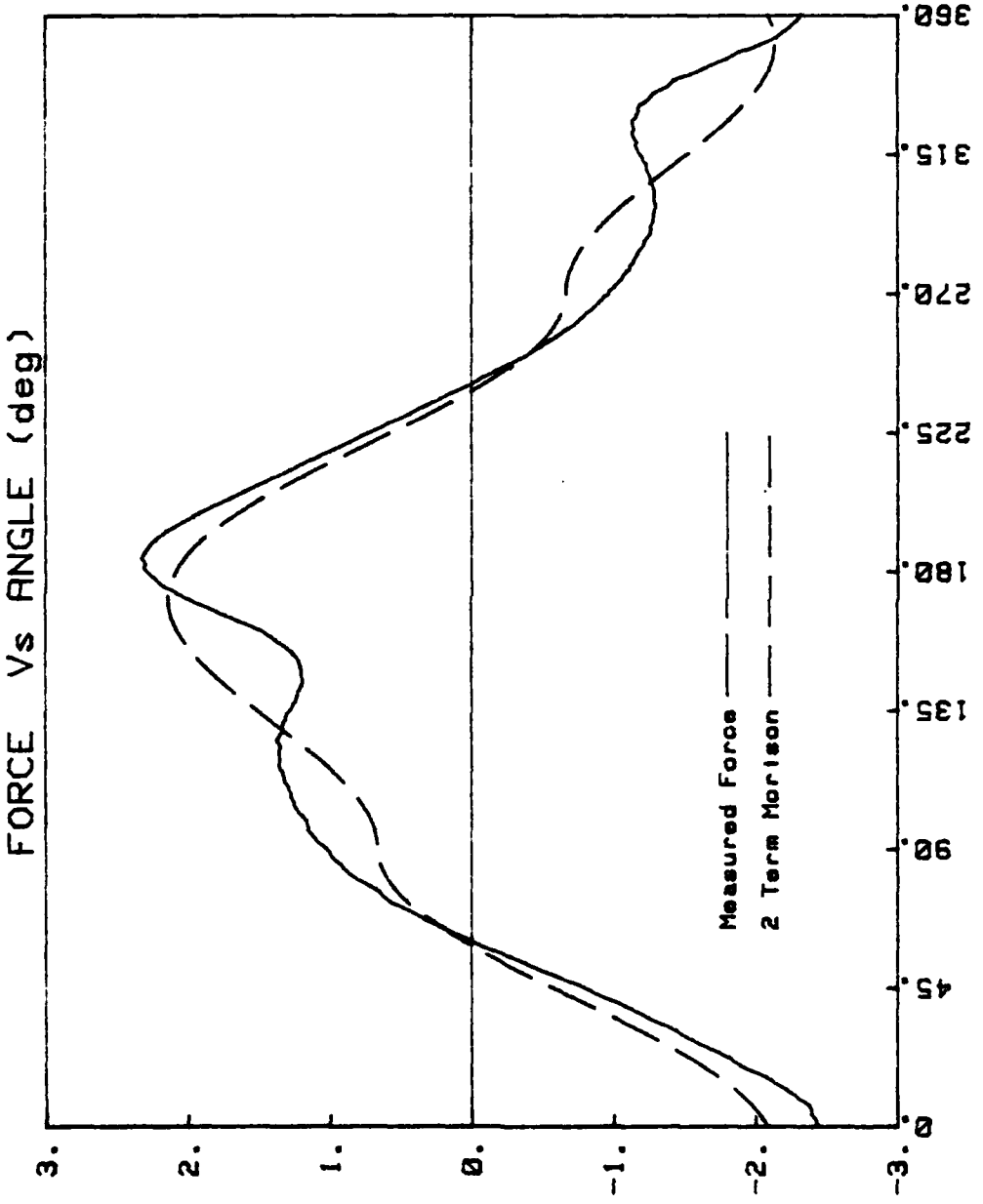

Figure 63. Comparison of Measured and Calculated Force (Two-Term Morison Equation) for K = 22.56, β = 4050, α = 90 Deg., k/D = 0.01

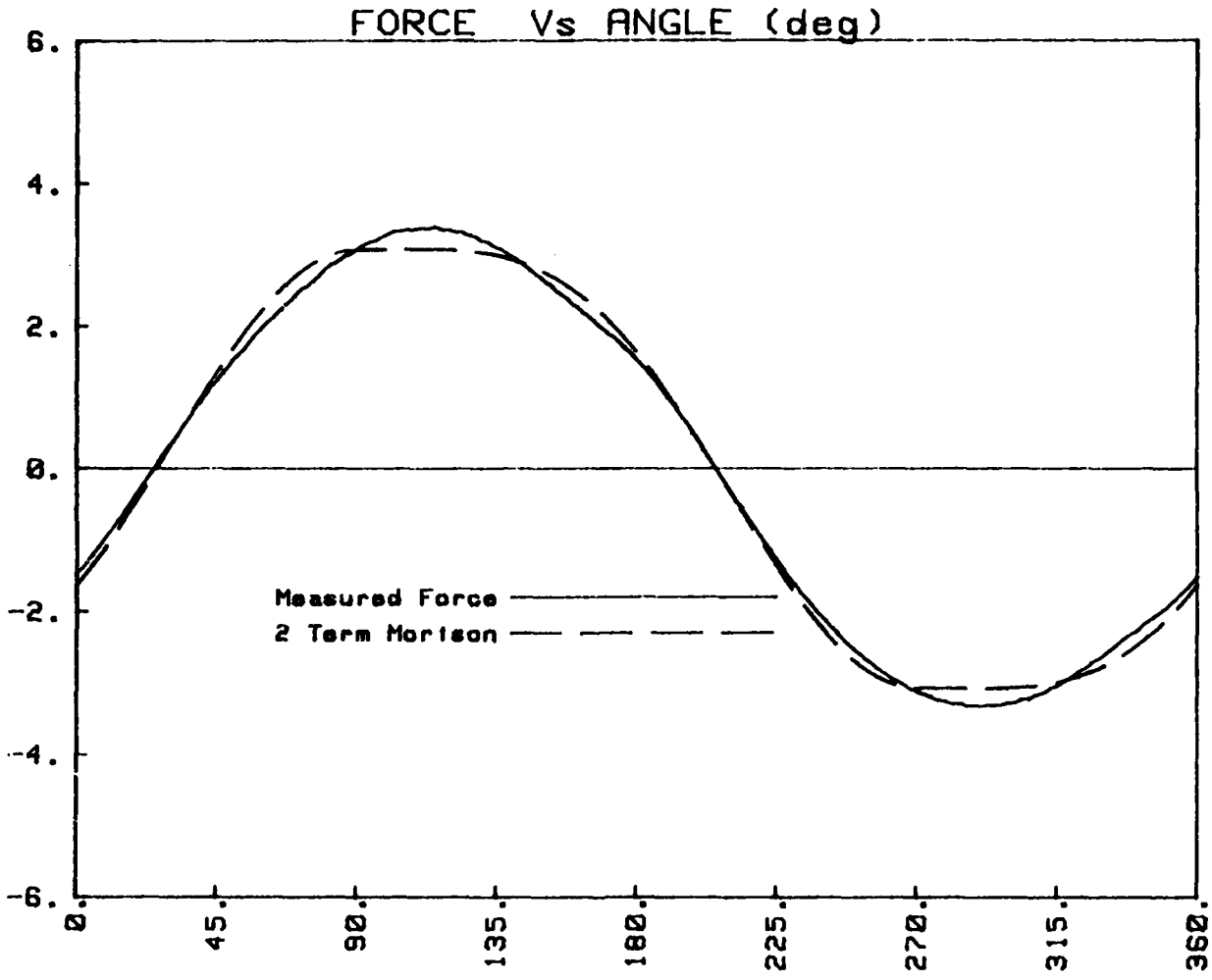

Figure 64. Comparison of Measured and Calculated Force (Two-Term Morison Equation) for K = 6.89, β = 4100, α = 60 Deg., k/D = 0.01

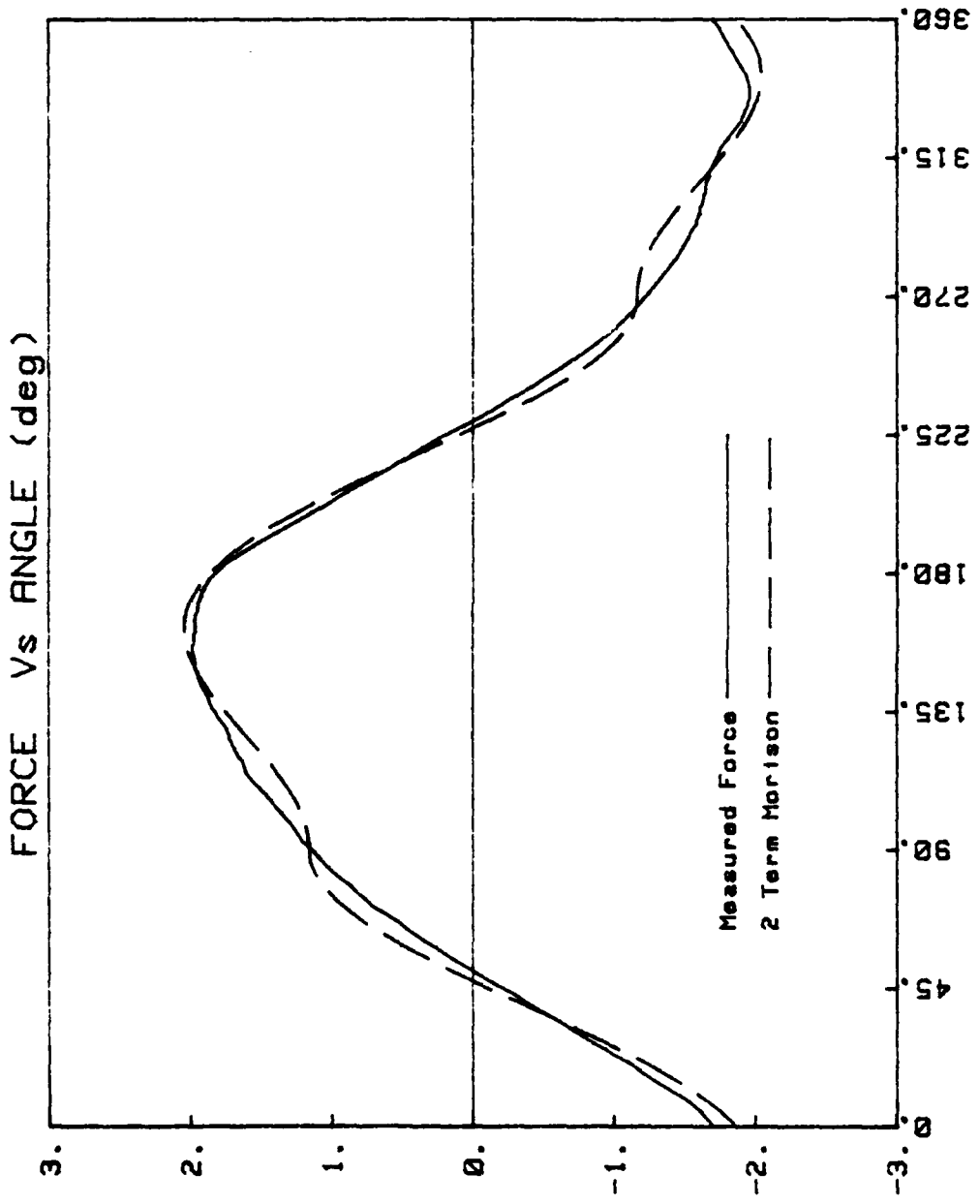

Figure 65. Comparison of Measured and Calculated Force (Two-Term Morison Equation) for K = 16.83, β = 4100, α = 60 Deg., k/D = 0.01

AD-A124 093 OSCILLATING FLOW ABOUT YAWED CYLINDERS(U) NAVAL POSTGRADUATE SCHOOL MONTEREY CA T SARPKAYA MAR 83 NPS-69-83-001 NSF-CEE82-10248 2/2

UNCLASSIFIED F/G 20/4 NL

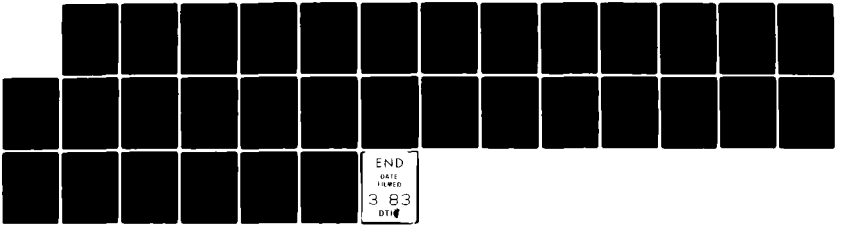

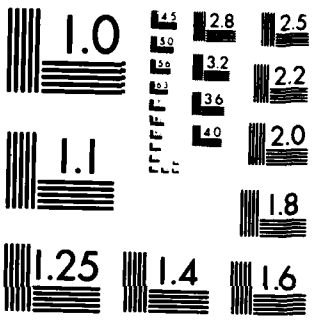

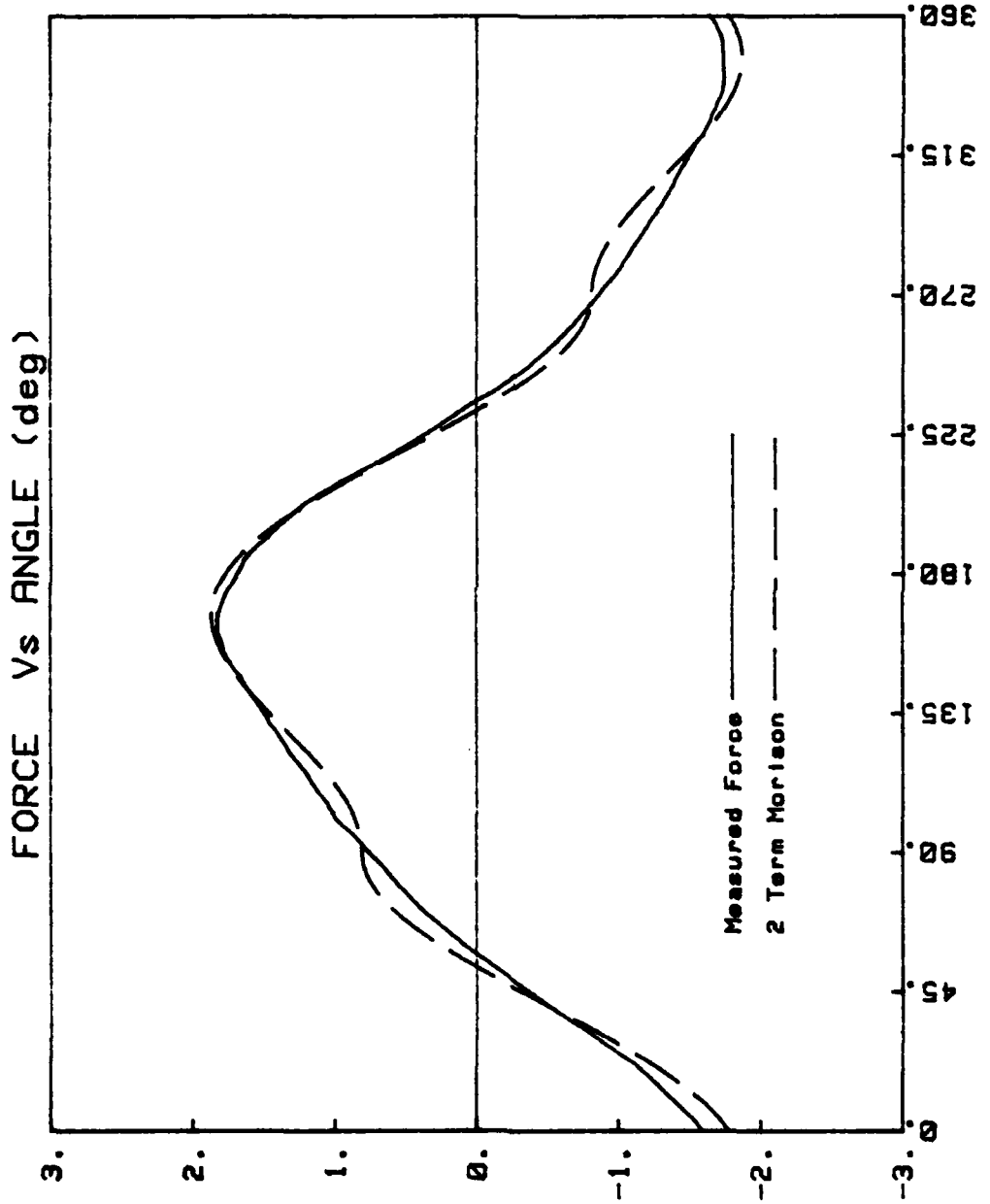

Figure 66. Comparison of Measured and Calculated Force (Two-Term Morison Equation) for K = 23.94, β = 4100, α = 60 Deg., k/D = 0.01

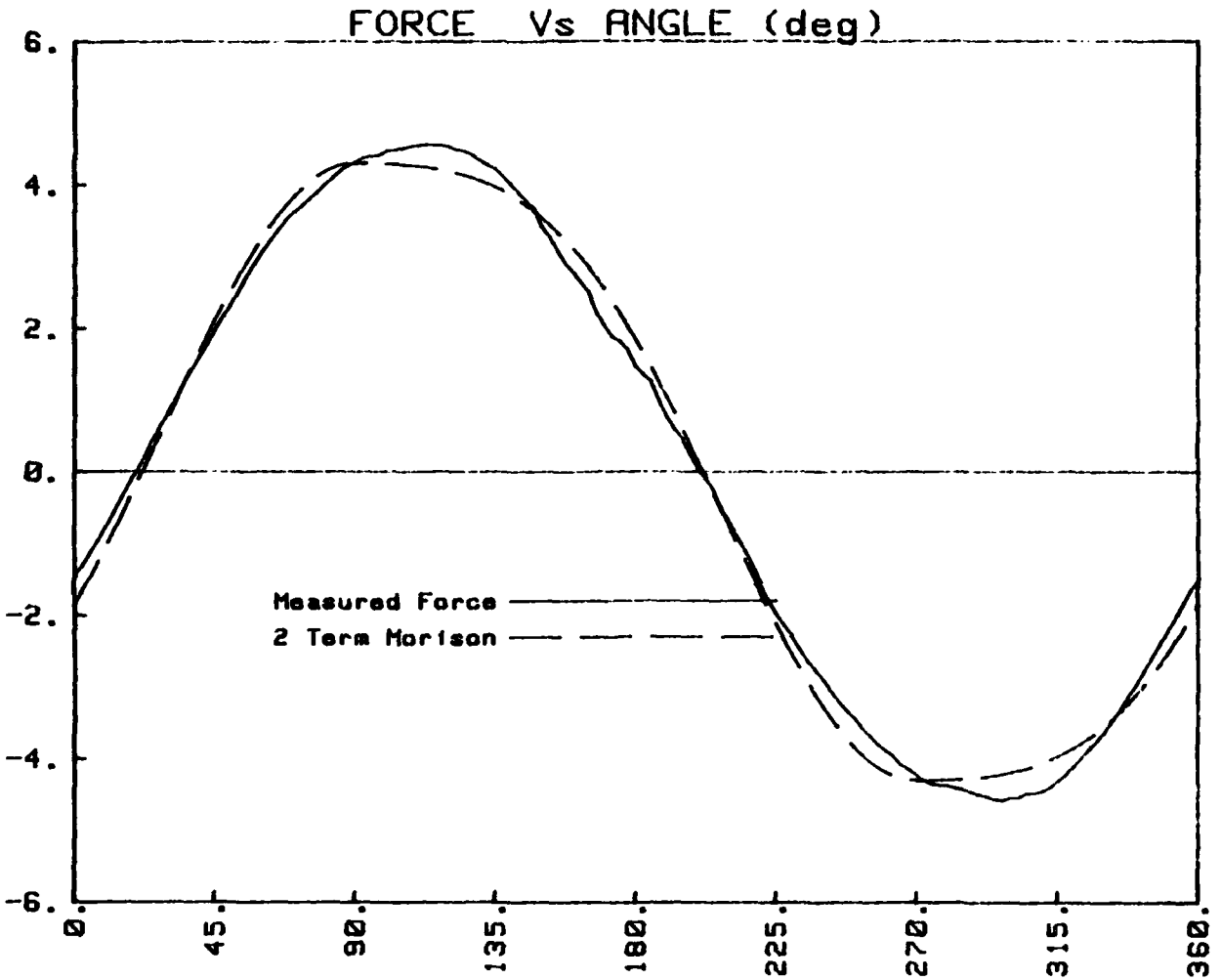

Figure 67. Comparison of Measured and Calculated Force (Two-Term Morison Equation) for K = 7.90, β = 4150, C 4' eg., k/D = 0.01

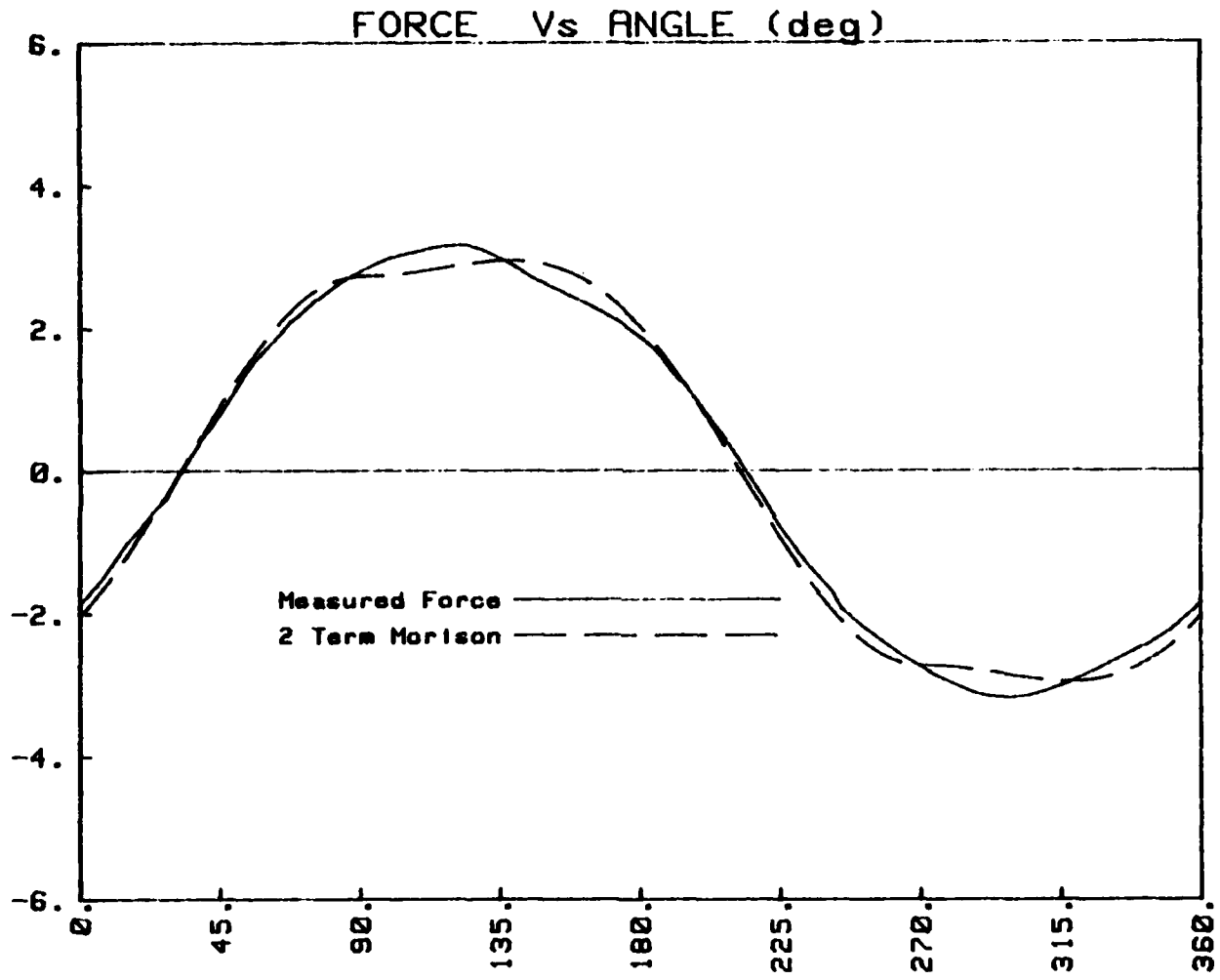

Figure 68. Comparison of Measured and Calculated Force (Two-Term Morison Equation) for K = 10.05, β = 4150, α = 45 Deg., k/D = 0.01

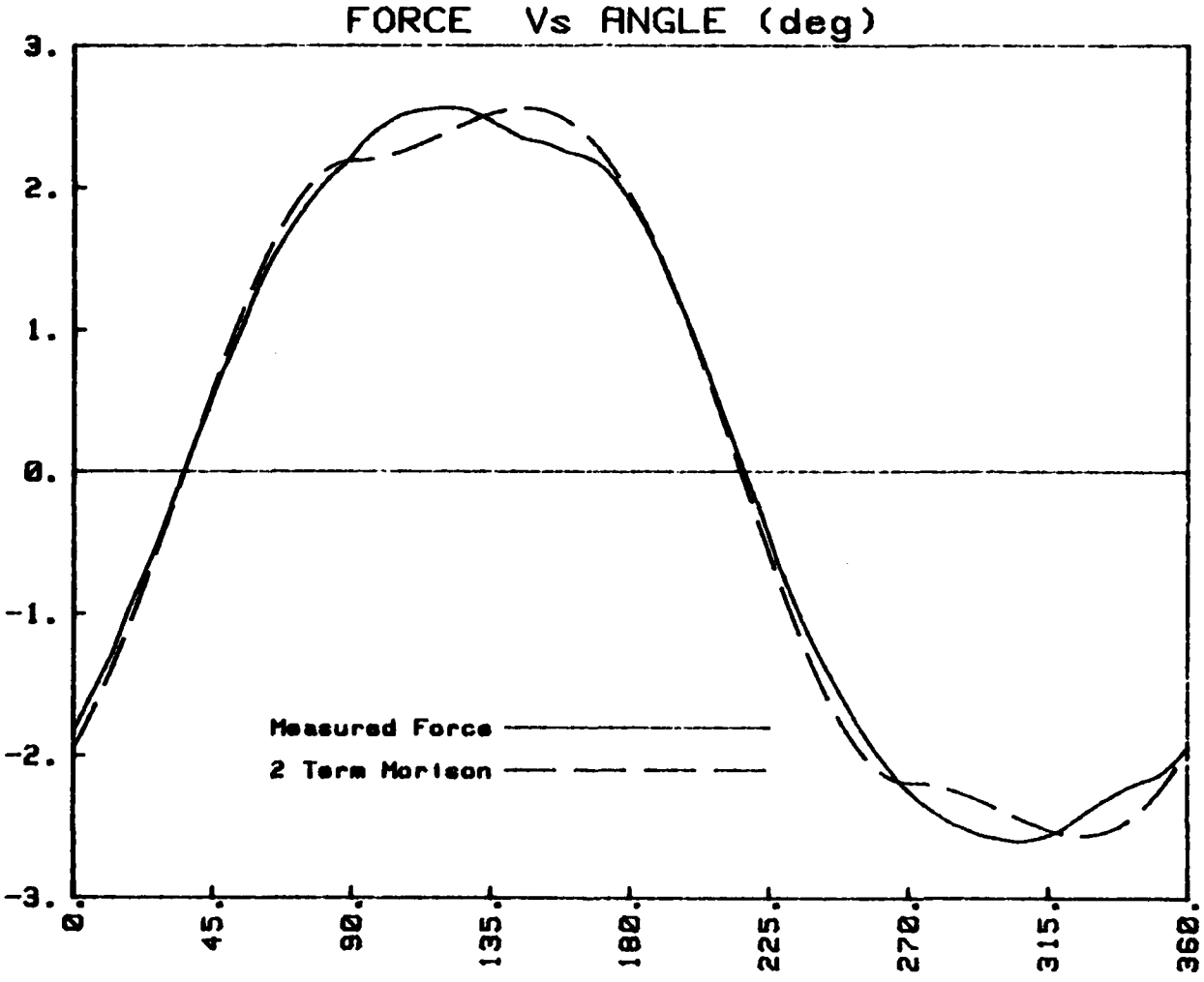

Figure 69. Comparison of Measured and Calculated Force (Two-Term Morison Equation) for K = 12.50, β = 4150, α = 45 Deg., k/D = 0.01

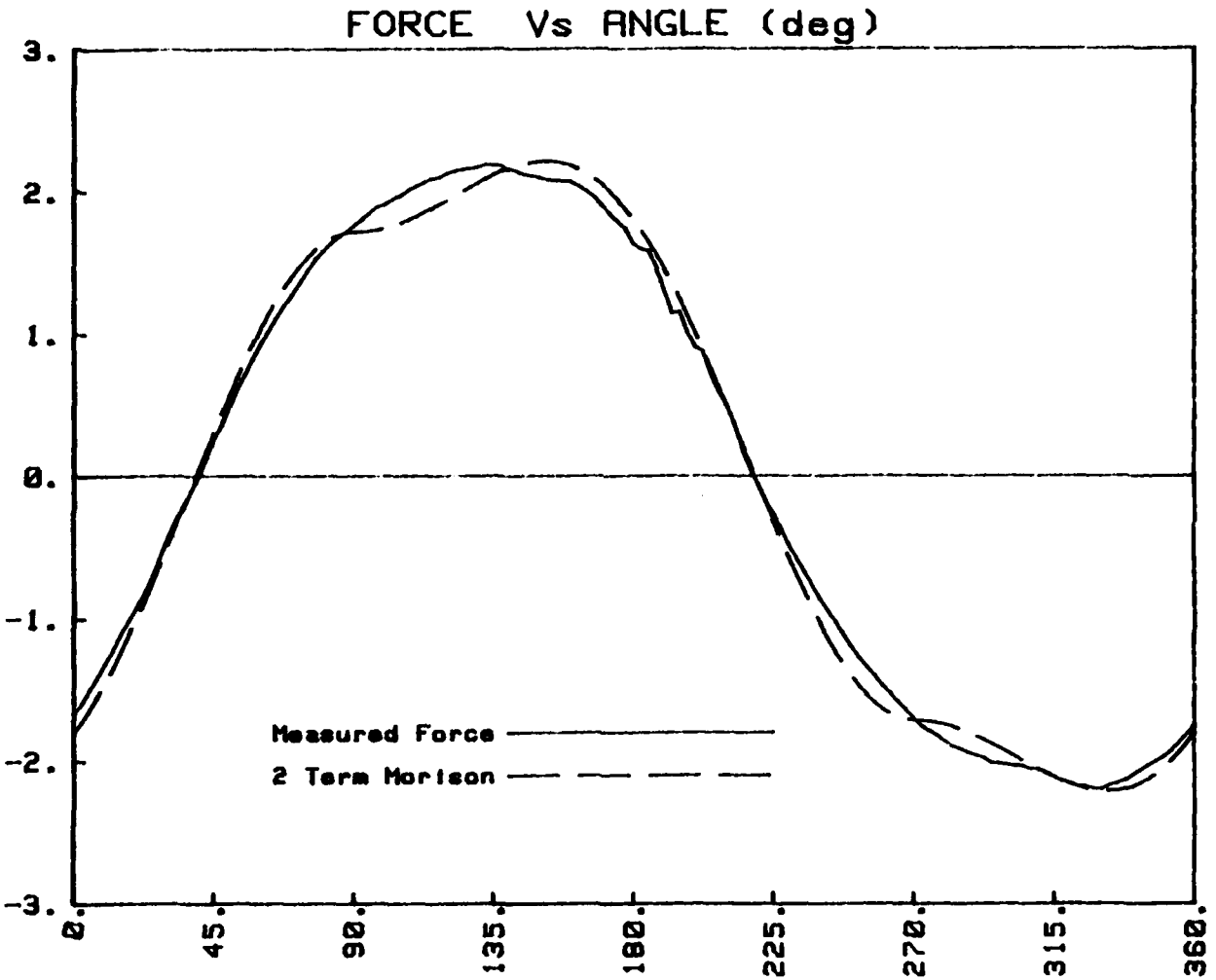

Figure 70. Comparison of Measured and Calculated Force (Two-Term Morison Equation) for K = 16.35, β = 4150, α = 45 Deg., k/D = 0.01

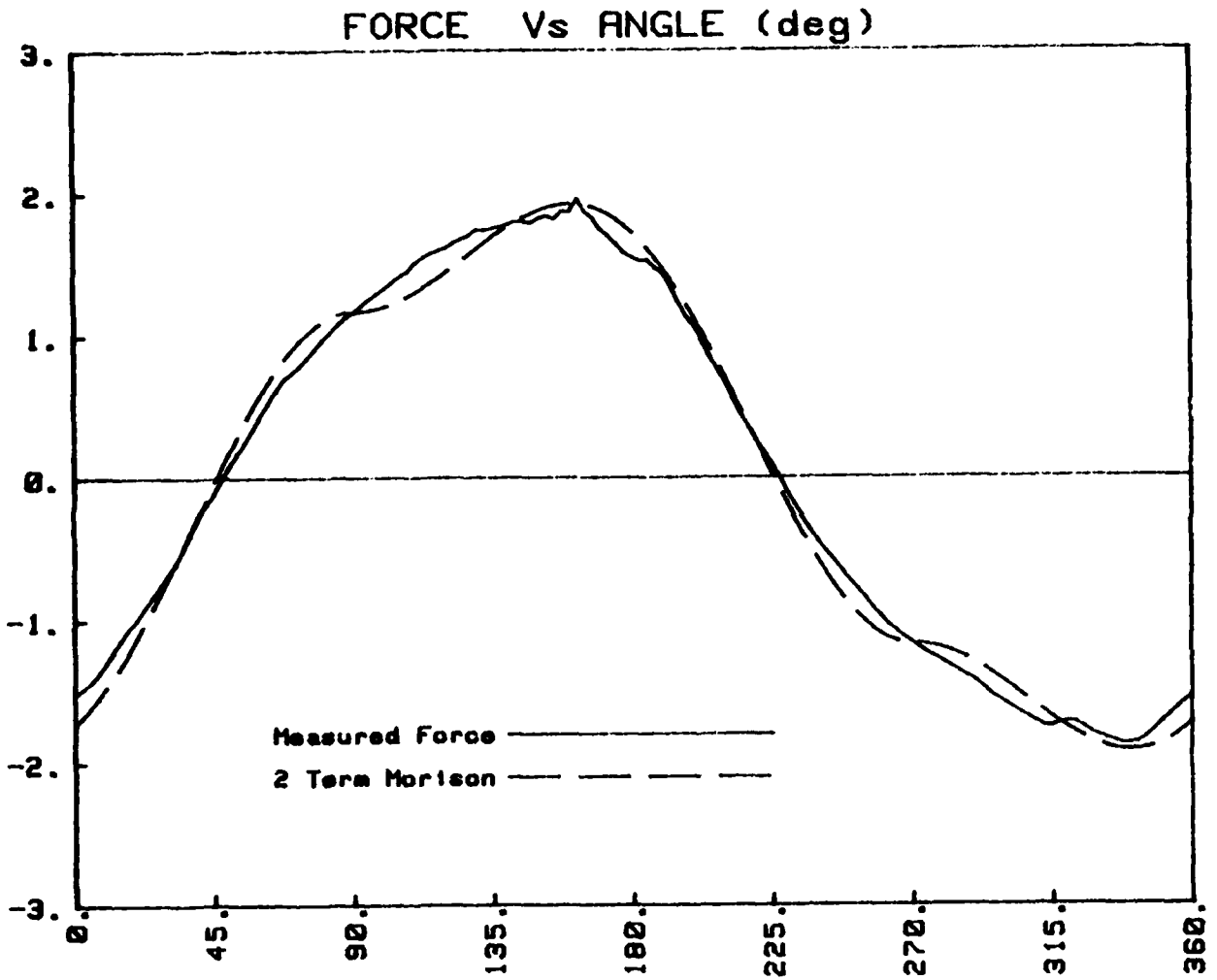

Figure 71. Comparison of Measured and Calculated Force (Two-Term Morison Equation) for K = 24.04, β = 4150, α = 45 Deg., k/D = 0.01

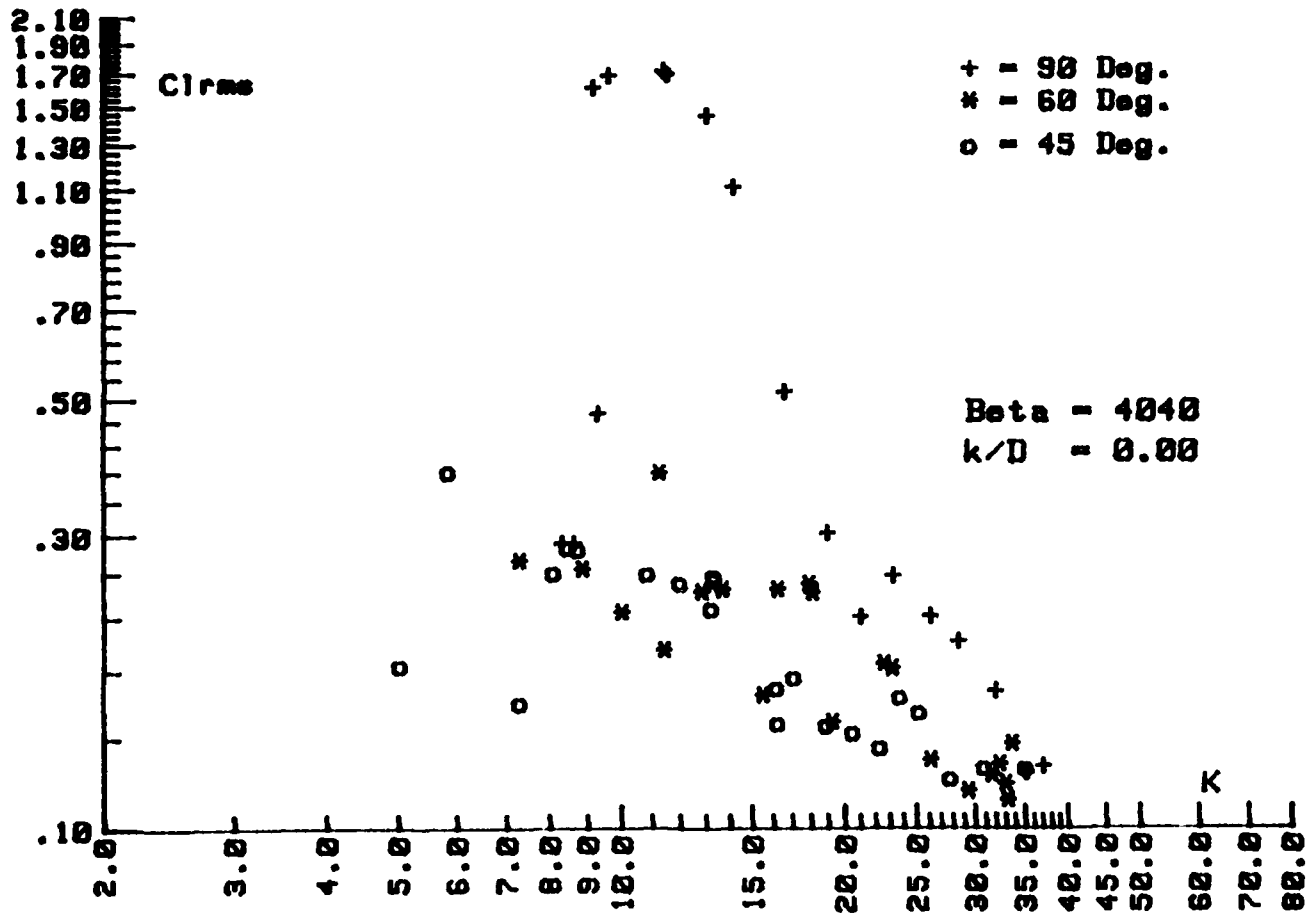

Figure 72. Comparison of C_{lrms} Versus K for β = 4040, k/D = 0.00, α = 90, 60, and 45 Deg.

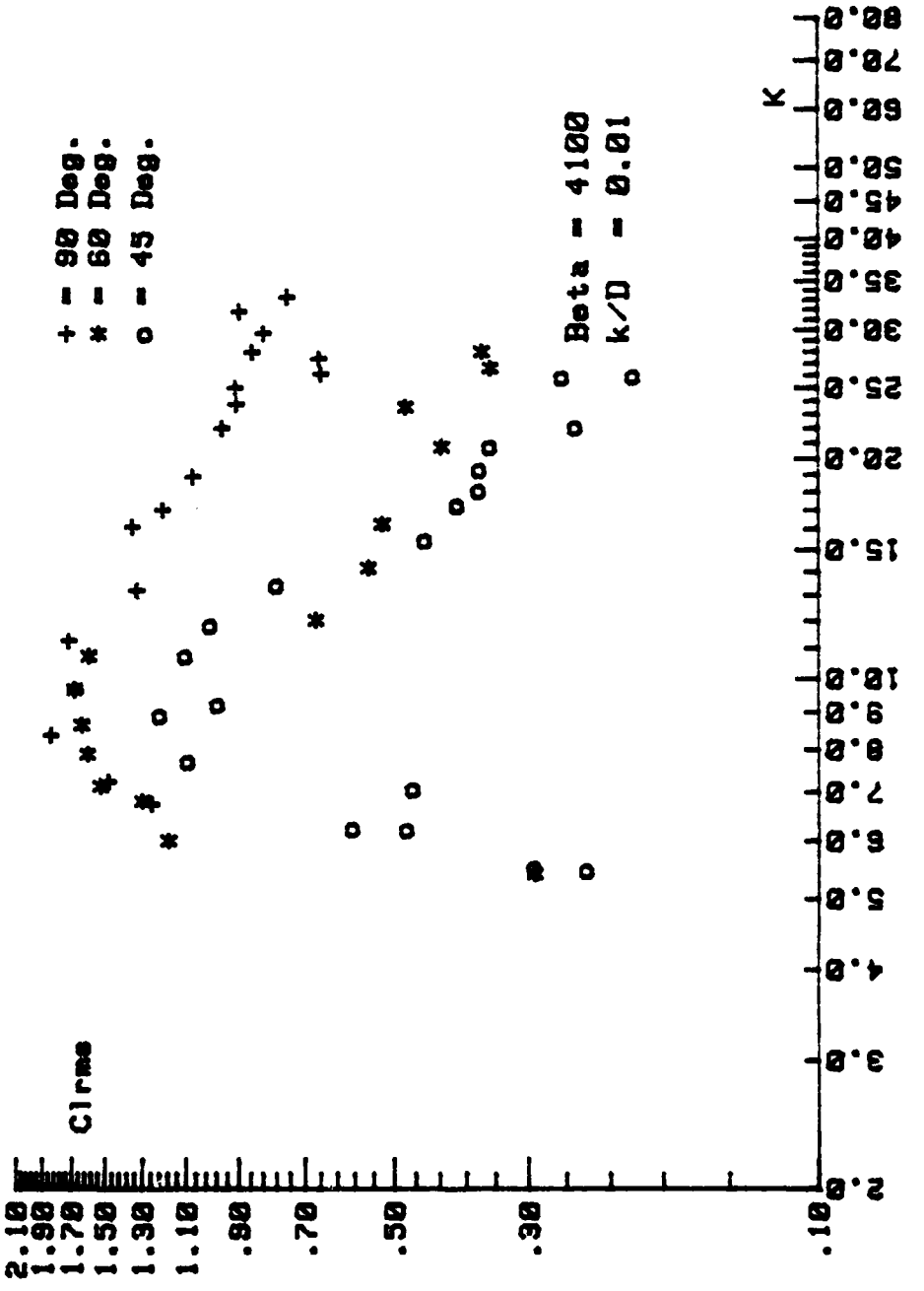

Figure 73. Comparison of C_{lrms} Versus K for β = 4100, k/D = 0.01, α = 90, 60, and 45 Deg.

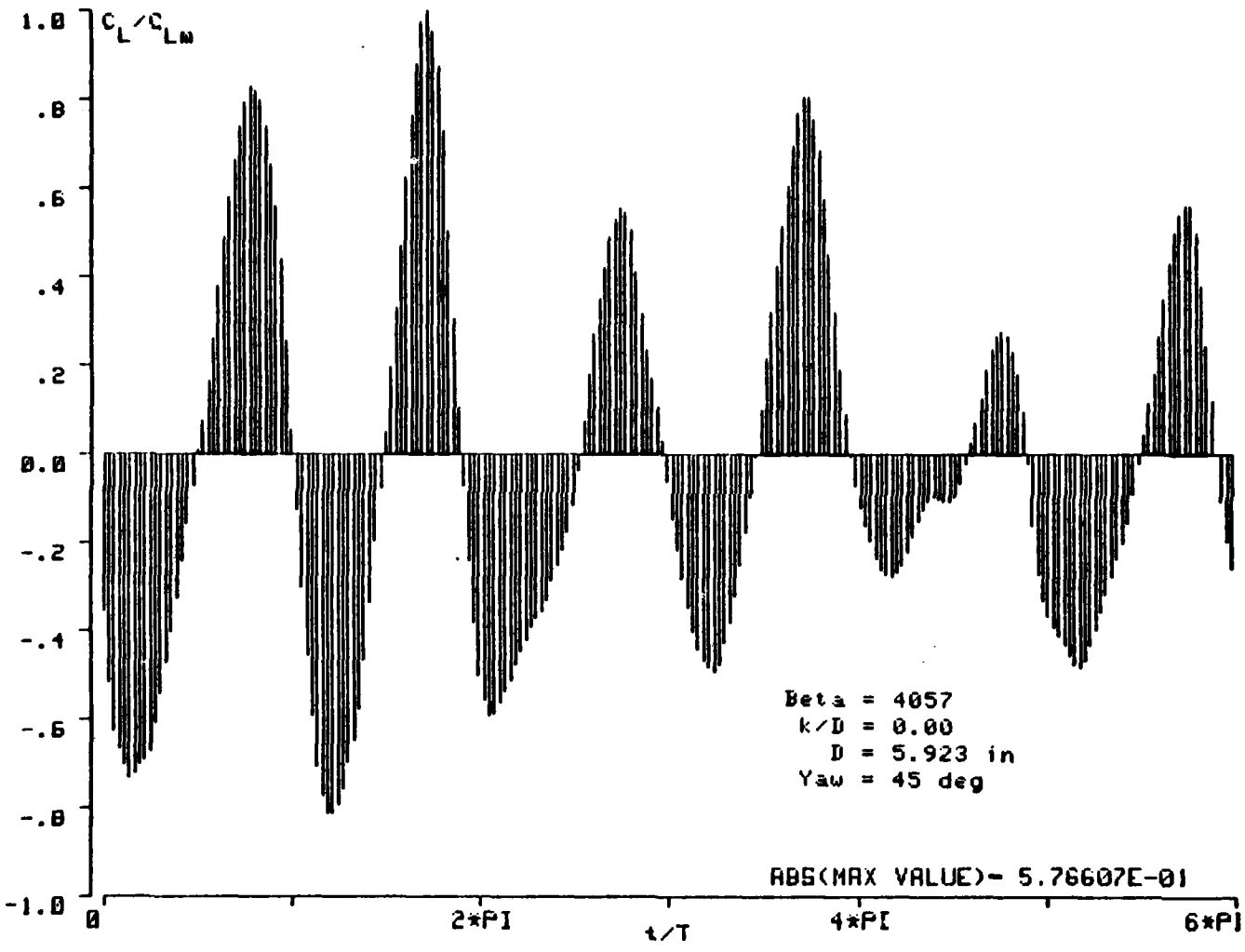

Figure 74. Normalized Lift Force Data for $\hat{K}$ = 8.38, β = 4090, α = 45 Deg., k/D = 0.00

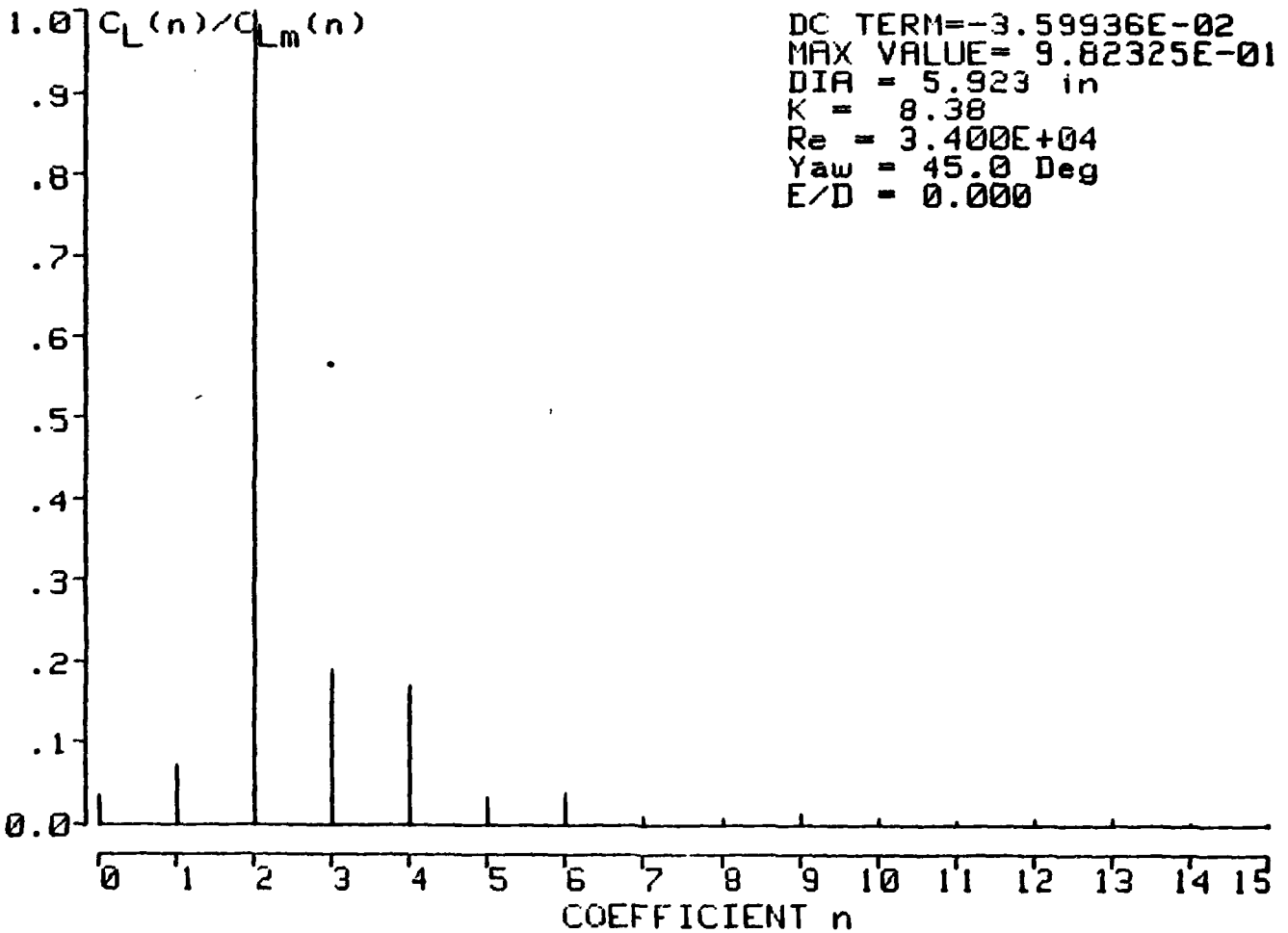

Figure 75. Normalized Fourier Coefficients for K = 8.38
β = 4090, α = 45 Deg., k/D = 0.00

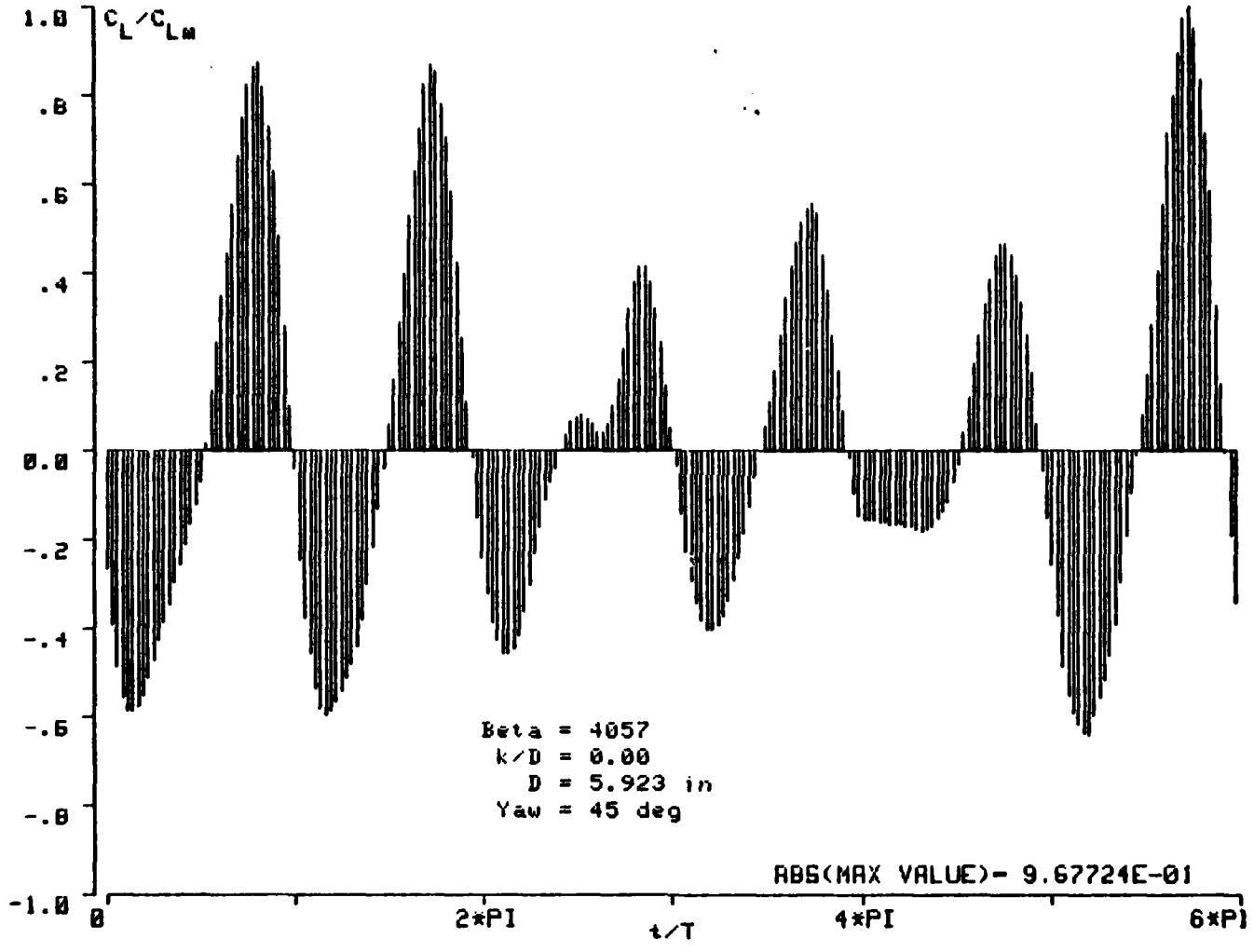

Figure 76. Normalized Lift Force Data for K = 10.62, β = 4090, α = 45 Deg., k/D = 0.00

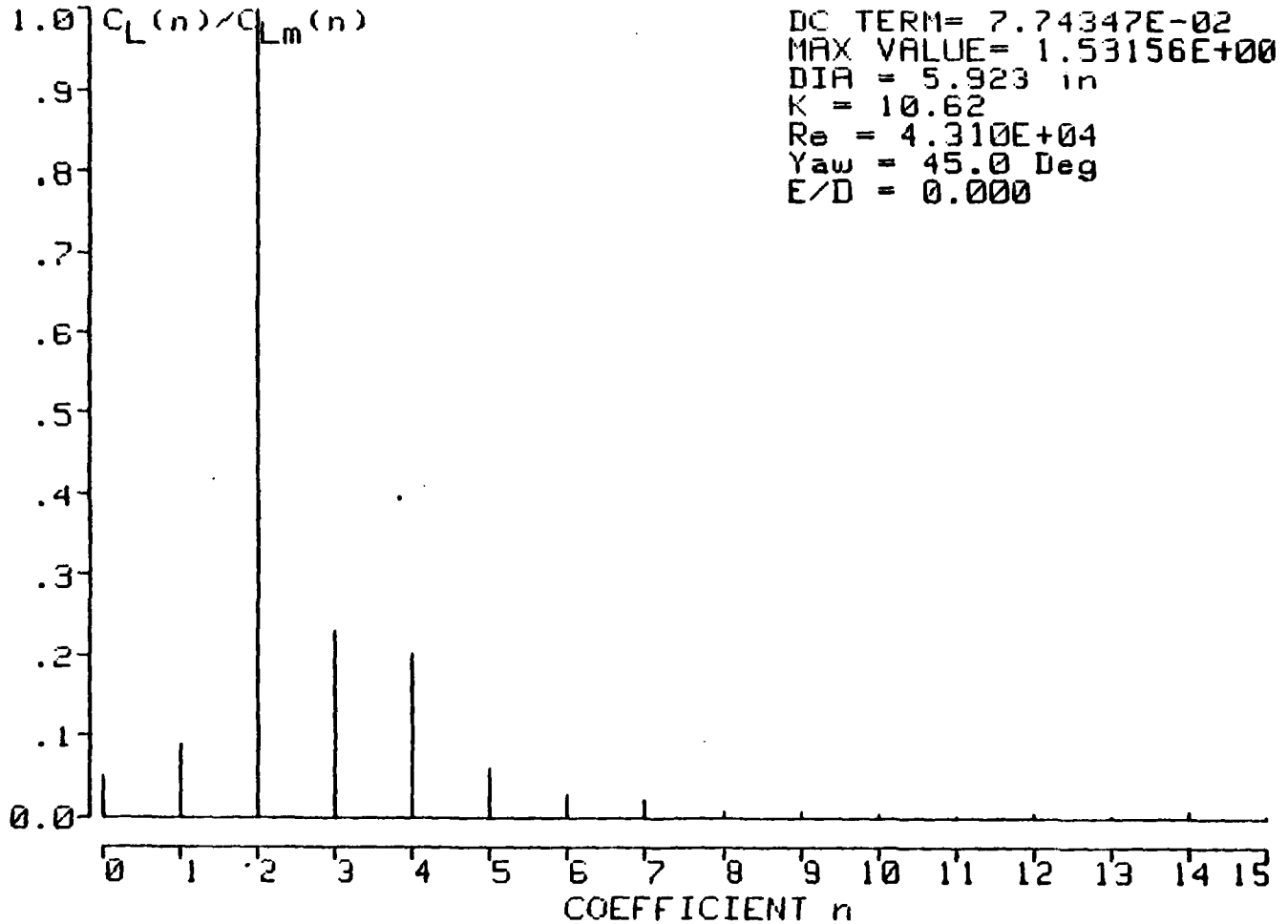

Figure 77. Normalized Fourier Coefficients for K = 10.62
β = 4090, α = 45 Deg., k/D = 0.00 .

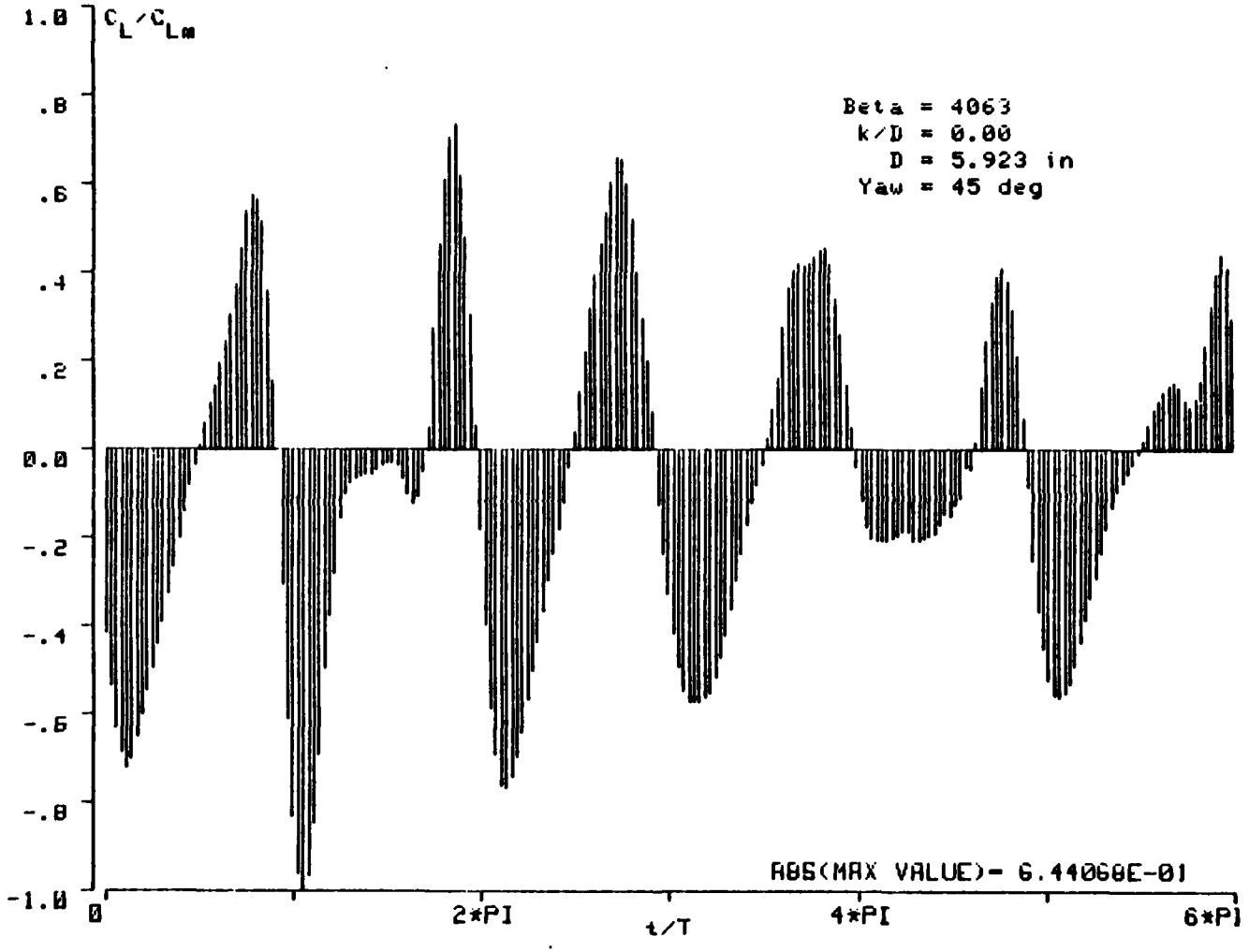

Figure 78. Normalized Lift Force Data for R_e = 13.79, β = 4090, α = 45 Deg., k/D = 0.00

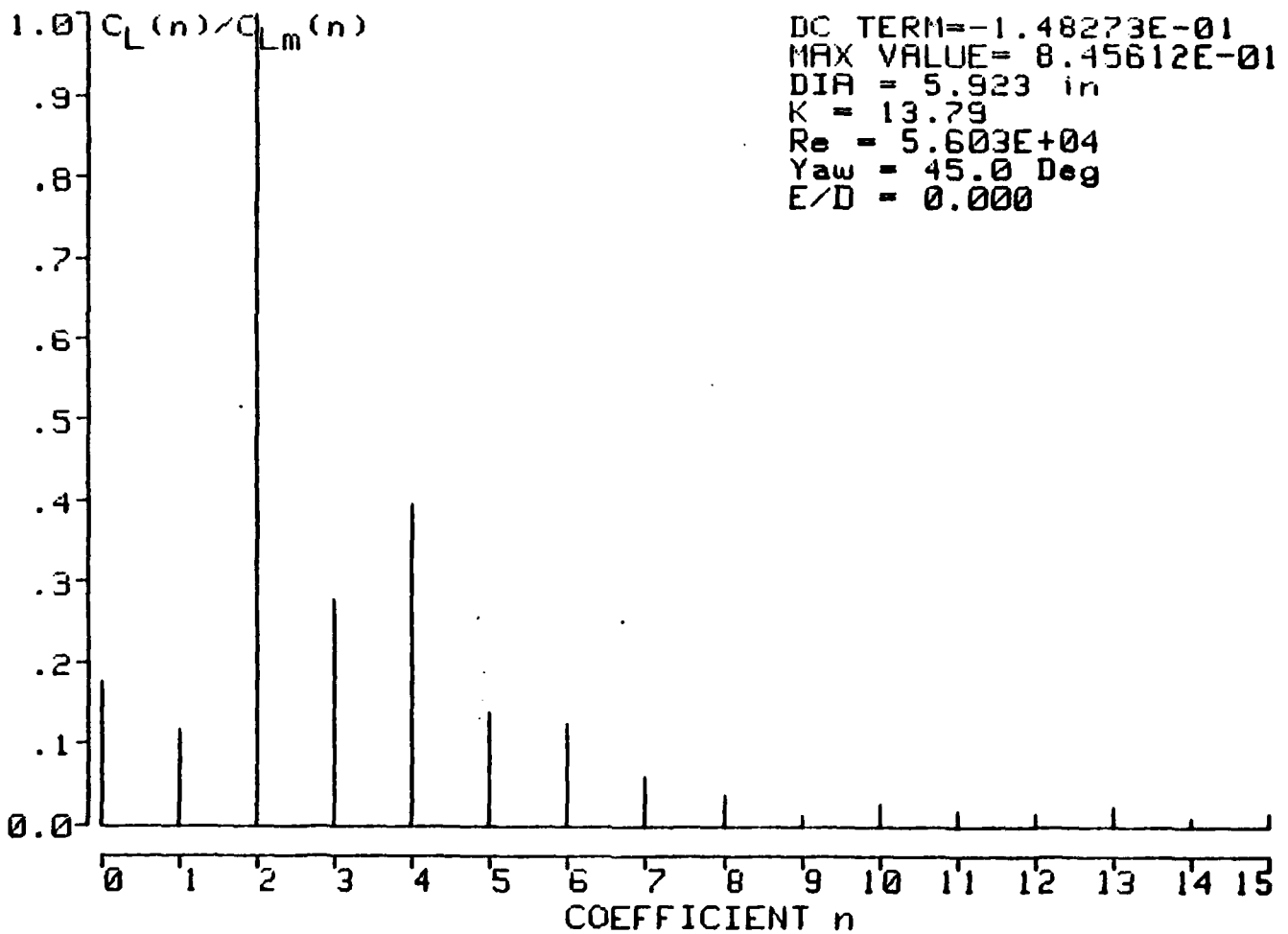

Figure 79. Normalized Fourier Coefficients for K = 13.79, β = 4090, α = 45 Deg., k/D = 0.00

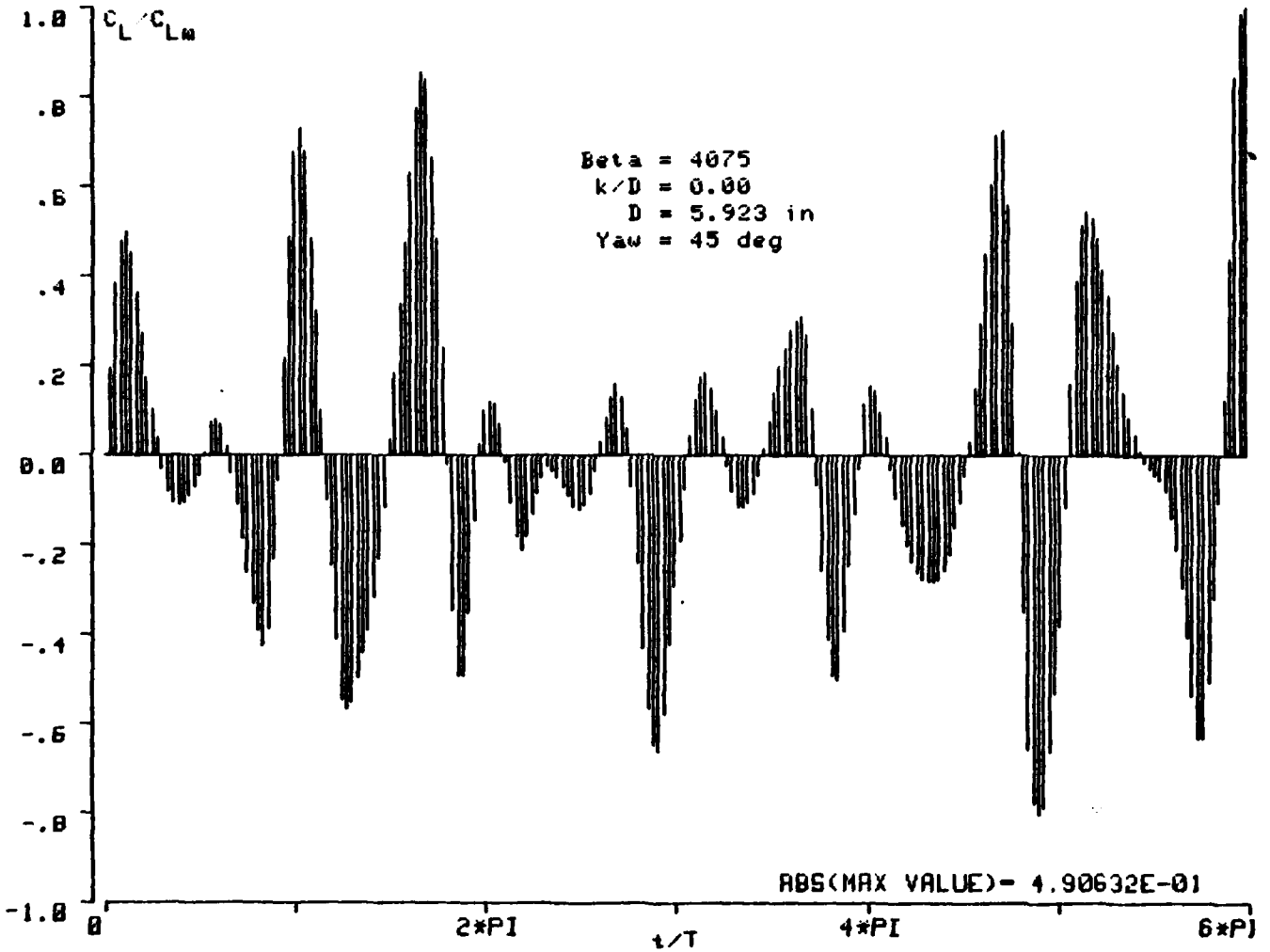

Figure 80. Normalized Lift Force Data for K = 17.63, β = 4090, α = 45 Deg., k/D = 0.00

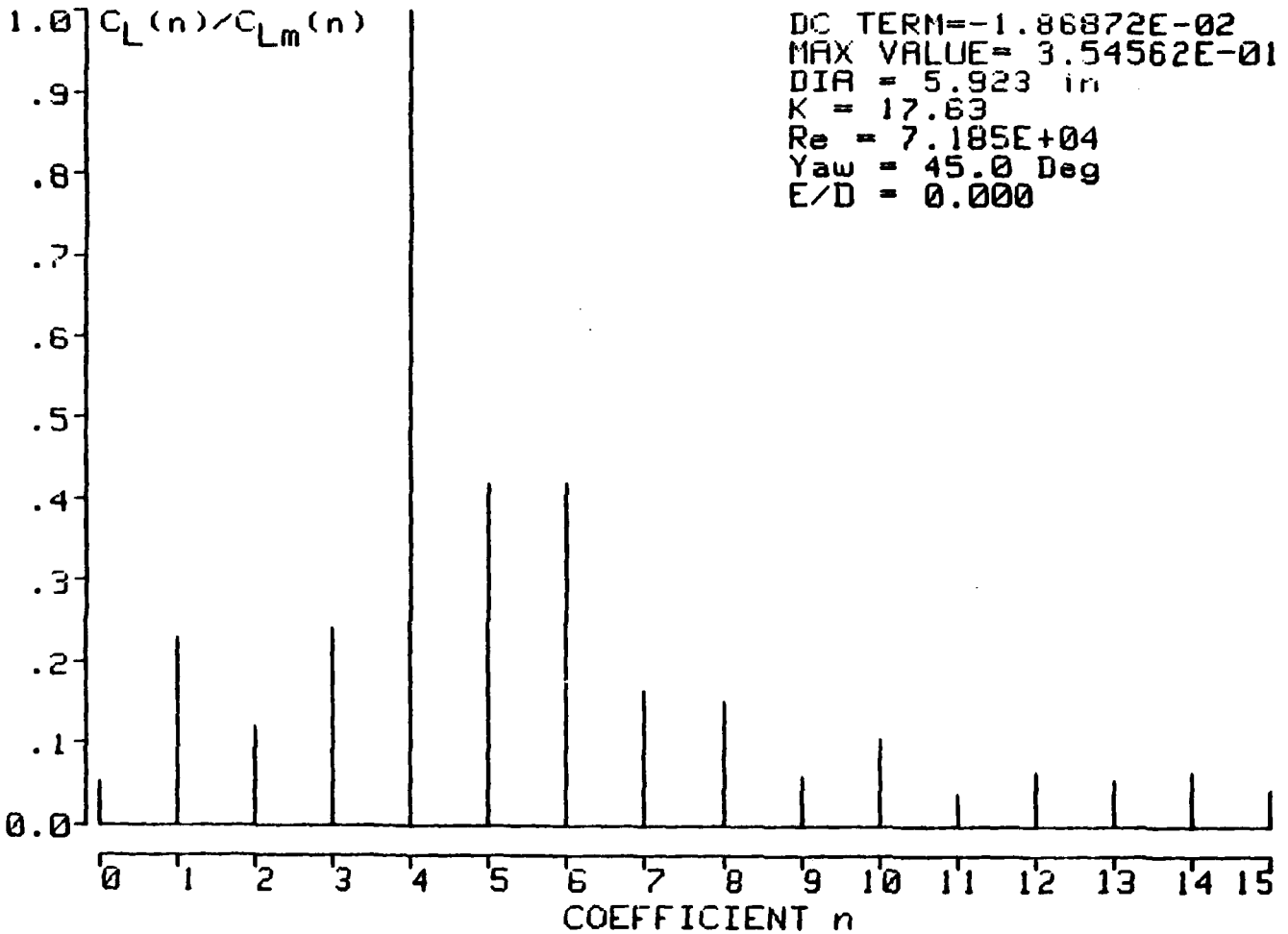

Figure 81. Normalized Fourier Coefficients for K = 17.63, β = 4090, α = 45 Deg., k/D = 0.00

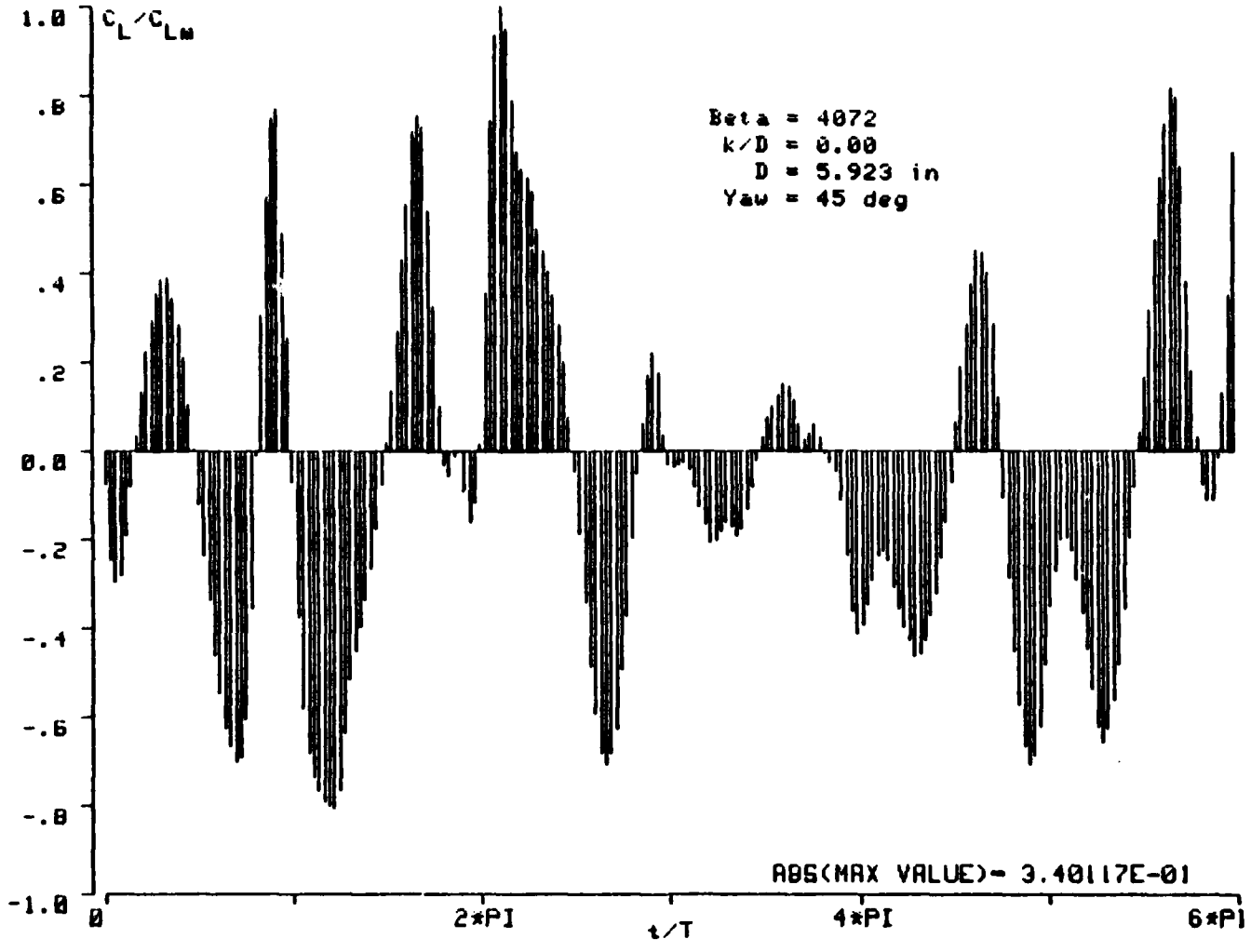

Figure 82. Normalized Lift Force Data for K = 21.18, β = 4090, α = 45 Deg., k/D = 0.00

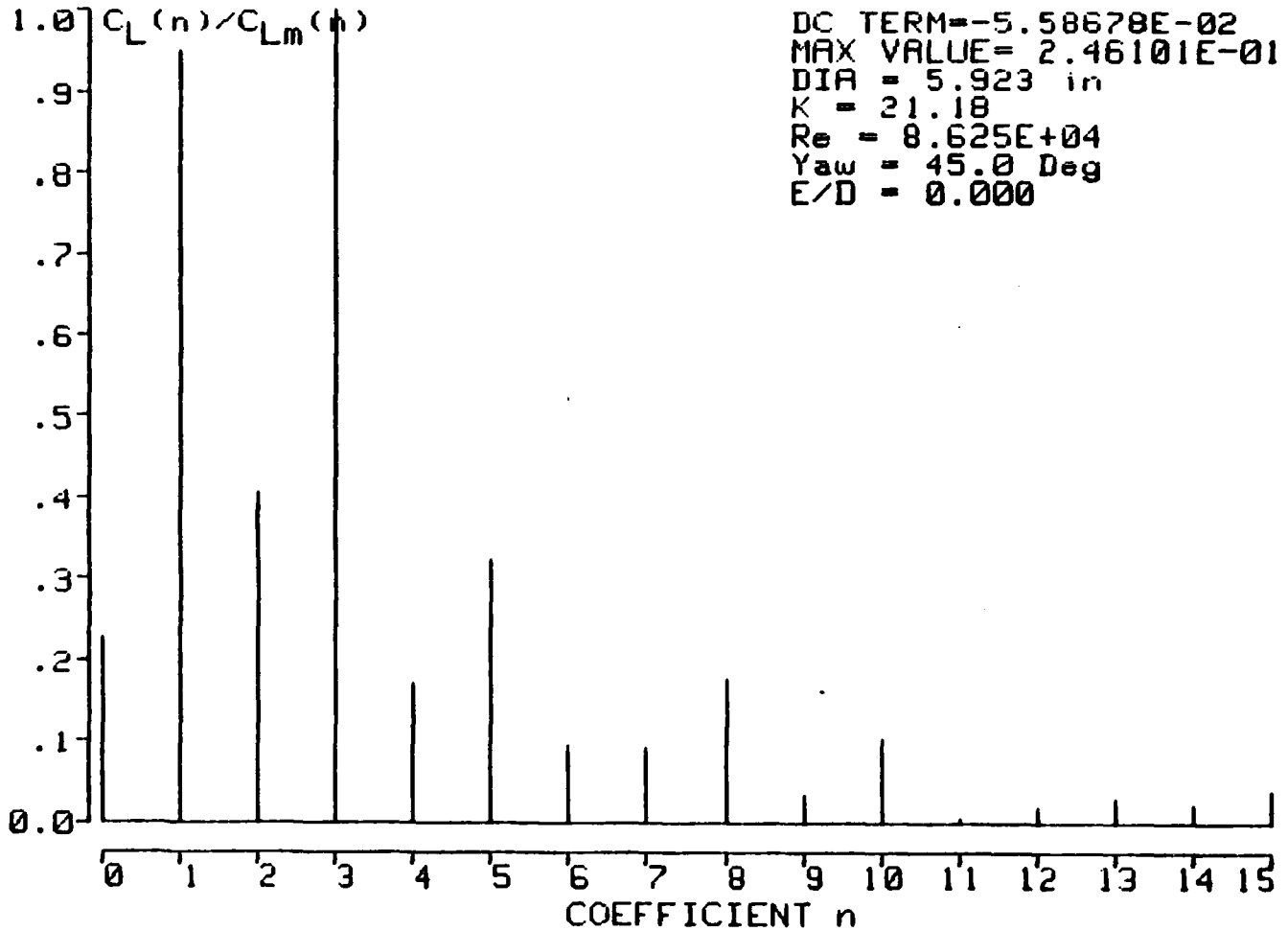

Figure 83. Normalized Fourier Coefficients for $\dot{K}$ = 21.18, β = 4090, α = 45 Deg., k/D = 0.00

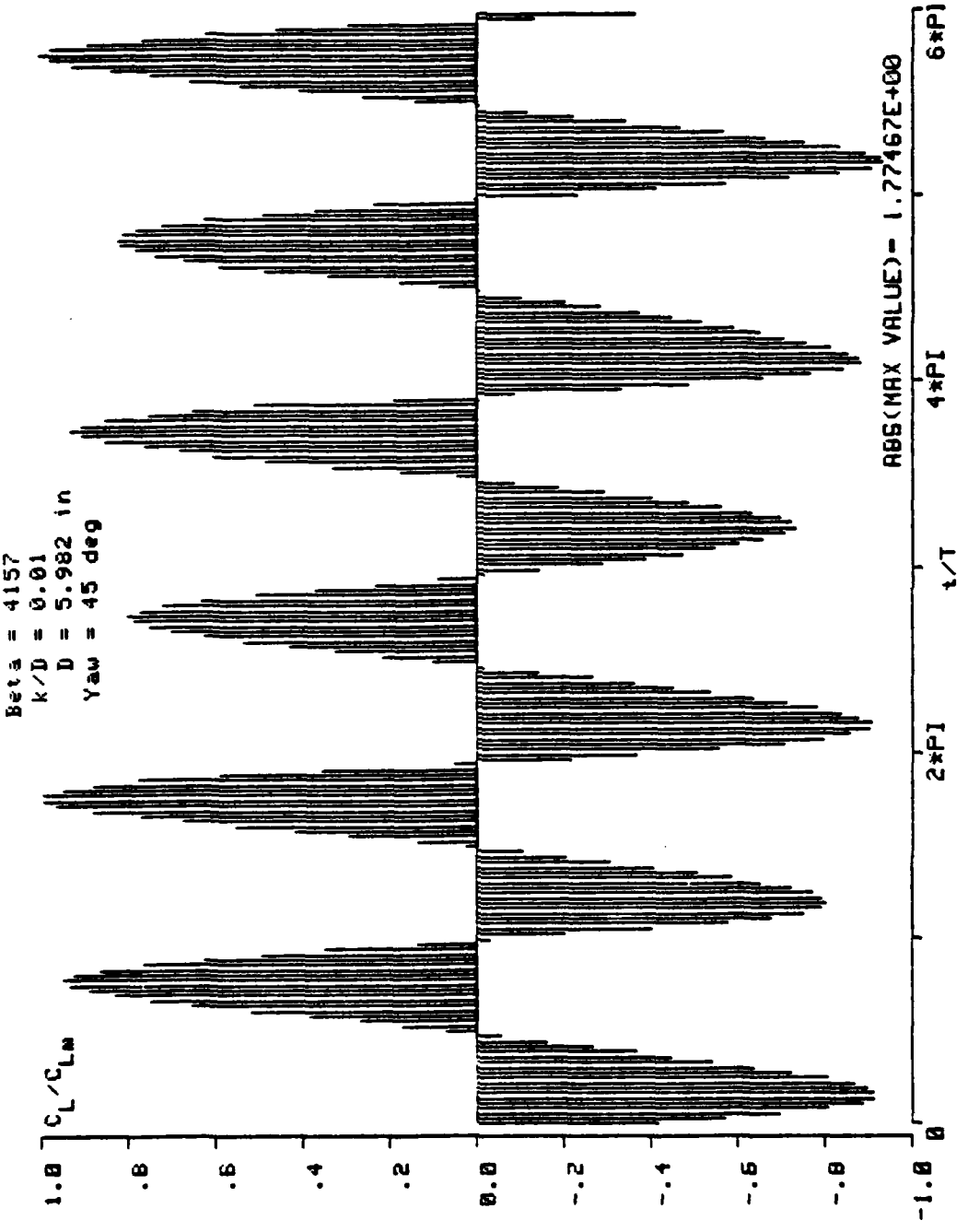

Figure 84. Normalized Lift Force Data for K = 7.86, β = 4150, α = 45 Deg., k/D = 0.01

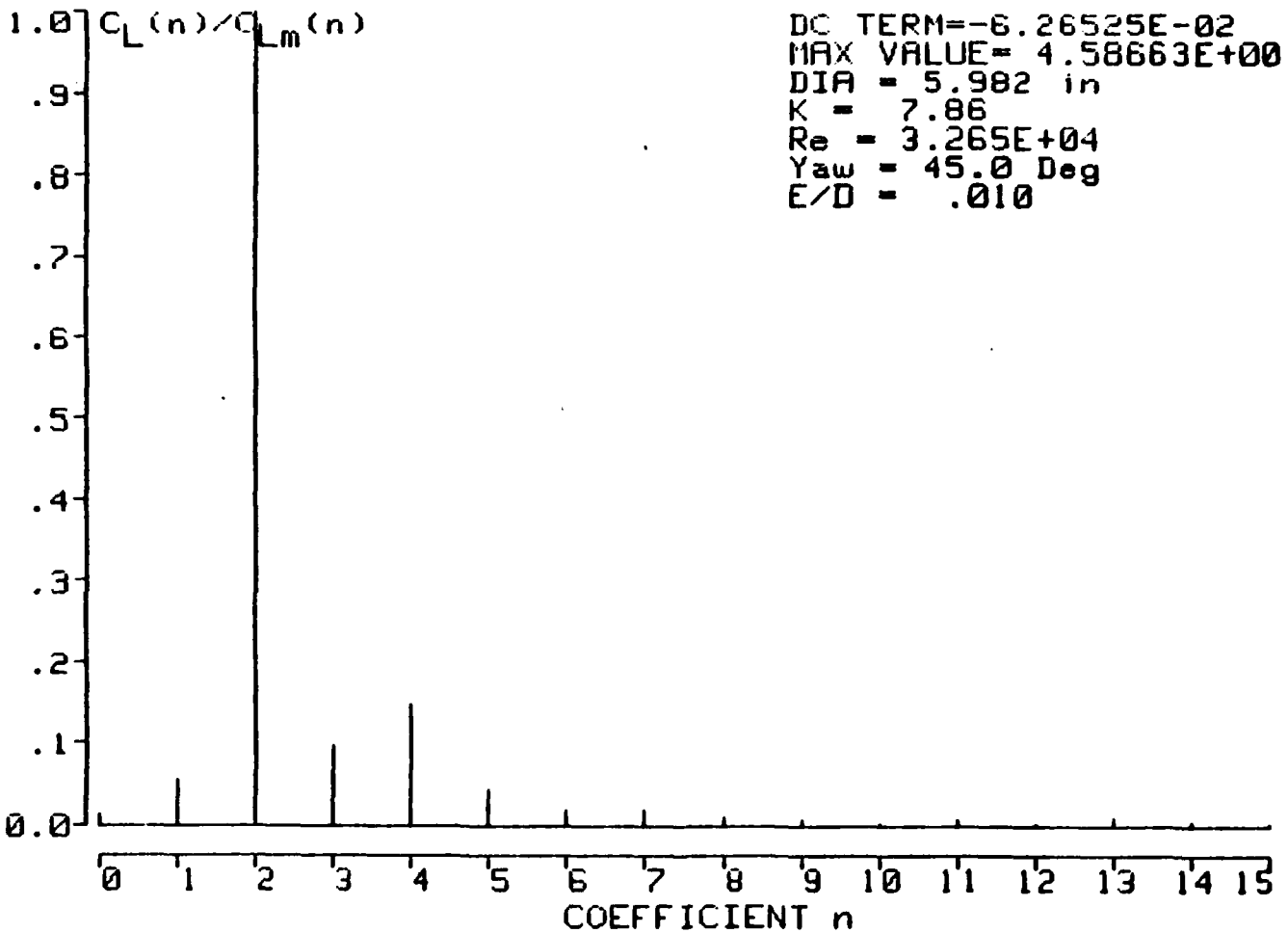

Figure 85. Normalized Fourier Coefficients for K = 7.86, β = 4150, α = 45 Deg., k/D = 0.01

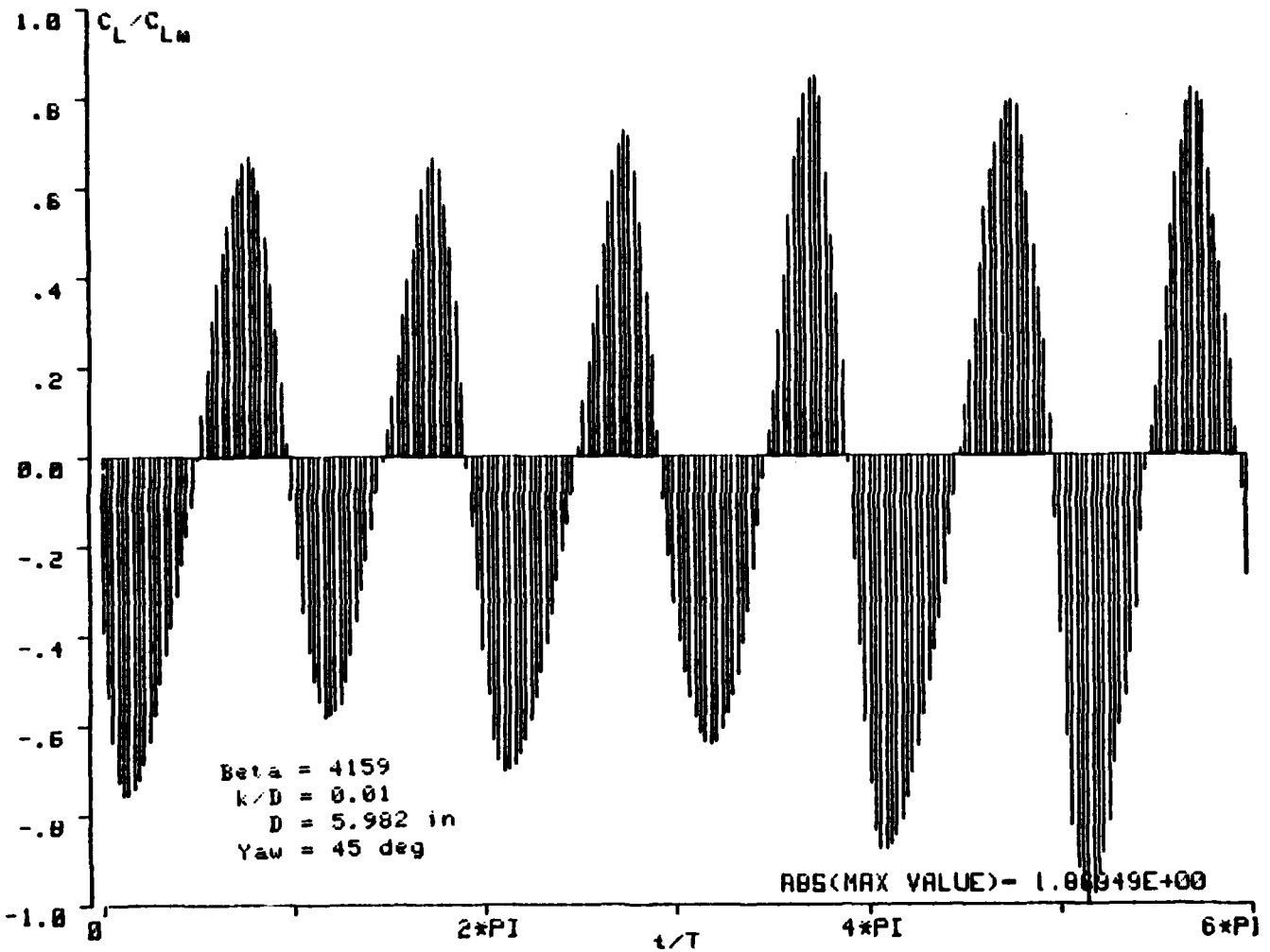

Figure 86. Normalized Lift Force Data for K = 9:39, β = 4150, α = 45 Deg., k/D = 0.01

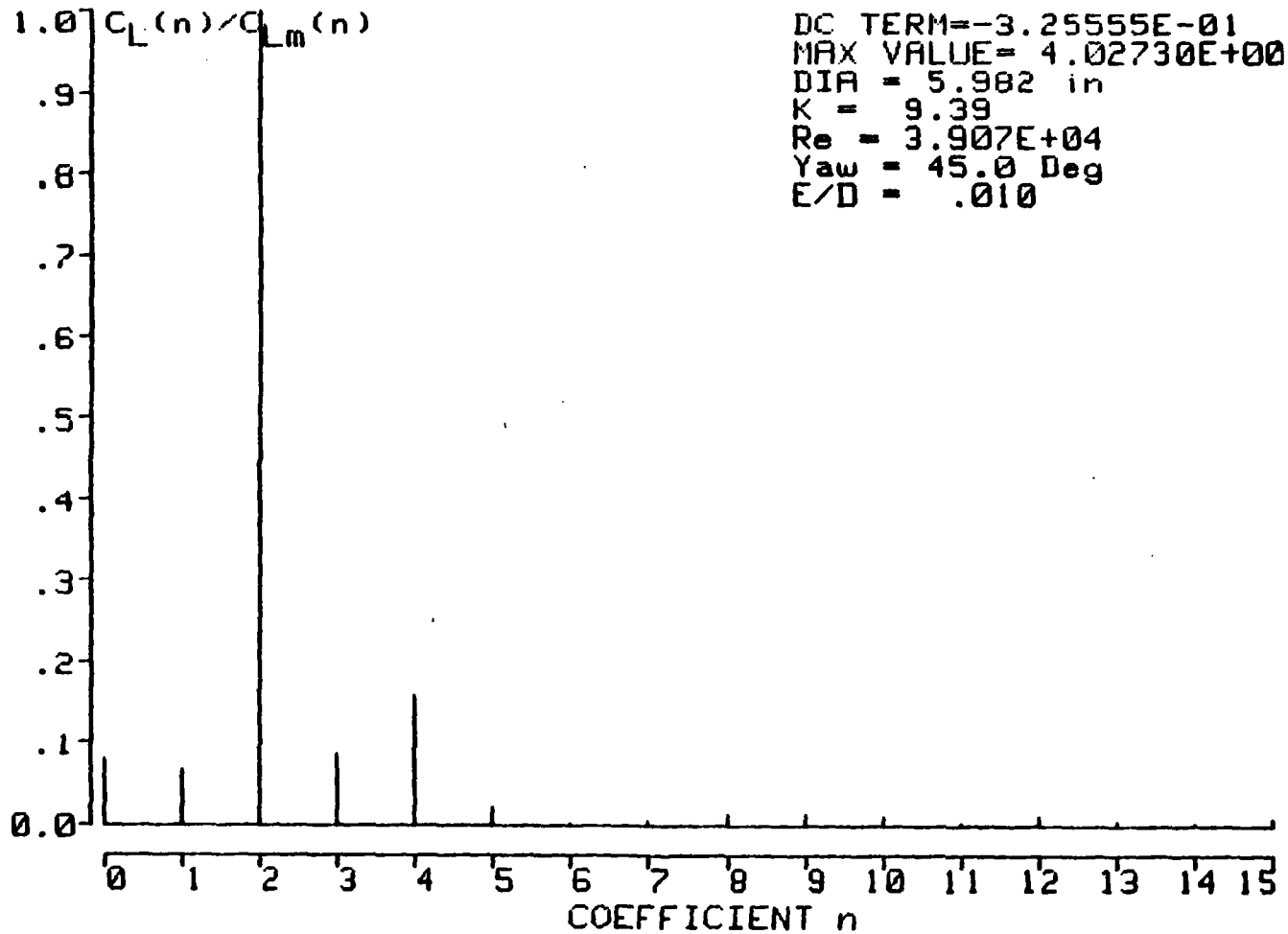

Figure 87. Normalized Fourier Coefficients for K = 9.39, β = 4150, α = 45 Deg., k/D = 0.01

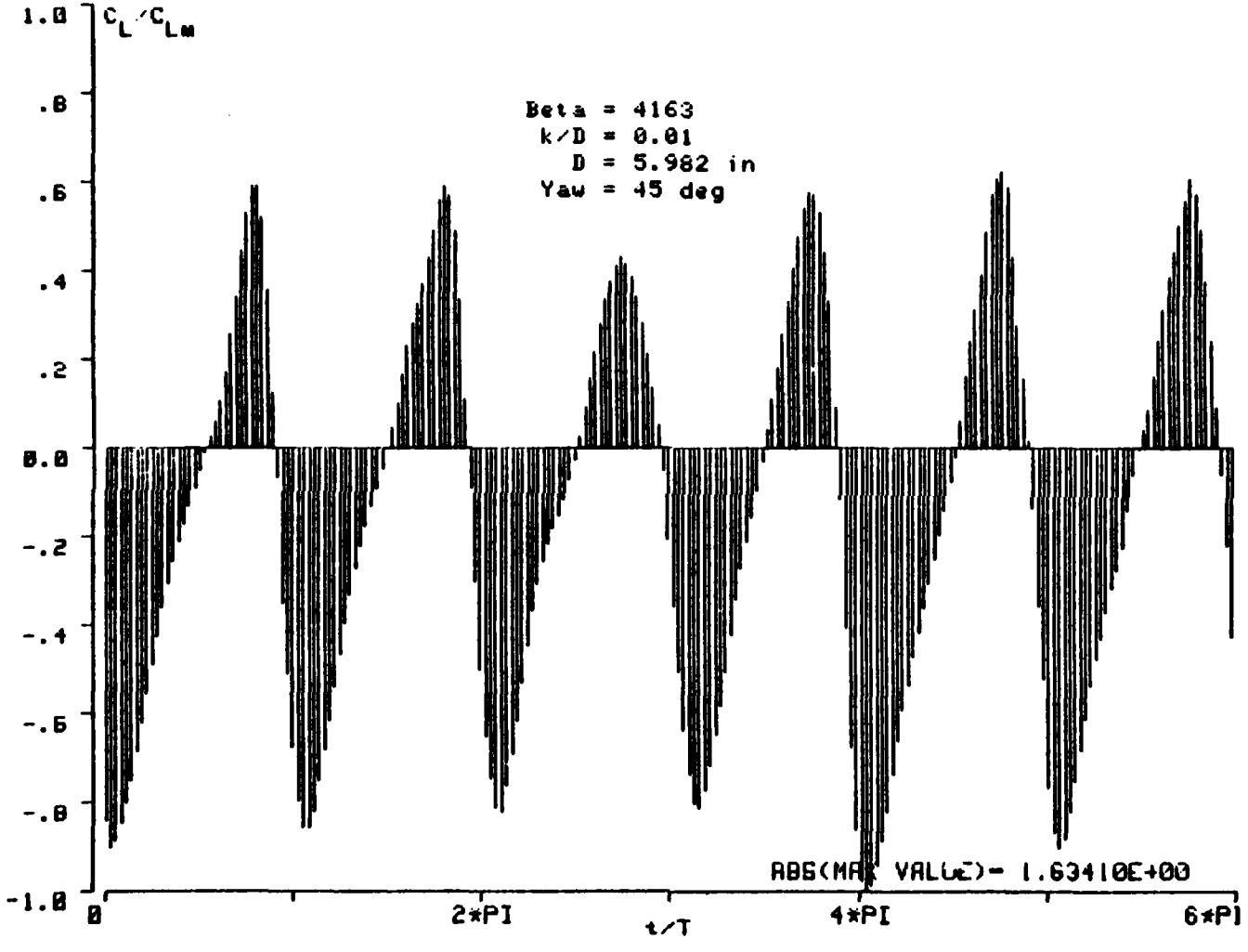

Figure 88. Normalized Lift Force Data for K = 13.69, β = 4150, α = 45 Deg., k/D = 0.01

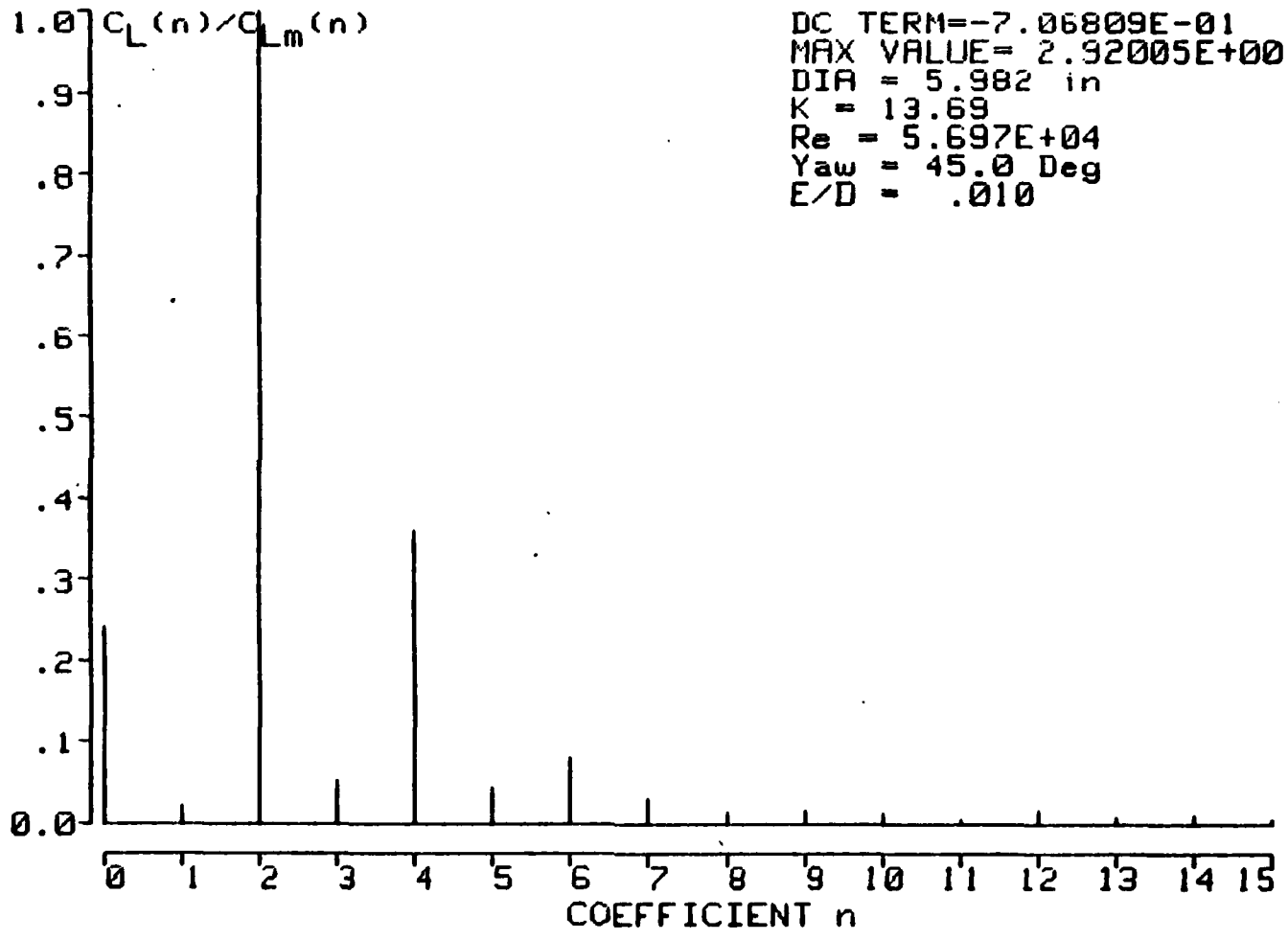

Figure 89. Normalized Fourier Coefficients for K = 13.69, β = 4150, α = 45 Deg., k/D = 0.01

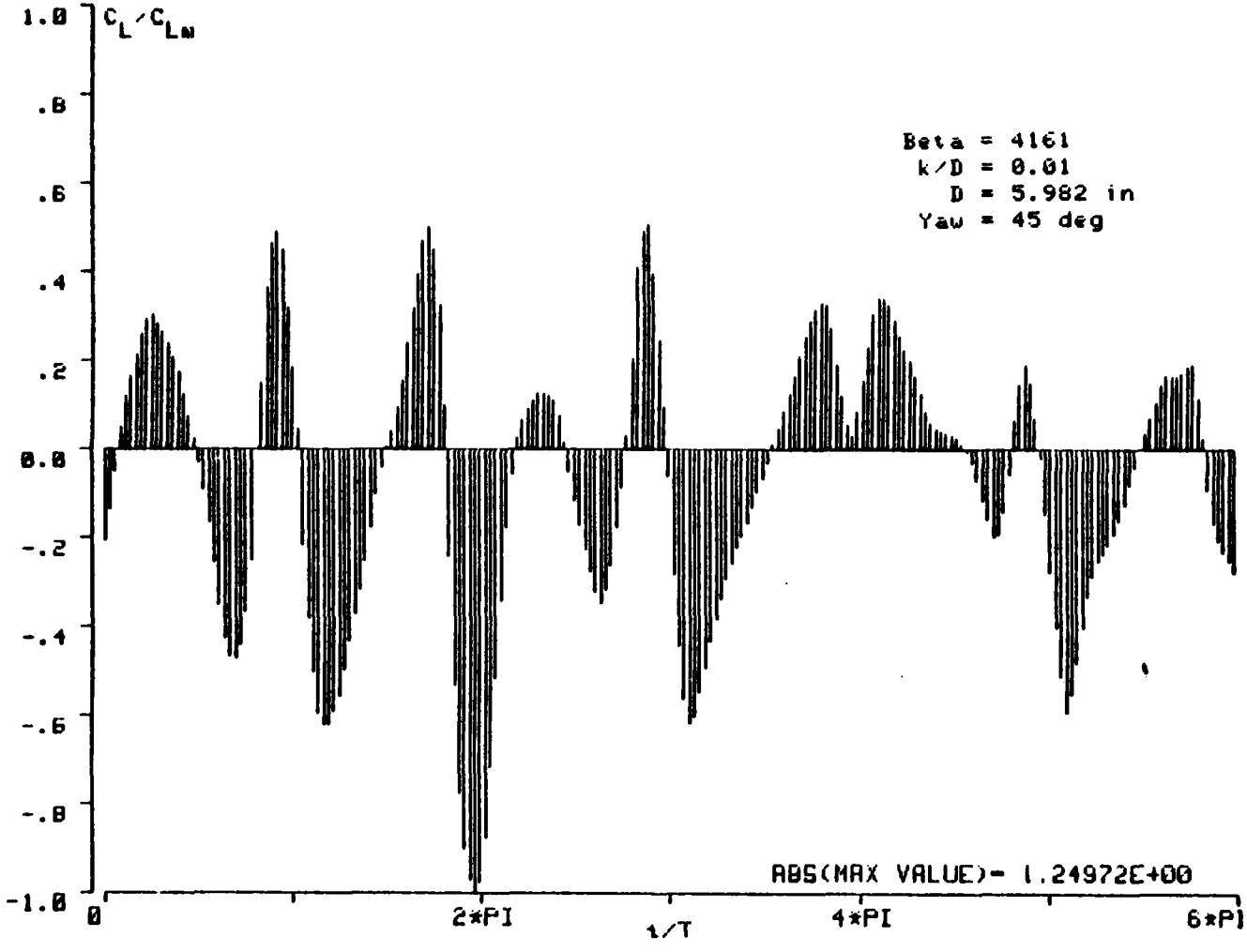

Figure 90. Normalized Lift Force Data for K = 17.57, β = 4150, α = 45 Deg., k/D = 0.01

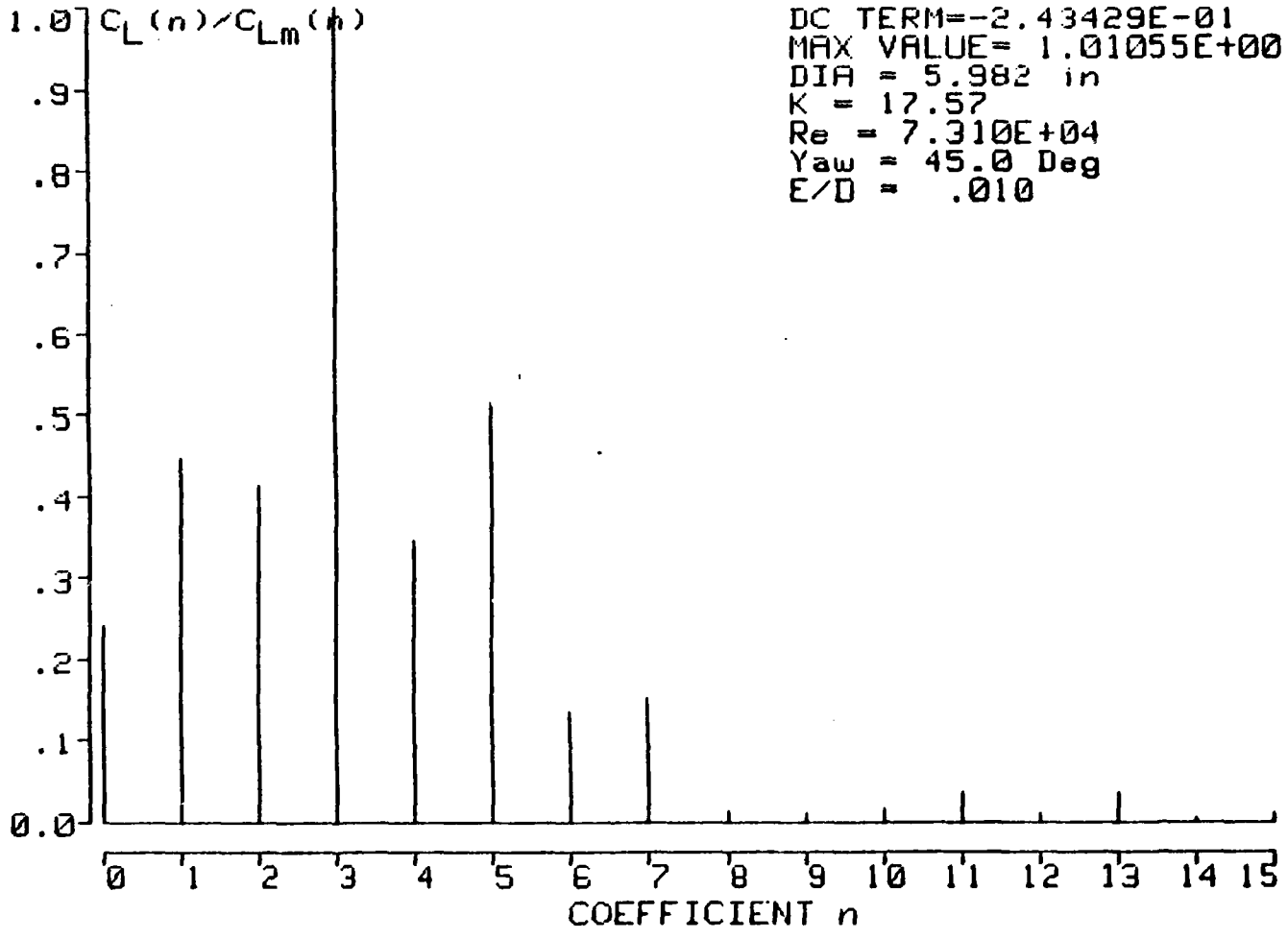

Figure 91. Normalized Fourier Coefficients for K = 17.57, β= 4150, α= 45 Deg., k/D = 0.01

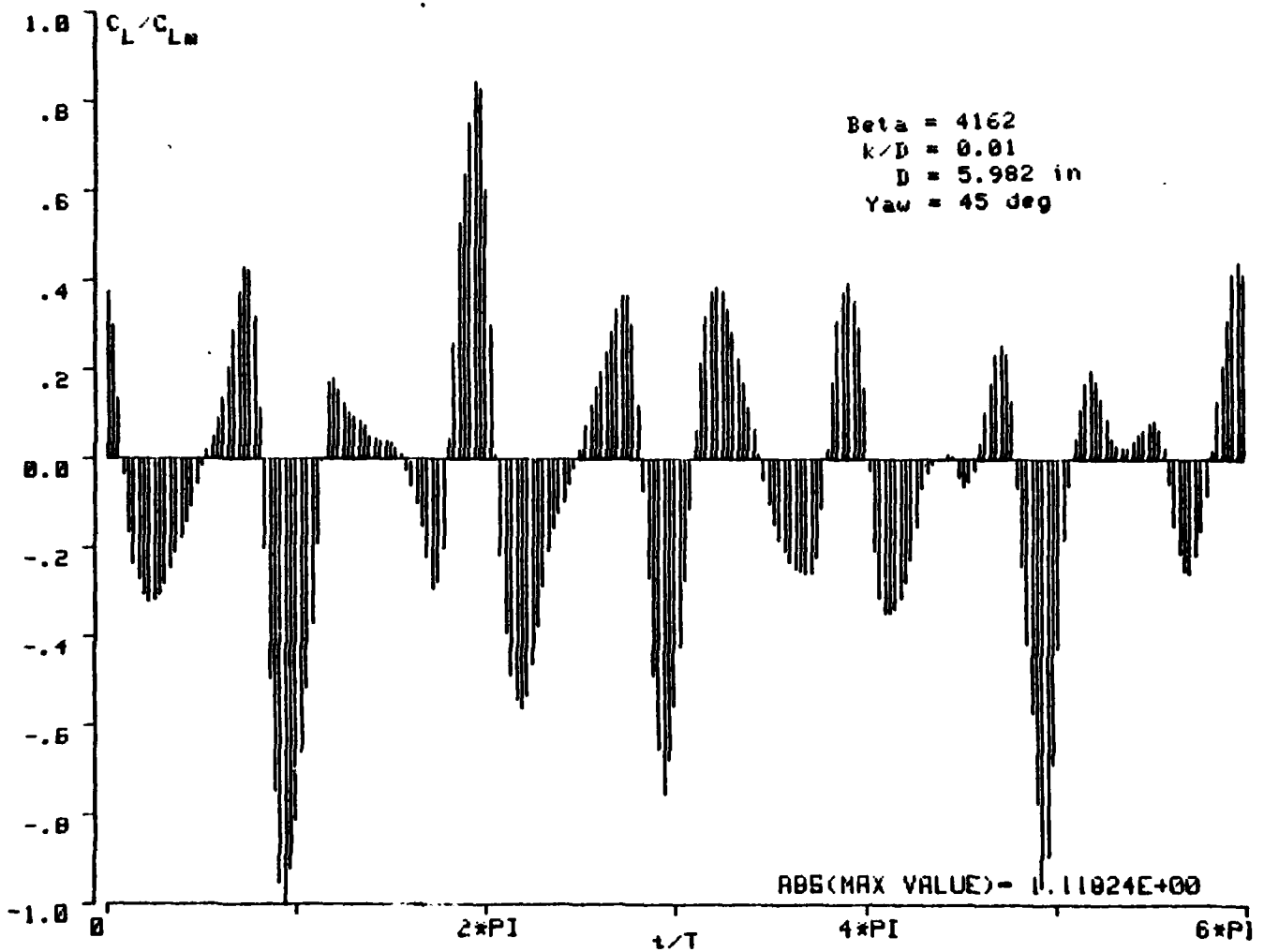

Figure 92. Normalized Lift Force Data for K = 19.68, β = 4150, α = 45 deg., k/D = 0.01

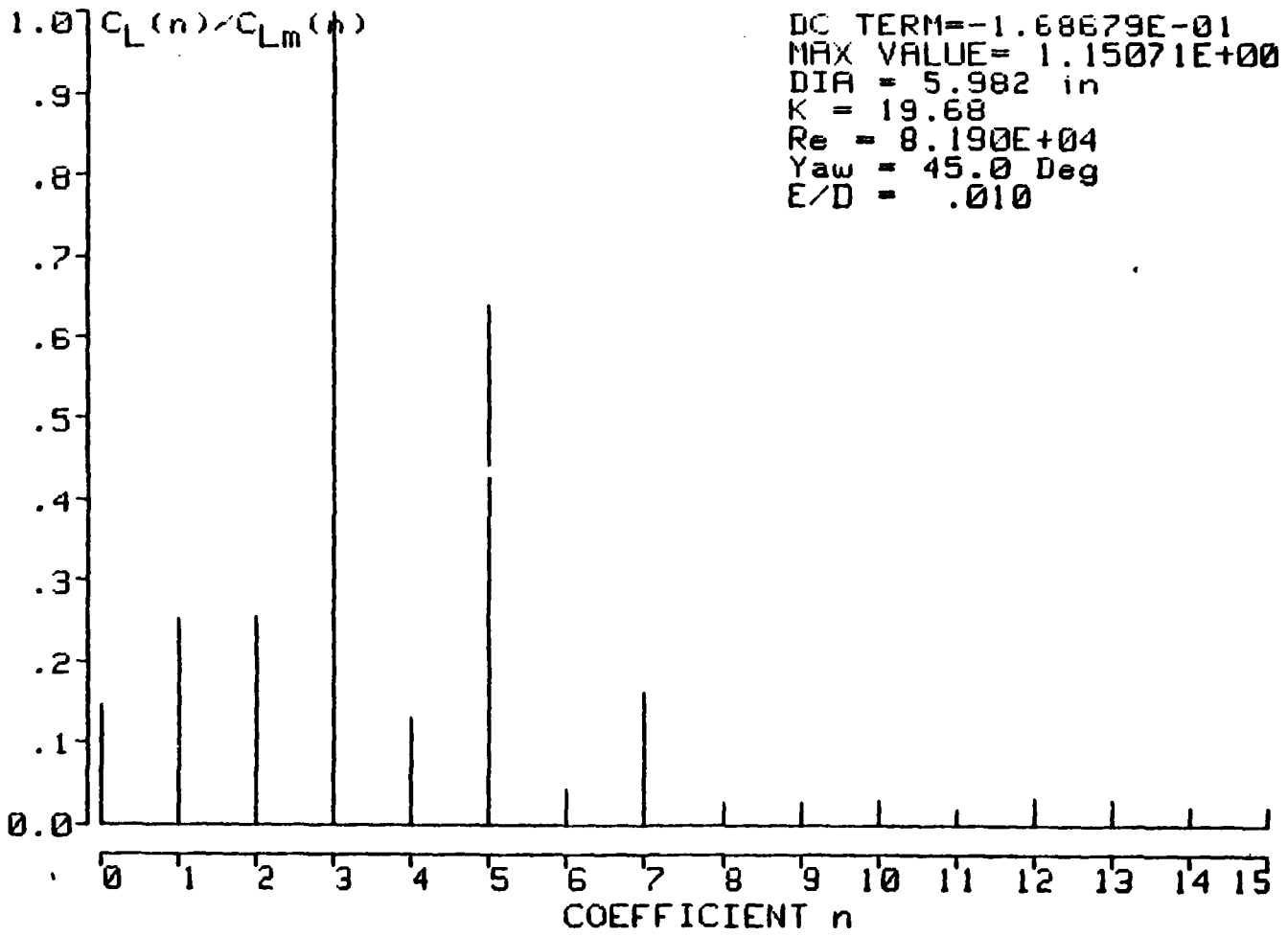

Figure 93. Normalized Fourier Coefficients for K = 19.68, β= 4150, α= 45 Deg., k/D = 0.01

LIST OF REFERENCES

1. Morison, J. R., O'Brien, M. D., Johnson, J. W., and Schaaf, S. A., "The Force Exerted by Surface Waves on Piles", Petroleum Transactions AIME, Vol. 189, 1950, pp. 149-157.

2. Sarpkaya, T., "Morison's Equation and the Wave Forces on Offshore Structures", Naval Civil Engineering Laboratory Report No. CR 82.008, Naval Facilities Engineering Command, Port Hueneme, CA., 1982.

3. Heideman, J. C., Olsen, O. A., and Johansson, P. I., "Local Wave Force Coefficients", Civil Engineering in the Oceans IV, ASCE, Vol. 1, 1979, pp. 684-699.

4. Sarpkaya, T. and Isaacson, M., Mechanics of Wave Forces on Offshore Structures, Van Nostrand Reinhold, New York, 1981.

5. Hoerner, S. F., Fluid Dynamic Drag, 3rd Ed., Book Published by the author, New Jersey, 1965.

6. Bursnall, W. J. and Loftin, L. K., "Experimental Investigation of the Pressure Distribution About a Yawed Circular Cylinder in the Critical Reynolds Number Range", NACA Technical Note 2463, 1951.

7. Norton, D. J., Heideman, J. C., and Mallard, W. W., "Wind Tunnel Tests of Inclined Cylinders", Proceedings of the Offshore Technolofy Conf., Vol. IV, 1981, pp. 67-75.

8. Sarpkaya, T. and Collins, N. J., Discussion of "Drag and Inertia Forces on a Cylinder in Periodic Flow", Journal of Waterways etc. Div. ASCE, WW1, 1978, pp. 96-98.

9. Sarpkaya, T., "Vortex Shedding and Resistance in Harmonic Flow About Smooth and Rough Circular Cylinders at High Reynolds Numbers", Naval Postgraduate School Report No: NPS-59SL76021, 1976, Naval Postgraduate School, Monterey, CA.

10. Sarpkaya, T., "In-line and Transverse Forces on Smooth and Sand-Roughened Cylinders in Oscillatory Flow at High Reynolds Numbers", Naval Postgraduate School Report No: NPS-69SL76062, Naval Postgraduate School, Monterey, CA.

11. Keulegan, G. H. and Carpenter, L. H., "Forces on Cylinders and Plates in an Oscillating Fluid", Journal of Research of the National Bureau of Standards, Vol. 60, No. 5, 1958, pp. 423-440.

INITIAL DISTRIBUTION LIST

1.	Defense Technical Information Center Cameron Station Alexandria, Virginia 22314	2
2.	National Science Foundation Washington, D. C. 20550 Attn: Dr. Arthur A. Ezra	2
3.	National Science Foundation Division of Grants and Contracts AAEO/ENG Branch 1800 G. Street, N. W. Washington, D. C. 20550	2
4.	Library, Code 0142 Naval Postgraduate School Monterey, CA 93940	2
5.	Dean of Research Naval Postgraduate School Monterey, CA 93940	1
6.	Professor T. Sarpkaya, Code 69SL Mechanical Engineering Naval Postgraduate School Monterey, CA 93940	10
7.	Chairman, Department of Mechanical Engineering Code 69 Naval Postgraduate School Monterey, CA 93940	2
8.	National Maritime Institute Teddington, Middlesex England Attn: Superintendent	1
9.	Prof. R. L. Wiegel Hydraulic Engineering Lab., University of California Berkeley, CA	1
10.	Dr. Yoshimi Goda Port and Harbour Institute Ministry of Transport Nagase, Yokosuka, Japan	1

11. Prof. John H. Nath — 1
Oregon State Univ.,
Corvallis, Oregon

12. Prof. Robert G. Dean — 1
Ocean Engineering
University of Delaware
Newark, Delaware

13. Dr. David J. Maull — 1
Engineering Department
University of Cambridge
Trumpington Street
Cambridge, England

14. BHRA — 1
Cranfield, Bedford
England

15. Dr. M. M. Zdravkovich — 1
Mechanical Engineering
University of Salford
Salford M5 4WT
England

16. National Bureau of Standards — 1
Washington, D. C.
Attn: Dr. G. Kulin

17. Hydronautics, Inc. — 1
Pindell School Road
Howard County
Laurel, MD 20810

18. Commander — 1
Naval Ship Research and Development
Center
Bethesda, MD 20034

19. Commander — 1
Naval Sea Systems Command
Washington, D. C. 20362

20. Office of Naval Research — 1
800 North Quincy Street
Arlington, VA 22217

21. Director — 1
Naval Research Laboratory
Washington, D. C. 20390

22. Library of Congress
Science & Technology Division
Washington, D. C. 20540 — 1

23. Southwest Research Institute
P. O. Drawer 28510
San Antonio, TX 78284 — 1

24. University of California
College of Engineering
Berkeley, CA 94720 — 1

25. Harward University
Pierce Hall
Cambridge, MA 02138 — 1

26. Department of Ocean Engineering
MIT
Cambridge, MA 02139 — 1

27. Webb Institute of Naval Architecture
Crescent Beach Road
Glenn Cover, L.I., NY 11542 — 1

28. Davidson Laboratory
Stevens Institute of Technology
711 Hudson Street
Hoboken, NJ 07030 — 1

29. Library (code 1640)
Naval Oceanographic Office
Washington, D. C. 20390 — 1

30. Ocean Engineering Department
Woods Hole Oceanographic Institute
Woods Hole, MA 02543 — 1